0 0 0 0 4 7 0 4 8 3 0

LBL-5787
c.1

THE INFLUENCE OF RETAINED AUSTENITE ON THE THICK SECTION MECHANICAL PROPERTIES OF A COMMERCIAL LOW ALLOY ULTRA-HIGH STRENGTH STEEL

Ronald Martin Horn
(Ph. D. thesis)

RECEIVED
LAWRENCE
RADIATION LABORATORY

MAR 9 1977

LIBRARY AND
DOCUMENTS SECTION

December 1976

Prepared for the U. S. Energy Research and
Development Administration under Contract W-7405-ENG-48

For Reference

Not to be taken from this room

LAWRENCE BERKELEY LABORATORY
UNIVERSITY OF CALIFORNIA
BERKELEY

LBL-5787
c1

LEGAL NOTICE

This report was prepared as an account of work sponsored by the United States Government. Neither the United States nor the United States Energy Research and Development Administration, nor any of their employees, nor any of their contractors, subcontractors, or their employees, makes any warranty, express or implied, or assumes any legal liability or responsibility for the accuracy, completeness or usefulness of any information, apparatus, product or process disclosed, or represents that its use would not infringe privately owned rights.

Table of Contents

ABSTRACT v

I. INTRODUCTION 1

II. EXPERIMENTAL PROCEDURE 4

A. Material Preparation 4

B. Heat Treatment 4

C. Mechanical Testing 5

1. Impact Testing 5

2. Tensile Tests 6

3. Fracture Toughness Tests 6

D. Austenite Characterization 7

1. Magnetic Saturation 7

2. X-Ray Methods 7

E. Transformation Behavior 9

F. Microscopy 9

1. Optical Microscopy 9

2. Transmission Electron Microscopy 9

3. Scanning Electron Microscopy 10

III. RESULTS 11

A. Transformation Behavior 11

B. Cooling Process Determination 12

C. Mechanical Properties 13

1. Tensile Properties 13

2. Fracture Properties 16

0 0 0 0 4 7 0 4 3 3 H

D. Fracture Appearance 17

E. Retained Austenite Behavior 19

1. Oil Quenched - 300-M 20

2. 2.5 cm Air Cooled - 300-M 20

3. 5.0 cm Air Cool - 300-M 21

4. 10 cm and 15 cm Air Cool - 300-M 23

5. 2.5 cm Air Cool - 4340 23

F. Microstructure Characterization 24

1. Optical Metallography 24

2. Transmission Electron Microscopy 26

IV. DISCUSSION 27

A. Transformation Characteristics 27

1. Continuous Cooling Behavior 27

2. As-cooled Structure 29

3. Tempering Transformation 32

4. Austenite Behavior 36

B. Mechanical Behavior 37

C. Thick Section Steel Evaluation 50

V. SUMMARY AND CONCLUSIONS 54

ACKNOWLEDGEMENTS 56

APPENDIX I 57

APPENDIX II 60

REFERENCES 70

TABLES 75

FIGURE CAPTIONS 89

FIGURES 96

0 0 0 0 4 7 0 4 3 3 3

THE INFLUENCE OF RETAINED AUSTENITE ON THE THICK SECTION MECHANICAL PROPERTIES OF A COMMERCIAL LOW ALLOY ULTRA-HIGH STRENGTH STEEL

Ronald Martin Horn

Materials and Molecular Research Division, Lawrence Berkeley Laboratory
and Department of Materials Science and Engineering,
University of California, Berkeley, California 94720

ABSTRACT

The relationships between microstructure, mechanical, and fracture properties were investigated for thick sections (up to 15 cm) following air cooling and tempering in a silicon-modified 4340, 300-M. This steel which has high pearlite hardenability achieves high strength levels after very slow cooling. Slow cooling also leads to high levels of retained austenite (up to 30%). Properties were determined for microstructures equivalent to those developed through air cooling and tempering of 2.5, 5.0, 10.0 and 15 cm thick plates. Simulated slow cooling was performed on small specimens to model the thicker sections. Fracture toughness and Charpy V-notch behavior were used to evaluate fracture properties while both round and flat tensile specimens were used to measure mechanical properties. Emphasis was placed on determining the role of the austenite on these properties. The morphology, amount, and mechanical stability of the austenite were characterized using transmission electron microscopy and magnetic saturation techniques. It was found that the stability of the austenite, which changed with tempering treatment, had a major influence

0 0 0 0 4 7 0 4 2 3 3

on the fracture properties. Specifically, if the austenite was stable the material had good fracture resistance, while if the austenite was unstable the fracture toughness was poor. Destabilization of the austenite after tempering was found to be associated with tempered martensite embrittlement. Finally, it was found that for 300-M there was an optimum slow cooling rate which led to a good combination of strength, ductility and fracture resistance.

00 00 00 00 41 77 00 40 78 33 47

I. INTRODUCTION

Low alloy ultra-high strength steels have been commercially important for many decades. In these materials there is a compromise between strength and toughness. Consequently, much work has been aimed at increasing one without affecting the other. Several approaches have been used to make this improvement. The cleanliness of the steel is one characteristic shown to influence only the toughness. Recent improvements in manufacturing methods, e.g. vacuum arc remelting, have led to lower inclusion contents which in turn have been shown to improve ductility.[1] Composition changes are another method used to improve properties.[2-4] The alloy modifications explored by various steel companies have led to several steels of similar yield strength with widely varying composition. Significant work has also been undertaken to effect improvements through process modification.[5-7] These processing modifications change the amount and morphology of the phases present. Often, as well, combined approaches are used to develop desired microstructures.[2,8]

Most work on low alloy ultra-high strength steels has involved conventional quenching and tempering heat treatments; this process, however, restricts the versitility possible of other treatments, such as isothermal transformations or slower cooling. It also limits the usefulness of the research to thin section products. A significant proportion of steel components constitute thick section and cannot be heat treated in a manner to achieve a uniform microstructure during rapid cooling.

The work on quenched and tempered steel has shown that one constituent, retained austenite, can have significant influence on properties. High carbon austenite of the type retained in tool steels (due to a low M_s) has a deliterious effect. The role of austenite in lower alloy, lower carbon steel after quenching and tempering, is more ambiguous. In fact, austenite of a lath morphology has been associated with increases in fracture toughness in these steels.[9]

The constituent which has the major influence on the properties of steel is the carbide. Its structure, size, and distribution determines strength level as well as fracture properties. Carbides which are fine and unformly distributed often lead to excellent properties while carbides in the form of long continuous plates can lead to much lower fracture resistance. It has been found that the addition of silicon has a marked influence on both retained austenite[10] and carbide structure in quenched and tempered steels.[11] Silicon can also influence the continuous cooling transformation behavior in low alloy heat treatable steels.[12,13]

With the need to broaden research applicability to thicker section sizes, it was considered desirable to look at microstructures achieved by slower cooling processes. This study was aimed at investigating the microstructure-property relationships in air cooled (normalized) steel of varying section size (thickness). The investigation centered around air cooling because it leads to uniform microstructures in section thicknesses of up to 15 cm. The steels used for the investigation were 4340 and 300-M, a silicon modified version of 4340. These

0 0 0 0 4 7 7 0 4 7 3 3 5 3

steels were chosen for several reasons. First, they are the most widely used commercial high strength steels. Secondly, they are obtainable in vacuum arc remelted form. Finally the modified version, 300-M, retains large levels of austenite after slow cooling.

The study had several objectives. First, a goal of the research was to establish a method for investigating thick section properties. Secondly, the study set out to characterize microstructural-mechanical property relationships in different section sizes. Finally, a major goal of this work was to unambiguously assess the role of retained austenite (with respect to amount, distribution and mechanical and thermal stability) on the properties of these steels.

II. EXPERIMENTAL PROCEDURE

A. Material Preparation

The ultra-high strength low alloy steels used in this study were all vacuum arc remelted aircraft quality material. The heats used were certified to meet commercial specification AMS-2300 and military specification MIL-S-8844C. The certification included mechanical tests as well as inspection tests to verify upper limits on inclusion levels. Jernkontoret charts per ASTM specification E45-63 were used to check for silicate and oxide inclusions, verifying low levels of each. The chemical compositions of the steels used are listed in Table I. It should be noted that the phosphorus and sulfur levels were low compared to air melted steels. The material was purchased as annealed bars which were hot forged and then hot rolled in our laboratory to the desired thickness. The material was slow cooled after fabrication and then spheroidized at 650°C for one hour to insure good machinability.

B. Heat Treatment

Heat treatment consisted of austenitization, cooling, and tempering. The austenitization treatments were all carried out at 870°C for one hour per inch of thickness. Austenitization treatments were performed either in a vertical tube furnace in an argon atmosphere or in a resistance heated conventional furnace in stainless steel bags to prevent decarburization. The cooling processes were performed using several methods. Oil quenching was performed by directly dropping the

0 0 0 0 4 7 0 4 7 8 3 5 9

specimen(s) into agitated room temperature oil. Air cooling, however, was performed differently for the different thickness evaluations. The 2.5 cm and 5.0 cm thicknesses were cooled directly. When the specimen's thickness was smaller than the thickness of interest, steel plates were used to build up the specimen's dimensions. Figure 1 shows the molds used for the round tensile specimens. The simulations of the 10.0 cm and 15.0 cm slabs were performed by matching numerically determined cooling rates in two step heat treatments using insulating material (vermiculite) to slow cooling rates in the 500°C to 870°C range and using a programmed salt pot to match rates in the 200°C to 500°C range. The cooling was monitored using a thermocouple. Tempering was performed in salt pots at the desired temperature for one hour. All specimens were directly water quenched from the tempering temperature for standardization.

C. Mechanical Testing

1. Impact Testing

Charpy V-notch tests were performed to ASTM E23-72 specification. Specimens were tested primarily on a 223 ft-lb. capacity machine with the tests for the oil quenched material conducted separately on a 60 ft-lb. capacity machine. All specimens were made to the dimensions shown in Fig. 2a. The test temperatures other than room temperature were obtained by using either methyl alcohol-liquid nitrogen mixtures, heated water, or a furnace with thermocouple monitoring.

2. Tensile Tests

Two types of tensile tests specimens were used. These are shown in Figs. 2b and 3. The cylindrical specimens, following ASTM specifications, were 0.63 cm in diameter and had a 2.54 cm gage length. The flat tensile specimens were 0.1 cm thick and had the same gage length. The cylindrical specimens were tested using a 300,000 lb. MTS universal testing machine at a crosshead displacement rate of 0.1 cm/min. The flat tensile specimens were pulled using an Instron testing machine at a crosshead speed of 0.05 cm/min. The yield strength and tensile strength values were averaged for both tests. However, elongation and reduction in area measurements were only made on the cylindrical tensile specimens.

3. Fracture Toughness Tests

All fracture toughness tests were performed according to ASTM specification E399-72. Standard compact tension specimens shown in Fig. 4 were used. The specimens were all 2.54 cm thick except for the oil quenched material where some specimens were only 1.8 cm thick. The specimens were fatigued on a 20,000 lb. MTS machine at 50 Hz. Fatigue cracking procedures conformed with ASTM specifications with effort made to achieve an a/W ratio of .5. The K_{Ic} tests were performed on a 300,000 lb. MTS at an acceptable ram speed of 0.005 in/sec (.00125 cm/sec). The fracture toughness was evaluated using the following formula:

$$K_I = \frac{P}{WB^{1/2}} \cdot f(a/W)$$

0 0 0 0 4 7 0 4 7 3 7
0 0 0 0 4 7 0 0 8 4 0

with

$$f(a/W) = 29.6\left(\frac{a}{W}\right)^{1/2} - 185.5\left(\frac{a}{W}\right)^{3/2} + 655.7\left(\frac{a}{W}\right)^{5/2}$$

$$- 1017.0\left(\frac{a}{W}\right)^{7/2} + 638.9\left(\frac{a}{W}\right)^{9/2}$$

where K_I is the stress intensity, P the load, B thickness, W the specimen width, and a the crack length. In the case of ductile specimens non-valid estimates of the fracture toughness were made by using the 95% secant line intersection with the load curve to determine the load of interest.

D. Austenite Characterization

1. Magnetic Saturation

Flat tensile specimens, as described earlier, were used for austenite characterization with a saturation permeameter. The apparatus has been described by de Miramon.[14] The volume of austenite was determined through the measurement of the specimen's saturation induction using the method described in Appendix I. Because the specimens were essentially 70-100% magnetic, as opposed to fully non-magnetic as with austenitic TRIP steels, it was necessary to use calibration standards for reference. These methods for calibration are also described in Appendix I.

2. X-Ray Methods

The amount of retained austenite was also determined using X-ray techniques for certain treatments as a check on the magnetic saturation

technique. The estimate was made using a direct comparison of integrated intensities as described by Cullity.[15] A Picker diffractometer was used for measurement. The X-ray source was copper K_α radiation produced at 40 kV and 14 mA. A lithium fluoride monochromator was used to reduce florescent radiation.

Following Cullity[15] it can be seen that the amount of retained austenite present is given by the following equation (assuming that the carbide level is zero):

$$\frac{I_\gamma}{I_\alpha} = \frac{R_\gamma C_\gamma}{R_\alpha C_\alpha}$$

where $I_{\alpha(\gamma)}$ = integrated intensity for ferrite (austenite)

$C_{\alpha(\gamma)}$ = concentration for ferrite (austenite)

$$R_{\alpha(\gamma)} = \frac{1}{v_{\alpha(\gamma)}} \; |F|^2 \; p \left(1 + \frac{\cos^2 2\theta}{\sin^2 \quad \cos}\right) \quad e^{-2m}$$

where v is the volume of a unit cell, F the structure factor, p the multiplicity, and e^{-2m} the temperature factor. This yields the following equation for the concentration of austenite:

$$C_\gamma = \frac{1}{1 + \frac{I_\alpha}{I_\gamma} \cdot \frac{R_\gamma}{R_\alpha}} \; .$$

Areas under the 220_γ and 311_γ peaks were calculated and compared with the 211_α peak area. The calculated concentrations were then averaged to reduce preferred orientation effects.

E. Transformation Behavior

To check transformation characteristics that had been previously measured, a Theta dilatometer was used. Specimens were austenitized for one half hour and continuously cooled under vacuum. A Datatrak program was made using numerically calculated cooling profiles and was used to control the specimen's cooling rate. The calculation of transformation levels was made using a four step procedure. First, the final level of austenite was evaluated for the cooling treatment. Then initial and final expansion rates were extrapolated from either the pre-transformation or post-transformation region into the transformation regime. This transformation was then used to calculate the amount of transformation at any given temperature. These data allowed the construction of the continuous cooling transformation (CCT) diagram.

F. Microscopy

1. Optical Microscopy

Specimens for optical metallography were sectioned from fracture toughness specimens. They were mounted in Koldmount, ground on successive papers to 600 grit and then polished first using 1μ diamond paste and then using .05μ alumina. Specimens were etched with a 5% nital solution for ten seconds, and viewed using a Zeiss Ultraphot metallograph.

2. Transmission Electron Microscopy

Material slices for specimen preparation were taken from fracture toughness specimens. Thin slices were abrasively cut and ground under

coolant, and were then chemically thinned in an $HF-H_2O_2$ mixture to between 50 μm and 75 μm in thickness. Discs from the foils were both spark cut and punched out, lightly ground, and electropolished in a twin jet polisher using a chromic-acetic acid solution at a voltage of 25-35 volts. Transmission foils were examined using a Siemens Elmiskop IA operated at 100 kV.

3. Scanning Electron Microscopy

Fracture surfaces of selected specimens were examined with an AMR 1000 scanning electron microscopy at 20 kV. Fatigue fracture interfaces as well as fracture areas were studied.

0 0 0 0 4 7 0 0 8 4 2

III. RESULTS

A. Transformation Behavior

The isothermal (TTT) and continuous cooling (CCT) transformation behavior of 4340 type steels has been previously characterized. Ericsson[12] and Yuen[13] used a magnetic permeability method to study the differences between 4340 and 300-M, cooled isothermally and cvntinuously, respectively. Although differences in isothermal behavior were small, the continuous cooling behavior was distinctly different. Pearlite reactions were found with cooling rates of ~0.4 °C/sec in 4340 while none were found in 300-M with rates as low as 0.07 °C/sec. Bainite transformations were delayed significantly in the 300-M as well. Large changes in the amount of retained austenite were also found in the silicon modified steel. While present data verified Yuen's trend in austenite levels, magnetic saturation and X-ray analysis led to revised estimates of the actual austenite quantities. Dilatometry results developed from the cooling paths of interest to this study are shown in Fig. 5. This study verified the general shape of the CCT curves. However, the relative percentages transformed as determined by proportion were much different from Yuen's data for the 300-M alloy at slow cooling rates. The curves suggest that cooling rates slower than 0.3 °C/sec (around 450°C) lead to microstructures containing bainite (diffusion dependent transformation). It also shows that the transformatons are confined to a narrow region of temperature for cooling rates less than 0.3°C/sec. This implies no pearlite formation for any

practical cooling rate.

B. Cooling Process Determination

The purpose of this study was to characterize the properties of thick section steels containing large levels of retained austenite. The cooling process of interest was the air cooling process due to its ease of implementation and to the uniformity of microstructure it imparts. The determination of the cooling rates that thick sections would experience if air cooled was necessary. By matching this rate in small specimens, the same microstructure could be achieved. To account for conduction in the metal as well as convection and radiation at the plate surface, numerical techniques were used to model the heat transfer process. The methods used and the computer program which resulted are given in Appendix II.

Prior to the selection of air cooling for investigation it was necessary to ascertain that the process would lead to uniform microstructures in the section thicknesses of interest i.e., no significant gradation from center to edge would exist in the transformation regime. Computer analysis verified that the gradient is small [$< 15°C$] in the transformation temperature range [$< 450°C$] in slabs up to 15 cm in thickness. Moreover, the cooling rate difference, edge to center, is essentially identical. Thus it can be assumed that uniform microstructures are obtained in the section.

Having substantiated the absence of a temperature gradient in the steel structure, it was necessary to determine the heat transfer parameters giving best fit cooling profiles with laboratory determined

rates. Figure 6 shows the laboratory rates compared with the numerically calculated rates for 2 cm thickness steel. This best fit was obtained using a heat transfer coefficient of .00085 and an emissivity of 0.9. These parameters also gave the best fit for 3 cm thickness steel air cooled. These parameters were used to develop numerically determined cooling rates for the thicknesses of interest: 2.5 cm, 5.0 cm, 10.0 cm, and 15.0 cm. Figures 7 and 8 show the profiles as determined for these thicknesses with both center and edge rates shown as they intersect the transformation curve. It became clear that slabs of up to 5 cm thickness contain significant martensite levels, while the 10 and 15 cm thick, air cooled slabs contain predominantly diffusion controlled transformation products.

C. Mechanical Properties

1. Tensile Properties

Tensile properties depend directly on cooling rate. Normally, untrahigh strength steels are oil quenched to produce fully martensitic structures and are then tempered at a temperature that will give the material the optimum level of ductility and toughness. In this study, the cooling rate was the primary variable used to produce microstructure variation. Figures 9 through 13 show comparisons of the yield strength and ultimate tensile strength (UTS) properties for 300-M. Oil quenched and air cooled material of 2.5 cm, 5.0 cm, 10.0 cm and 15.0 cm thickness in the as-cooled condition as well as in the tempered condition are shown. Figure 14 shows the tensile properties for air cooled 4340 of 2.5 cm thickness. Tables II through IX list these properties. Finally,

Figs. 15 through 20 show the elongaton and reduction in area for these same treatments. Generally, with the slow cooling process there is a drop in both yield and ultimate strength. The air cooling treatments do, however, lead to strength levels comparable to some quenched and tempered steels. The alloy additions to 4340 steel have a significant effect as verified by the air cooled properties of the unmodified steel.

a. Oil quenched properties - 300-M. The properties of 300-M have been previously characterized very thoroughly.[7,16,17] However, it has been shown that heat-to-heat variation in phosphorus and sulfur can significantly influence properties. Therefore, for evaluation of unconventional heat treatments, it is necessary to know base-line quenched and tempered properties. As seen in Fig. 9, tempering this steel at 300°C leads to a yield strength of 250 ksi and a UTS of 290 ksi. This treatment is the commercially used treatment for this silicon modified alloy steel.

b. 2.5 cm air cooled - 300-M. The tensile properties of the air cooled treatment are still high even after the accepted 300°C tempering treatment, leading to a 225 ksi yield and 270 ksi ultimate tensile strength. Tempering at higher temperatures leads to properties very close to those of the oil quenched material. The strength properties are essentially identical after tempering at 650°C. Double tempering, particularly in the 450°C range tends to increase the yield strength slightly. Reduction in area is somewhat lower than that of the oil quenched steel, with a decrease observed after the 450°C temper. Elongation levels follow those of the oil quenched and tempered material.

c. 5.0 cm air cooled - 300-M. Figures 11 and 17 characterize the behavior of the 300-M following this heat treatment. The tensile properties are lower reflecting a change in microstructure from one which is fully martensite. The peak yield strength of over 200 ksi, however, does suggest the presence of significant amounts of transformation products formed at low temperatures (< 350°C), as indicated by the dilatometric studies. Double tempering leads to some increase in yield strength in the 450°C range. The elongation and reduction in area are below those of the quenched and tempered material with a noticeable dip in the 450°C tempering temperature range.

d. 10 cm and 15 cm air cooled - 300-M. The tensile properties for these two conditions are shown in Figs. 12, 13, 18, and 19; the properties for both are very similar. Yield strength levels, particularly after tempering in the 300°C to 400°C regime, are around 160 ksi. This result indicates that the microstructures are considerably different from those of the oil quenched steel. The elongations also changed significantly with values increased to between 18 and 20 per cent. The transformation behavior supports these differences in that the transformations on cooling are essentially completed above 325°C. Both conditions, however, do show significant "secondary hardening" with large increases in UTS after tempering in the 450°C to 550°C temperature range. Severe degradation in ductility is concurring with this strengthening. Only tempering at 650°C restores the air cooled properties to those of the other treatments.

e. 2.5 cm air cooled - 4340. The air cooled tensile properties are displayed in Figs. 14 and 20. The strength levels are significantly below those of the oil quenched 300-M as well as the air cooled 300-M of equivalent thickness. This is due to the higher transformation start tempertures for 4340, seen previously by Yuen.[13] The strength properties remain lower throughout the tempering range. The ductility is consistent with the low strength values observed.

2. Fracture Properties

The fracture toughness (K_{Ic}) dependence with tempering temperature is displayed in Figs. 21 through 26 for the six conditions investigated. The Charpy V-notch impact energies are shown in Figs. 27 and 28, with Fig. 29 showing the transition temperature behavior for the 2.5 cm air cooled 300-M. Tables X through XIII list results.

The oil quenched base line K_{Ic} properties show a peak value at a tempering temperature of 300°C. There is a slight dip at 400°C with recovery up to the spheroidized (650°C temper) condition. The properties for the 300-M structures for the four air cooling treatments show consistent behavior. The as-cooled properties improve with tempering with peak values experienced at 300°C. However, tempering in the 450°C to 470°C range produces a precipitous drop in toughness. This drop is emphasized with double and triple tempering. Recovery of toughness does occur with tempering at 650°C. The recovery becomes more limited with increasing thickness, with the 10 cm and 15 cm thickness material showing brittle fracture characteristics.

0 0 0 0 0 4 7 0 0 4 0 7 8 3 4 5

The 4340 air cooled sample shows behavior similar to the 300-M air cooled material. Improvements with tempering occur up to the spheroidization treatment, where ductile behavior is seen. Only in the 275°C tempering temperature range is there a slight drop in toughness.

Charpy impact behavior is similar to that of the fracture toughness. In particular, peak Charpy energies are found for treatments giving peak K_{Ic} values. The oil quenched and tempered 300-M gives a minimum with a 400°C temper, while all air cooled thicknesses give minimums after tempering at 450°C to 470°C. The air cooled 4340 shows the minimum at the much lower temperature of 275°C. The 10 cm and 15 cm thicknesses mirror the K_{Ic} behavior by showing significant embrittlement with tempering at 650°C. However, the peak values of Charpy energy in the best condition are good, as exemplified by the 30 ft-lb value for 10 cm air cooled material tempered at 300°C.

Transition temperature behavior, which was only studied for the 2.5 cm air cooled 300-M, is shown in Fig. 29. Only the spheroidized structure (tempered at 650°C) exhibits high Charpy energies at low temperatures, typical of high strength material. The tempering treatment with the lowest energies is that one performed at 450°C. At this temperature, using 15 ft-lb as an indicator of ductile brittle transition temperature (DBTT), this treatment leads to a DBTT above 165°C.

D. Fracture Appearance

Fracture appearances of K_{Ic} specimens are displayed in Figs. 30 through 35 for the oil quenched and air cooled 300-M, and for the air

cooled 4340. Figure 30 shows the fracture appearance as a function of tempering for the oil quenched 300-M. While the as-quenched material displays a mixed mode fracture, quasi-cleavage with dimpled regions, the optimum 300°C tempering treatment shows only shallow dimpled rupture. Tempering at 400°C, which leads to a slight fall off in K_{Ic}, develops a mixed mode fracture, intergranular and dimpled rupture. Spheroidization leads to re-development of a dimpled rupture appearance with fine deep dimples, indicative of severe plastic flow prior to failure.

The air cooled fracture appearances are somewhat different. The fracture features are larger in size. The 2.5 cm thick material as show in Fig. 31 exhibits mixed fracture features in the as-cooled and tempered states up through 400°C tempering temperatures. The amount of dimpled rupture increases with tempering, but the quasi-cleavage is still very predominant. Tempering at 450 to 470°C leads to elimination of dimpled rupture with quasi-cleavage as the only fracture feature. This coincides with the large drop in fracture toughness. The 5.0 cm material exhibits similar fracture features to those of the thinner section material (Fig. 32). The amount of dimpled rupture present, particularly after tempering at 300°C, is greater, reflecting the high ductility. The 470°C temper treatment, however, shows the same shift to quasi-cleavage characteristics. Tempering at 650°C led to a ductile fracture appearance.

Figure 33 shows the various surfaces for the 10 cm section air cooled 300-M. The behavior follows that of the thinner sections. The material never exhibits total dimpled rupture. The 650°C treatment does

not, however, lead to any recovery of fracture toughness. This is supported by the cleavage fracture mode observed on the fracture surfaces. The slower cooled material, 15 cm thick, exhibits less dimpled rupture at all tempering ranges, as shown in Fig. 34. Both the 450°C and 650°C treatments show quasi-cleavage (cleavage) modes operative during fracture.

Figure 35 shows only two treatments for the 4340 air cooled material. It shows a shift in mode after tempering in the embrittlement region. The 4340 steel, however, does show ductile fracture appearance in most conditions, particularly after the 650°C temper.

E. Retained Austenite Behavior

Figures 36 through 41 characterize the behavior of the retained austenite for the conditions investigated. Tables VI through IX list results. Magnetic saturation was used to determine the behavior of the austenite. X-ray results were used for spot checking. However, as shown by the behavior with loading, particularly in the as-cooled form, the unstability of the austenite could lead to low X-ray values.

Prior to discussion of each individual condition, it is necessary to discuss the general behavior of the austenite particular to the air cooled structures. Figure 42 shows an example of the stress-strain behavior. The austenite in this form is basically stable to stress, with transformation taking place primarily in the unform elongation region of the stress-strain curve. The uniform elongation region is therefore extended in the conditions which contain large amounts of austenite. Specific behavior for the condition studied now follows.

1. Oil Quenched - 300-M

Figure 36 shows the level of austenite in this condition as a function of tempering temperature and strain. The austenite levels prior to loading, at yield, and after 2% plastic strain are shown. The as-quenched material had approximately 5.5% austenite initially. This initial level decreased slightly with tempering [~2% decomposes] through 400°C. Tempering at 470°C reduced the level significantly to less than 1%. The amount of austenite after varying levels of plastic strain, however, changed drastically with tempering. The as-quenched austenite essentially transformed by yield with none remaining after 2% strain. Tempering at 300°C led to marked changes in behavior; the austenite that remained was much more stable to loading. Approximately 30% of the austenite was still present after 2% plastic strain. However, after the 400°C temper the austenite reverted to the behavior exhibited in the oil quenched condition, was unstable to load, and transformed by 2% strain. The austenite in the 470°C temper had transformed by yield.

2. 2.5 cm Air Cooled - 300-M

The austenite level and stability are characterized in Fig. 37. The initial percentage was significantly higher following the air cooling treatment, approximately 14.5%. Tempering reduced this amount substantially as it did in the quenched and tempered 300-M. Magnetic saturation showed that the level of austenite was less following tempering at 300°C than at 350°C or 400°C. The drop off did not take place at 400°C as it did after oil quenching. Tempering in the 450-470°C range led to a significant reduction in the initial austenite level. Double

0 0 0 0 0 4 7 0 0 7 8 0 7

tempering at up to 400°C also shown, had little effect on the initial austenite level. Double tempering at temperatures above 400°C, however, led to a large reduction in the austenite present. The effect of loading is also shown in Fig. 37. In the as-cooled condition there was a substantial amount of transformation with load after 2% plastic strain, essentially a 60% reduction in level. This was consistent with the behavior of the oil quenched material. Following tempering in the 300-400°C range, the remaining austenite was more stable to load. The absolute level as well as the percentage transforming was significantly different from the as-cooled austenite. Tempering in the 425-470°C range, however, reversed this trend. The austenite lost its stability to loading and after the 470°C treatment it was, essentially, fully transformed after 2% strain. Double tempering seemed to affect only the initial levels, with the amount transforming with the first increment of strain basically constant.

3. 5.0 cm Air Cool - 300-M

Figure 38 shows the behavior for the microstructure developed through air cooling a 5.0 cm thick slab. The initial austenite level was higher than either of the other two conditions discussed with the initial level approximately 17.5%. Tempering in the 300°C to 450°C temperature range led to a decrease in the austenite level from that of the as-cooled material. The same behavior, as observed in the 2.5 cm material, was observed in the 300 to 400°C range where the austenite level was lower with lower tempering temperature. Higher temperatures

of tempering [> 400°C] led to a significant decomposition of the austenite with only 8% austenite retained after a one hour temper at 470°C.

The stability of the austenite with loading is shown as well. The behavior is similar to the previous treatments. However, the as-cooled stability while lower than that of the austenite conditioned by tempering was more stable than the austenite found in the oil quenched and 2.5 cm air cooled material prior to tempering. The stability was maximized in the 300-400°C tempering temperature regime. Instability to load set in again after tempering between 425° and 470°C with 2% strain eliminating all austenite after the highest tempering temperature. Double tempering led to behavior similar to that found in the thinner section. It reduced the initial austenite level in the unstable regime (425-470°C). However the austenite behavior with strain, specifically the absolute amount of austenite transforming with strain, was constant. Figure 43 compares the behavior for the 400° and 470°C temper conditions of this 5.0 cm section. The slope of the line representing the austenite level serves as a good measure of the austenite stability as a function of strain. The decomposition rate is much greater after tempering at 470°C. This leads to a higher work hardening rate, as expected, when austenite transforms to martensite. Table XIV shows the levels of austenite present for the 5.0 cm thick material as determined with X-rays for several conditions of interest. The levels correlate well with the magnetic saturation levels. The table also shows the lattice parameter for the austenite peaks of interest. There seems to be a decrease in a_o

0 0 0 0 0 4 7 0 0 7 0 4 3

after tempering in the 470°C range, implying the formation of carbides concurrent with the decrease in austenite stability.

4. 10 cm and 15 cm Air Cool - 300-M

Figures 39 and 40 show the austenite levels and austenite behavior for these two thicknesses. The initial levels in the as-cooled conditions were essentially the same, approximately 29%. The levels present after tempering in the 300°C to 400°C range were similar to other treatments with decomposition more rapid at lower temperatures, leading to higher austenite levels after the 400°C temper. Then, as with the other treatments, the austenite level fell off at 450°C, particularly sharply in the 10 cm thick material. The stability of the austenite was high in the 300°-400°C range with lower stability in both the as-cooled and 450°C temper conditions. However, the as-cooled instability was less pronounced than for the thinner air cooled sections.

5. 2.5 cm Air Cool - 4340

In an attempt to understand the role of silicon on the austenite level and stability, the austenite behavior was also explored in this steel. Figure 41 shows the behavior of the austenite, as a function of tempering temperature. The retained austenite level was significantly below that of the counterpart treatment in the 300-M, 4.5% compared with 14.5%. The level of austenite was essentially unchanged with tempering at 200°C. However, tempering at 275°C led to a drastic decrease in the austenite level, with even higher treatments leading to total decomposition. The behavior of the austenite when subjected to a load was similar in both the as-cooled and 200°C temper conditions

with all the austenite transforming with 2% strain. The austenite level decreased following tempering at 275°C and was essentially eliminated by yield.

F. Microstructure Characterization

1. Optical Metallography

Figures 44 through 49 characterize the basic microstructural features of the treatments of interest.

a. Oil quenched - 300-M. Figure 44 shows the microstructural features of the as-quenched, 470°C temper, and 650°C temper conditions. The as-quenched sample is typically martensitic with no discernable transformation products present in some alloys with lower hardenability. The 470°C temper shows the structure beyond the normal use range. The attack is heavy revealing the formation of carbides throughout the microstructure. Finally, the 650°C temper shows the typical spheroidized structure, containing fine, uniform carbides.

b. 2.5 cm air cool - 300-M. The as-cooled, double tempered at 450°C, and 650°C temper microstructures are displayed in Fig. 45. The as-cooled microstructure is bainitic in general appearance. The transformation temperature, however, indicates that the structure must also contain significant levels of martensite. The double tempered microstructure shows a characteristic carbide-containing morphology. It is also noteworthy that the etchant reveals accentuated boundary attack implying significant carbide precipitation. The 650°C temper shows a much coarser structure than that shown by the oil quenched material tempered at the same temperature. However, all areas show

evidence of uniform carbide precipitation.

c. 5.0 cm air cool - 300-M. Figure 46 shows the as-cooled, 300°C, and 470°C temper treatments. The as-cooled structure is again typically bainitic [lower] with feature sizes larger than those observed in the thinner section. The structure tempered at 300°C still retains the basic microstructural features with some boundary enhancement. The 470°C temper is now very similar to the 2.5 cm air cool material with boundary precipitation. Although not displayed, the 650°C temper also shows microstructural features similar to the thinner section; i.e., more pronounced features.

d. 10 cm air cool - 300-M. Figure 47 depicts optically the microstructural features of the as-cooled, 300°C temper, 450°C temper, and 650°C temper treatments. The as-cooled structure is a bainitic structure, more characteristically formed at higher temperatures (350°C to 450°C range). There appear to be possible areas of ferrite, characteristically light etching. The 300°C treatment lead to structures more typically bainitic in appearance, while the 470°C temper shows distinct grain boundary attack suggesting extensive precipitation. This boundary accentuation remains even after tempering at 650°C. The microstructure is much more non-uniform than that exhibited by the oil quenched material given the same tempering treatment.

e. 15 cm air cool - 300-M. The microstructure for the as-cooled structure and the 450°C temper treatment are displayed in Fig. 48. The slow cooling rate experienced by this material developed a microstructure that, optically, shows little change with post-cooling treatment.

The structures are bainite. There also appear to be areas of ferrite, as with the 10 cm thick section material. Carbide precipitation is present in both the as-cooled and tempered structures.

f. 2.5 cm air cool - 4340. The as-cooled and spheroidized conditions are shown by Fig. 49. The as-cooled structure is significantly different from that of the 2.5 cm thick, air cooled 300-M. Considerable carbide formation seems to have occurred during the initial heat treatment. There are also areas of ferrite in the as-cooled microstructure. Little change in optical appearance takes place with tempering. The 650°C tempering treatment does not produce homogeneously distributed carbides throughout the structure.

2. Transmission Electron Microscopy

A necessary part of an adequate characterization of the complex microstructures is transmission electron microscopy. Figures 50 and 51 characterize the oil quenched 300-M microstructures, while Figs. 52 through 57 characterize the air-cooled 300-M microstructures of different thicknesses. Finally, Figs. 58 through 61 characterize the microstructural features developed in selected conditions after tempering. All micrographs will be discussed in further detail in the following section to explain microstructure-property relationships. Conventional methods of indexing[18] were used to identify various phases where possible. In most cases where both austenite and ferrite phases were present the phases exhibited the Kurdjumov-Sachs relationship[19] with $[111]_{\alpha} \parallel [110]_{\gamma}$.

0 0 0 0 9 7 0 9 7 8 5 0

IV. DISCUSSION

Having presented the basic data and figures, it is now necessary to present a coherent discussion of the factors that influence the specific properties and general behavior of the slow cooled material.

A. Transformation Characteristics

1. Continuous Cooling Behavior

Although the majority of attention in high strength steels has been focused on the rapid cooling treatments that lead to fully martensitic structures, there has been interest in the thick section microstructures which necessarily are not fully martensitic. There has been much interest in the area of using TTT diagram information to construct continuous cooling transformation (CCT) diagrams.[20,21] These attempts are based on the assumptions that (1) the amount of nucleation for transformation on a continuous cooling path is never greater than the isothermal nucleation rate, and (2) the amount of transformation is to a first approximation the amount transformed at an average temperature for that time. These assumptions lead to CCT diagrams which are shifted to the right and down from standard TTT diagrams. These assumptions apply to all materials. A comparison of diagrams for 300-M and 4340 (TTT with CCT), shows these assumptions to be valid. The assumptions apply particularly well to the pearlite transformations. However, typical additions to highly hardenable low alloy high strength steels effect bainite transformations to a much

smaller degree. Therefore, continuous cooling can lead to predominantly bainitic microstructures. The effect of elemental additions on continuous cooling behavior must be evaluated in all regions. The primary additions common to 4340 and 300-M are nickel, chromium, and molybdenum. These elements retard pearlite formation.[22,23] Isothermal transformtion studies have shown that the levels found in 4340 yield adequate pearlite hardenability. The bainite transformations start, isothermally, more rapidly (~15 seconds as compared with 250 seconds) than do pealite transformations. Continuous cooling behavior has been shown to be analogous using primary end quench methods.[24] The bainite reaction in continuous cooling processes start if cooling to ~400°C is not achieved in around 25 seconds. Therefore 4340 cooled in any significant section size will contain some bainite.

The elemental additions which distinguish 300-M from 4340 are approximately 1.4 wt% silicon, 0.1 wt% vanadium, and 0.2 wt% additional molybdenum. Both vanadium and molybdenum are strong carbide formers and retard pearlite formation. The addition of silicon has been shown to have a strong influence on the bainite transformation by Babu.[25] He found that silicon additions retarded the bainite incubation time slightly, particularly in the 350°C to 400°C range. The transformation kinetics were more drastically affected, with the time for completion significantly lengthened. In many cases, the reactions were found to be stabilized short of completion. Isothermal studies using metallographic techniques are not as conclusive. However, continuous cooling work does point out the effectiveness of the additions to 4340 in

0 00 01 00 04 47 70 04 07 84 54 1

altering bainite transformations, and therefore the hardenability. Yuen's data[13] as well as published data[26] support this change in CCT behavior. Hardness levels are high, also indicating that the transformations take place at lower temperatures. The transformation behavior derived from the air cooling processes is not in agreement with Yuen's findings. The magnetic technique used by Yuen was difficult to calibrate, leading to unusually high estimates of retained austenite levels. Yuen also found a discontinuity in the transformation levels in the region where the microstructure changed from a "lower bainite" - martensite mixture to an "upper bainite" morphology. This was found to be much less pronounced using dilatometric techniques, showing a continuous change in behavior. The levels of retained austenite found in slow cooling treatments using X-ray and magnetic saturation techniques while not as high as those estimates made by Yuen, were nonetheless very substantial. Silicon, therefore, seems to be the major factor leading to these changes in structure with slow cooling.

2. As-cooled Structure

The as-cooled microstructures found in 300-M through continuous (slow) cooling can be divided into three classes: martensitic, martensitic-bainitic, and bainitic. The oil quenched (untempered) material is fully martensitic with ~5% retained austenite. An optical micrograph of this structure is shown in Fig. 44 indicating typical medium carbon martensite appearance. Transmission electron microscopy (TEM) can give a better evaluation of the microstructural features present. Figure 50 shows the typical lath structure with retained

austenite films present between the laths. The laths themselves show heavy dislocation tangles. Figure 51 shows one different area of a large lath. There appear to be some internal precipitation; too fine, however, to lead to any diffraction spots. Again, boundary films of austenite appear to be present. There also appear to be selected areas of twinned martensite, as expected for the high carbon content. More extensive twinning was seen in adjoining areas. This morphology has been seen before in similar steels.[27-28] The amount of twinning does, however, seem to be present to a greater extent than in oil quenched 4340.

Slower cooling rates produce distinctly different microstructures as revealed by optical metallography discussed earlier. The 2.5 cm thick air cooled material and the 5.0 cm air cooled material show similar microstructural features optically with both having characteristic bainite microstructures. Transmission electron microscopy is able to reveal more about the structure. Figure 52 shows the mixed microstructure that is present in the 2.5 cm air cooled material along with significant amounts of retained austenite, as indicated by dark field imaging. The austenite is clearly interlath in character with varying width. The austenite is at times surrounded by bainitic ferrite indicating that the ferrite really has a packet structure consisting of several laths close in orientation. Figure 53 shows austenite of slightly different morphology. The austenite is wavy in nature as seen earlier by Huang[29] in an isothermally transformed bainite formed in a silicon steel. The bright field shows evidence of internal

0000100044770040784552

precipitation as well as martensite laths between the bainite, which are twinned and thus exemplify the mixed morphology present.

The microstructure of the 5.0 cm air cooled 300-M is similar to that of the thinner section material. It also contains a significant amount of retained austenite as shown by dark field analysis. The austenite is perhaps more extensive as would be expected. Figure 54 shows TEM of different areas at the same magnification as in Fig. 53. The austenite laths are longer and thicker indicating that the transformation had longer time for carbon segregation. There appears to be little internal precipitation in the laths which contain austenite. The austenite has a wavy morphology as seen in the 2.5 cm thick material. The structures from both continuous cooling treatments have microstructures that strongly resemble the isothermal structures in a silicon steel characterized by Huang.[29] He found similar ferrite-austenite mixtures after isothermal transformation at 315°C, and was able in certain locations to resolve carbide films in conjunction with the austenite, which had the same wavy morphology.

The structures formed through cooling at the slower rates (<0.15 °C/sec), corresponding to 10 cm air cool and 15 cm air cool material, do not show the same differences in transmission micrographs as are seen in optical micrographs. The thick plates of austenite are shown in Fig. 55 for the 10 cm slab. The austenite is extensive as verified by magnetic saturation and X-ray results. Figure 55 shows that the austenite has the same morphology as seen before. The ferrite has an appearance that is similar to that seen in the higher isothermal

treatments.[29] Figure 56a shows another area of the as-cooled structure. Again, stringer-type austenite is extensively found, with little evidence of extensive carbide precipitation. The 15 cm air cooled structure is shown in Fig. 57. The plates of retained austenite are characteristically seen as long, thick films and imaged in dark field. Figure 56b show another region where the austenite morphology resembles that found in more rapidly cooled structures. There is evidence of twinned structures present, although not extensively seen. The microstructures support the conclusion that the structures are complex and that different morphologies are associated with the various transformation temperatures.

The microstructures found in the air cooled 4340 are markedly different. The retained austenite level is very similar to that of the oil quenched 300-M, containing approximately 4%. There are fewer ferrite-austenite regions as found in the slow cooled 300-M. Substantial carbide precipitation has occurred. The optical micrographs also reveal significant ferrite which would partially account for the lower strength.

3. Tempering Transformation

The tempering behavior of 300-M is interesting. It has been well established that the addition of silicon to hardenable steels can significantly influence the tempering behavior.[10,30-32] Tempering of martensitic steels can be divided into the following four stages:[33-35] (1) the formation of ε-carbide, (2) the decomposition of retained austenite, (3) the formation of cementite, and finally (4) secondary

0000000447700407845 63

hardening. These stages can overlap and at times are changed in order with temperature ranges subject to composition. Secondary hardening is usually associated only with steels having appreciable levels of alloy carbide formers. Silicon has been shown to have the largest effect on the tempering response of ultrahigh strength low alloy steels. In particular, it has been found that silicon extends the range over which ε-carbide is stable and retards the decomposition of retained austenite. Owen[31] has suggested that silicon is rejected by the carbides, leading to a buildup of silicon and thereby increasing the carbon activity surrounding the particle. This leads to a significant reduction in the carbide growth rate. Reisdorf[32] has suggested that ε-carbide is actually an iron-silicon carbide. With this background, a discussion of the tempering behavior of the oil quenched material and of the tempered (or thermally conditioned) slow cooled 300-M is in order.

The 300-M material in the oil quenched condition exhibits tempering behavior similar to other silicon-containing high strength steels. Tempering at 300°C leads to a structure that still contains retained austenite while having extensive amounts of carbide, as demonstrated by the microstructure displayed by Fig. 58a. Others have shown that ε-carbide is present in this steel after a 300°C treatment.[36] This structure is similar to the oil quenched structure. The retained austenite has not decomposed at 300°C, the normal tempering temperature. Tempering at higher temperatures, 400°C to 470°C, leads to the decomposition of the retained austenite; this decomposition is

concurrent with the occurrance of cementite in the microstructures.[37] Figure 58b shows carbide precipitation at the lath boundaries after tempering at 470°C.

The tempering process in the other air cooled conditions is analogous to the process in the oil quenched 300-M. However, there is progressively less and less effect on the structure with tempering up to 400°C as the cooling rates become slower (equivalent to thicker slabs.) Tempering at temperatures below the transformation temperature does not seem to influence the microstructure significantly. There are, however, subtle differences which are observed between the behavior of the various slab thicknesses. The 2.5 cm air cooled material does show a significant change in yield strength with little change in ultimate strength with tempering. This is probably due to (1) the formation of additional ε-carbide from the martensite formed at lower temperatures, and (2) the transformation of high carbon austenite to martensite. Although no microscopy was performed on the material tempered at 300°C, magnetic saturation showed significant austenite present which was highly stabilized. The features of the material tempered at 470°C, a temperature where austenite was unstable, were examined. Transmission electron microscopy revealed that the microstructure had changed. There were internal carbides present, taking on the same morphology as the austenite had in the as-cooled condition.

The characterization of 5.0 cm air cooled 300-M is the most complete. The 300°C tempered condition was examined first. This treatment led to good strength-toughness properties. Figure 59 shows

0 00 00 0 04 7 70 01 0 04 57 4

the austenite which is present in large amounts (~15%). The austenite retains the same structure as that present in the as-cooled material. This is to be expected since little transformation takes place below this temperature, as shown by dilatometry. Tempering at 470°C, however, leads to different morphologies and different properties. Figure 60 shows retained austenite that is still present in the structure. The diffraction pattern indicates a $(\bar{2}10)$ orientation of cementite present with the austenite and ferrite orientations. Figure 61 shows a different area that does not contain austenite. The morphology of the carbide structures is similar to the austenite seen in the as-cooled material and in other silicon steels by Huang.[29] These films are not continuous implying that the carbide has precipitated during decomposition of the austenite.

The tempering response of the other slow cooled structures have not been characterized. However, from evaluation of tensile properties and retained austenite properties, their behavior would be similar with tempering up to 400°C.

Although no conclusive electron microscopy was performed in the tempered structures of the air cooled 4340, its tempering response fits the classical response of non-silicon containing ultrahigh strength steels. The three stages of tempering do take place in the conventional temperature ranges. Morphology of carbides in the as-cooled structures imply, however, that cementite might have formed on slow cooling. This would possibly eliminate the significant amounts of epsilon-carbide formation and imply that cementite formation would

follow directly from the retained austenite decomposition.

4. Austenite Behavior

Because the retained austenite content and its behavior are directly related to any thermal conditioning or tempering which follows the cooling process, these effects are discussed in detail. The behavior of retained austenite in ultrahigh strength steels has been treated thoroughly in the literature, particularly by Cohen and his co-workers.[38-40] In many instances the work was performed in higher carbon steels in order to achieve a significantly high level of austenite in the as-quenched condition. Others have also looked at the effect in 4340 type steels, noting that the austenite remained even after low temperature tempering.[30] Attention has been paid to the method of transformation of the austenite on cooling (continuous vs. isothermal) in certain steels.[11] Finally, significant work has been performed in an attempt to understand the level and effect on properties of austenite retained in highly alloyed steels.[41-45]

In the 300-M steel, the austenite retained shows significant stability after tempering at temperatures through 400°C and re-cooling to room temperature. In the quenched and tempered 300-M, a certain amount decomposes with low temperature tempering, leaving austenite that is stable up to thermal treatments as high as 400°C. Air cooling processes lead to a larger amount of austenite, as discussed earlier, which exhibits a different response to thermal treatment. Some small level is unstable with any tempering. However, a larger amount is retained following a 400°C temper compared to a 300°C temper (seen in

0 0 0 0 0 7 0 0 0 0 8 5

Figs. 37-40). It has been seen by other investigators[46,47] that the decomposition kinetics of the retained austenite on tempering follow those of the decomposition kinetics of the original austenite in the quenching (cooling) process. The behavior of 300-M should follow the behavior exhibited by the TTT diagrams for the silicon modified 4340 as seen by Babu.[25] Dilatometry substantiated this by showing less length change after tempering at 400°C than shown at 300°C. Material cooled at several decreased rates, representative of different air cooled thicknesses, all showed this same behavior. The stability of the initial austenite increased, however, with decreased cooling rate. This was most likely attributable to the increased time for carbon enrichment to take place during initial cooling.

B. Mechanical Behavior

The strength and fracture properties have been investigated in a variety of ultrahigh strength steels over many years. There have been two primary approaches to research in these steels. Efforts have been made to look at (1) the influence of composition on properties and at (2) the influence of novel heat treatments on properties in unmodified commercial steels. Alloy modifications have been used extensively to improved the medium carbon low alloy steels that were present well before the Second World War, i.e. 4130. The primary aim was to increase hardenability through alloy additions as well as to increase strength through solid solution hardening. Primary additions were small amounts of nickel, molybdenum, vanadium, and silicon.[4,48-50]

Efforts to develop alloys with improved properties in large sections with substantial amounts of additional nickel and chromium were also undertaken for specialized applications.[51] Recent interest has centered around controlling impurity levels in these steels.[1,52] It has been shown that sulfur and phosphorus influence the fracture properties as well as the transverse ductility. Therefore, investigative work has been performed on determining the influence of melting practice on these properties.[53,54]

The other approach to alloy design has been to select a heat treatment procedure to achieve desirable microstructural constituents or eliminate undesirable ones. Goolsby, Wood, and others[5,7,55] looked extensively at the role of austenitizing treatments on the fracture initiation properties of commercial steels as well as of developmental steels. They were able to show marked changes in properties by changing the prior austenite grain size as well as the undissolved carbide distribution. Fracture toughness increases of 50% were seen with little change in yield strength but with large decreases in ductility, e.g. reduction in area.

Beginning with Davenport,[56] many[57] have looked at the properties associated with bainitic structures, formed either by isothermal treatment or continuous cooling at rates slower than oil quenching. They found that optimum properties were achieved with treatments in specific transformation regimes. Other efforts have been made to investigate ausforming, martempering, and multiple austenization treatments in an attempt to improve properties.[58] Recently,

0 0 0 0 0 4 7 0 0 4 0 7 8 1 5 9 6

investigations have also concentrated on analyzing the microstructural constituents in detail in these high strength alloys. The goal of all research has been to develop microstructures that lead to better properties than exhibited by commercial steels after conventional treatments.

Some attention has been directed as well toward the properties of continuously cooled steels with heavy section applications. It has been documented that air cooled material does not have as good properties as does rapidly quenched material.[56] It has often been felt that the mixed microstructures present in thick section are not desirable. However, there is no way to avoid a range of transformation temperatures and corresponding range of structures in a part of any significant size.

The primary work toward achieving acceptable fracture properties has been directed toward bainitic steels which avoid pearlite formation. This can be accomplished with very small additions of boron which deter ferrite formation.[57,59] The bainitic transformations, however, do take place at high temperatures leading to low tensile properties. Efforts have been made to evaluate slow cooled conventional steels. Vadja, Hauser and Wells[11] looked at the effect of silicon on a 4340 type steel in end-quenched round bars to determine its influence on properties. This study and others pointed out qualitatively the large effect silicon additions have on transformation behavior and tensile properties.

A study of microstructures formed by slow cooling processes has a wide range of application, particularly in the manufacture of large

high strength parts. Silicon influences as-cooled properties as well as tempered properties through its significant solid solution strengthening as shown by Leslie,[60] and through its significant influence on carbide morphology as shown by Owen and others.[10,31]

Before discussing the specific properties of the air cooled 300-M, it is necessary to discuss the base line quenched and tempered properties to ascertain the role of the silicon. Wood and others[7,16,17] found the ultimate strength to be substantially higher than that of 4340 particularly after tempering at 300°C. This can be attributed primarily to the silicon additions and has presently been seen by Bhat[3] in other modified steels. The fracture properties of 300-M are not significantly different from the unmodified 4340. Both steels, when considered at equal strength levels out side the embrittling tempering regions, have similar properties.

The temperature range associated with tempered martensite embrittlement (TME), to be discussed later, is well documented to be 260°C to 315°C for 4340. This has been seen by Anctil and Kula[61] and others.[62] For 300-M, the slight minimum in toughness indicative of tempered martensitic embrittlement (TME) is shifted to the 400°C temper treatment. This toughness drop has been attributed, classically, to the dissolution of ε-carbide and concurrent precipitation of cementite.[63] Silicon as well as small additions of secondary hardening elements molybdenum and vanadium, have been recently used in other steel development because of their effects on strength and on tempering characteristics.[49]

The role of silicon on properties is emphasized by considering the air cooled properties of 300-M. First, the differences between 2.5 cm air cooled 300-M and 4340 emphasize its dramatic effects as an alloying addition. The microstructures, seen optically, are totally different. This is reflected in the tremendous differences in tensile properties. There are little strength differences (~20%) between the conventionally treated 300-M and the air cooled 300-M even though there is a one hundred fold difference in cooling rate which leads to bainitic structures. The 4340, however, shows a 40% decrease in UTS with this cooling rate change. Yuen's data indicates significant transformation differences for the 4340, leading to upper bainite in the slow cooled 4340. The 300-M, however, shows a very flat response to cooling rate. In comparing the properties, it can be seen that both air cooled steels exhibit similar fracture toughness behavior after low and high tempering temperature treatments with the spheroidized structure leading to very tough structures. There is an embrittlement regime for each steel. This regime occurs at a much higher temperature and is much more substantial for the 300-M.

The primary emphasis, however, was to investigate the properties that various section thicknesses would have in air cooled 300-M alone because of the variation in retained austenite levels. The yield strength is almost a linear function of austenite content. Work on cold rolled, slow cooled 300-M showed that the elimination of the austenite led to a linear increase in yield properties. The elongation is directly linked to the retained austenite in that great improvements

in properties were seen when the amount of austenite increased. The air cooled 4340 does not have the elongation of 300-M of similar yield [16% vs. 11.5%]. The reduction in areas are the same, establishing that the difference is in uniform elongation. The enhancement of elongation with retention of metastable austenite has been seen in the limiting case of TRIP steels where proper adjustment of composition and deformation led to tremendous increases in uniform elongation due to the austenite transformation characteristics.[64]

This improvement in per cent elongation is enhanced by tempering, which stabilizes the retained austenite with respect to load, allowing it to transform at only the appropriate strain. Elongations of 21 to 27% are seen in the 400°C temper in the 10 cm and 15 cm thick material. The elongations seen in the spheroidized condition do not match the levels of the air cooled condition irrespective of tempering treatment.

Although the yield strength behavior is directly related to cooling rate after low temperature tempering, the 5, 10, and 15 cm thick microstructures show increasing levels of secondary hardening in the 450°C to 550°C temper range, leading to an increase in the ultimate tensile strength. The secondary hardening is associated with the temperature range where the austenite stability changes drastically. The drop in yield strength at 450°C seems indicative of a stress-induced transformation. Cohen[38] has reported this type of drop in yield strength in high carbon steels exhibiting these transformations. The increased ultimate strength is indicative of the high hardness martensite that results from the transformation. This leads to composite

properties for the bainite-martensite material. The 550°C temper shows analogous behavior. The UTS and yield strength are higher than at 450°C, implying the presence of martensite, but absence, to a degree, of stress-induced transformation. It implies that the isothermal decomposition of the austenite during tempering was slow. However, destabilization occurred, allowing the austenite to transform to martensite upon cooling. Concurrent with this increase in UTS, there are both a drop in reduction in area and in elongation. This would be expected with large amounts of martensite present, giving the material characteristics of the untempered condition.

The fracture behavior of the air cooled material shows very distinct characteristics. The 2.5 cm air cooled 300-M has increased fracture toughness over the oil quenched material. The transformation characteristics of these two conditions are very similar even though there are distinct microstructural differences. The air cooled material shows a recovery of toughness with tempering. This improvement is evident with tempering up to 400°C. The air cooled material still has good fracture toughness at this temperature, where the oil quenched material shows a fracture toughness trough. However, higher temperature tempering, 450°C to 470°C, yields a much more significant drop in the toughness, from 60 ksi-in$^{1/2}$ to 40 ksi-in$^{1/2}$. This degradation is much more severe than the 5 ksi-in$^{1/2}$ drop exhibited in the quenched and tempered steel at 400°C. The Charpy data follow the K_{Ic} data for both treatments. The behavior of the 5 cm, 10 cm, and 15 cm air cooled material show somewhat different responses in the 300°C to 400°C range

with slight degradation in two cases with tempering above 300°C. The peak properties, however, do invariably occur in the 300°C temper condition. All these air cooled conditions do show as well tremendous degradation of toughness with tempering in the 450-470°C range. This degradation is very severe, with toughness always dropping to approximately 40 ksi-in$^{1/2}$. This degradation takes place over only 50°C in the tempering range. With the thicker sections, the drop is more dramatic. The Charpy energies also follow this trend with large drops after 450-470°C tempering. This behavior appears to be an enhanced tempered martensite embrittlement phenomenon.

Tempered martensite embrittlement has generally been associated with a drop in room temperature Charpy energy after tempering ultra-high strength low alloy steels in the 260°C to 350°C range.[65,66] While this association has been observed in notched tensile tests and torsion tests, the phenomenon is not always seen in K_{Ic} tests.[1,67] Plateau behavior in the embrittlement range is seen implying possibly some degradation. Anctil and Kula[61] were able to see it only in K_{Ic} tests at low temperatures. The mechanism for this embrittlement has not clearly been established. Initially, it was held that retained austenite might be at least partially responsible. However, metallographic evidence by Grossman seemed to dispell this.[65] Castleman, Averbach and Cohen[39] also showed that reducing retained austenite levels in quenched and tempered steel through refrigeration did not eliminate the Charpy energy trough. Lement, et al Baker, and Lui[1,68,69] attributed the drop in toughness to precipitation of lath boundary films of

0 00 0 0 04 7 70 01 0 85 29

cementite. Goolsby[55] was able to show this boundary precipitation with dark field analysis in a secondary hardening steel. However, earlier work by Capus[70] has shown that impurity elements seemed to influence this trough, and that elimination of these impurities eliminated any drop. The influence of silicon on retarding embrittlement to higher temperatures, however, substantiates the hypothesis that carbide precipitation at boundaries is the primary contributor to the embrittlement. The carbide theory does not always directly fit with the evidence of some prior austenite grain boundary failure in the embrittling region.

The embrittlement phenomenon seen in the air cooled 300-M is much more severe than that reported in the literature for quenched and tempered steel. The embrittlement, however, does appear at temperatures well below the temperatures for temper embrittlement (540°C), presently linked strongly with impurity segregation, and shown to be reversible.[71] The deep trough observed does coincide strongly with the change in austenite stability. This change appears consistently in the air cooled 300-M for all simulated thicknesses as does the fracture toughness drop. The Charpy energy, normally the most reliable measure, definitely shows the drop, as does the elongation and reduction in area for the thicker slab structures. These structures also contain much larger amounts of retained austenite. The fracture mode that is observed, however, does not show any clear evidence of grain boundary failure, with severe lath cleavage apparently the only mode. In these air cooled steels, it is seen that tempered martensite embrittlement (TME)

is exaggerated by the presence of 10-25% retained austenite. The retained austenite in the destabilized form transforms with stress to martensite, probably high in carbon. If this were the cause for the undesirable properties, double tempering, which eliminates some of the austenite, would also eliminate some of the degradation. In fact, it was seen in the 2.5 cm and 5.0 cm condition that this increased the embrittlement. Therefore it must be concluded that the retained austenite is destabilized through the precipitation of carbide at its austenite-ferrite interface. Table XIV gives an indication how the austenite lattice parameter changes with tempering temperature for different cooling treatments. It can be seen that with slow cooling rates there is partitioning of the carbon to the austenite. It can also be seen that destabilization is accompanied by a decrease in austenite lattice parameter implying a decrease in carbon content, and formation of carbide films. Huang[29] was able to show carbide films in a similar silicon steel. Transmission electron microscopy of the 300-M in cooled steels showed cementite structure with similar morphology to austenite. These long stringers would degrade fracture properties. If this behavior was indeed an exaggerated TME, it would be expected that similar austenite behavior would be seen in the quenched and tempered steel and in the air cooled 4340 since they contained austenite. Indeed, the embrittlement phenomenon occurs at the temperature range where the austenite is unstable. These temperatures are much different, 400°C for the quenched and tempered 300-M and 275°C for the air cooled 4340. Because of the small austenite level, however,

the effect is much smaller. Also, in the quenched and tempered 300-M, the austenite carbon level is initially lower, perhaps, accounting for the earlier destabilization. The main argument disproving the role of retained austenite in the embrittlement is the work by Castleman et al.[39] However, the morphology of the retained austenite was not known then. It seems possibly that the austenite that remained after refrigeration were the lath films which still could cause limited embrittlement. The air cooled 4340 also shows a destabilization of austenite after the embrittlement process. Previous investigators, although aware of the austenite level, were not aware of the austenite's characteristics.

This does not account for all the aspects of embrittlement in the quenched and tempered steel, in particular the grain boundary fracture. However, it does re-link austenite to embrittlement in these steels. Purity, while shown to eliminate the effect in other steels, can not really be evaluated. These steels are as pure as can be commercially manufactured. Therefore, the embrittlement phenomenon must be dealt with in real materials.

The air cooled steels do show other interesting features. For the steels showing moderate levels of austenite (5 to 17%) there is a recovery of properties in the spheroidized condition. However, this does not happen in the slower cooled steels. The fracture properties never recover and, in fact, show cleavage morphology. These steels exhibit an upper bainite structure with ferrite-austenite mixtures prevalent after primary cooling. Following high temperature tempering, the structure would degrade to the other microstructure, containing

stringer-like carbides. These carbides apparently do not spheroidize with normal high temperature tempering schedules. Higher temperatures or longer times must be necessary for spheroidization. The silicon, however, must slow growth even at these temperatures.

The total role of retained austenite on mechanical properties in ultra-high strength steels has been addressed by many investigators recently in their attempts to quantitatively access mixed microstructures. Webster[41] showed that retained austenite seemed to improve fracture toughness properties of martensitic stainless steels. Jin, et al.,[44] as well as Pampillo and Paxton,[42] have shown that the role of retained austenite is ambiguous in maraging type steels. It has been established, however, that austenite can be conditioned to give unique elongation and fracture properties in TRIP steels through its transformation properties by Fahr, Gerberich, Bhandarkar, Parker, Zackay, and others.[64,72,73] Finally, Lai, Rao, and others[2,8,9] have found that retained austenite is associated with higher fracture toughness values in ultra-high strength steels. This association with good properties does not imply that retained austenite has been unequivocally shown to be good. In the low alloy steels carbon partitioning to the austenite could lead to a much less tough austenite than found in TRIP steels. The present results provide an answer to the previously undetermined role of the austenite.

First, in quenched steels austenite seems to have little benefit. Even when stable it is still transformed after strain levels of 2-4%. This is significantly less strain than would be seen in front of a

crack tip in a fracture toughness test. When the austenite is unstable, the fracture properties of the material are deteriorated by the formation of the untempered martensite with stress or by the presence of carbide films formed during austenite destabilization. In the stable form, the austenite films replace carbide networks that provide a continuous crack path.

For the slow cooled structures, the austenite is present in larger amounts, leading to easier assessment of its role on properties. The austenite does improve the elongation properties. In its stable form, it is an integral part of a microstructure that exhibits good properties. When unstable, as with tempering above 400°C, the austenite destabilization is linked directly with carbide film formation, and severe degradation of fracture properties. The alloy additions to 300-M, particularly silicon, which lead to austenite retention also lead to higher strength levels through the retardation of pearlite formation and substantial solid solution hardening.

The investigation of air cooled thick section properties leads to another interesting phenomenon. This is the behavior exhibited by the material given a 650°C post cooling temper. Universally, this is expected to lead to normalization of properties, regardless of the prior microstructure. It is seen in lower strength pressure vessel steels that it is common practice to use this temper to equalize microstructure in spray quenched section of up to 12 in. thick, where the microstructure varies from martensite at the edge to upper bainite or pearlite in the center. The properties exhibited by the

as-cooled 300-M steel, however, show that the assumption of immediate normalization is not always true. It is seen that the yield properties change very little while fracture properties change significantly. The 2.5 cm material exhibits ductile properties characterized by a dimpled rupture fracture while the 15 cm air cooled material exhibits cleavage failure. The properties seem to be cooling path-dependent in the silicon modified steel. The large amount of austenite present in the thicker material, which experienced slower cooling, seem to lead to large cleavage facets attributable to a distribution of carbide plates. These features remain even after a 650°C temper. This result indicates that alloy additions can influence spheroidization processes indirectly through the initial microstructure present, or directly through their effect on diffusion or growth processes.

C. Thick Section Steel Evaluation

Besides evaluating the role of retained austenite on the thick section properties, it is also instructive to discuss (1) the method used to perform exploratory research on thick section, continuously cooled material, (2) the thick section properties of the steel itself, and (3) the methods of evaluating fracture properties. First, with today's needs for thicker structure sections, e.g. in pressure vessels, it will be necessary to evaluate higher strength materials for thick section application. The method of using simulated cooling paths is the only viable method of looking at composition effects. This method

also allows the evaluation of unusual heat treatments. The numerical approach used was necessary with high strength steels which transform at lower temperatures, giving off substantial latent heat. The method must not only rely on matching the rate in the higher temperature range, but also matching it in the low temperature region where transformation takes place. The use of simulation has been performed using insulated boxes to produce cooling rates similar to the center of thick slabs.[74] However, the region of good match is limited. Therefore it is necessary to control the cooling medium. The specimens used for the study, although cooled separately, did lead to consistent properties in post cooling treatment as well as from thickness to thickness, again substantiating the premise that the properties are a function of microstructure which in turn is only a function of cooling history.

To evaluate the properties of the steel for thick section applications it is necessary to concentrate on tempering levels below 425°C, the region below any tempering process which will lead to embrittlement. Figure 62 shows the normalized yield strength and fracture toughness plotted as a function of cooling rate. This comparison is for the 300-M having been tempered at 300°C following cooling, which led to the best properties for all treatments. The steel shows the normal trend of increased fracture toughness with decreased yield strength. This trend is true down to a cooling rate of 0.14 °C/sec at 450°C, which corresponds to the air cooling rate for the 10 cm slab. This condition had a yield strength of 160 ksi, an ultimate tensile strength of 205 ksi, an elongation of 18.1%, a fracture toughness of 100 ksi-in$^{1/2}$,

and a Charpy energy of 31.5 ft-lbs. These properties are very good. The material shows substantial hardenibility with the maintainance of good strength and toughness. There is, however, a degradation trend on going to slower cooling rates, implying that undesirable microstructural features tend to form with increased holding times in transformation regions. These properties are all dependent on the austenite stability. The stability allows maintainance of the good toughness and good elongation properties. It is not really possible to compare this steel in these conditions with normal thick section steels that are used for pressure vessels. Those steels are much lower in strength, (100-120 ksi ultimate tensile strength). However, the 5 cm and 10 cm material have similar ductility properties (elongations of 16 to 20 percent) at the significantly higher strength level.

The spheroidized properties are much different. While the strength level is unchanged with increase in thickness, the fracture properties vary drastically. The absolute strength level is very high, viz. 150 ksi yield strength. This is comparable with the yield strength after tempering at 300°C. The strength is maintained through the austenite transformation, allowing uniform strength levels throughout the thickness. However, the fracture properties also depend on the austenite decomposition, varying inversely with the austenite level in the as-cooled condition.

In investigating the fracture characteristics of any material there is the question of the materials sensitivity to sharp and blunt notches, and the question of what test is the best measure of fracture

0 0 0 0 0 4 7 0 0 7 5 6 3

resistance. Ritchie and others[75,76] have shown in high strength steels that there can be an inconsistency between fracture toughness and Charpy V-notch tests due to differences in the region of material that the different test sampled for its quantitative measure of fracture resistance. In the material treatments investigated in this study there seemed to be good correlation between charpy energy and fracture toughness trends. Both tests adequately showed the tempered martensite embrittlement phenomenon. The failure of certain spheroidization treatments to recover good fracture properties was also shown equally well by both tests. It therefore seems that both tests in this high strength steel study were useful in distinguishing the behavior. This was true because the initial air cooling treatment dictated the major microstructural features present.

V. SUMMARY AND CONCLUSIONS

This investigation has been aimed at widening the methods for conducting research in steels. Specifically, its purpose was to develop methods for investigating the microstructure-property relationships in thick section steels on a laboratory scale, and in 300-M, to investigate the role retained austenite had on the mechanical and fracture properties. From this study the following conclusions can be drawn:

1. Simulation methods allow assessment of thick section properties in small specimens. In this study center to edge variation in structure was avoided by investigating the slow air cooling process.

2. Using these techniques it was found that an air cooled ultra-high strength steel containing significant amounts of silicon was capable of developing thick-section microstructures with good fracture resistance and high strength.

3. In the steel, 300-M, it was found that retained austenite and its stability had significant effects on fracture properties, strength, and ductility. The austenite, if mechanically stable, improved uniform elongation without a deleterious effect on toughness.

4. It was found that the fracture toughness drop associated with tempered martensite embrittlement was increased by the presence of large amounts of retained austenite. The trough coincided with the temperature range where the austenite was destabilized by carbide film formation. This result was found for both 300-M and 4340 alloys.

0 0 0 0 4 7 0 0 8 3 4

5. Spheroidization treatment applied to this steel led to strength levels (~150 ksi yield strength) that were independent of thickness. The fracture properties, however, varied with thickness.

6. There appeared to be an optimum cooling rate, which defined the point where the properties started to degrade. In 300-M this cooling rate was about 0.15 °C/sec.

7. In general, silicon additions influence hardenability, carbide formation kinetics, and retained austenite levels in this ultra-high strength steel.

ACKNOWLEDGEMENTS

The author wishes to express his gratitude to Professor Earl R. Parker and Professor Victor F. Zackay for their guidance and encouragement throughout the investigation. He is also grateful to Professor Iain Finnie and Professor Lee Donaghey for their critical review of the manuscript. He would like to thank M. S. Bhat and John Wert for their many help discussions over the course of the work, and would especially like to thank Professor R. O. "Rob" Ritchie for his stimulating advice which was invaluable.

The assistance of the support staff of the Inorganic Materials Research Division of Lawrence Berkeley Laboratory is also acknowledged. In particular, the author wishes to thank Don Krieger, Lee Johnson, Jim Severns, "Pat" Patenaude, John Holthuis, Duane Newhart, Ed Edwards, Gloria Pelatowski, and Alice.

Finally, I would like to thank my parents for a lifetime of love and help that made it happen. FLA-TTY.

This research was supported by the U. S. Energy Research and Development Administration.

0 0 0 0 0 4 0 7 4 0 7 0 5 8 6 5

APPENDIX I.

Determination of Retained Austenite Levels Using Magnetic Saturation

The use of saturation induction for austenite determination during deformation in unstable austenitic steels has been described earlier. These measurements rely on the use of a permeameter built for use with with an instron testing machine. This permeameter uses two bucking detecting coils placed between the poles of an electromagnet to measure the flux change in a specimen. With an increase in the percentage of the specimen that is magnetic, there will be an associated increased in flux change. This flux change is measured by integrating the current from the detecting coil. By having two coils bucking each other, one a dummy coil containing no magnetic material, it is possible to eliminate the effect of the applied field. The energizing current in the large electromagnet is switched from positive to negative with a field strength of ~6,000 orsted; the field is easily enough to saturate the specimen. The equipment has been described earlier by de Miramon.[14]

Whereas previous work was concentrated with materials that were initially austenitic, this study was aimed at determining austenite levels in steel that were primarily martensitic or bainitic and were therefore primarily magnetic. Evaluation of these materials, therefore, required the use of careful calibration methods. It was necessary to use a standard to represent the signal of totally magnetic material. The standard had to have the same composition because of the significant influence of alloy additions on the saturation induction of the steel. The pure

magnetic condition was assured by spheriodizing the steel at 650°C following quenching. Initially, the saturation induction of pure iron was also checked against the textbook value to again assure accuracy. The following formula was used for the initial determination of the saturation induction:

$$B_S = \frac{1}{2NA} \times \Delta\phi_{SLFS} \times \frac{n}{n_o}$$

where

B_S = saturation induction

N = coil turns

A = area of the specimen

$\Delta\phi_{SLFS}$ = flux change due to square loop flux standard

n = voltage corresponding to integrated signal from coil containing the specimen

n_o = voltage corresponding to square loop flux standard.

Using this formula the following values for the saturation induction were calculated:

(a) Iron Standard - 21,300 gauss

(b) 300-M Standard - 19,300 gauss

(c) 4340 Standard - 20,100 gauss

These values agree very well with (1) the measured values for iron and (2) the calculated value for the alloy steels.

Knowing the valued for the standards it is easy to simplify the formula to determine austenite contents of unknown treatments. The following formula was used for the austenite percentage:

0 0 0 0 0 4 7 0 4 7 8 9 6

$$\%\text{Austenite} = \frac{n}{n_{std}} \times \frac{A_{std}}{A}$$

where

$n, (n_{std})$ = voltage of specimen (standard)

$A, (A_{std})$ = cross section area of specimen (standard)

To determine the amount of austenite in the deformed specimen, it was assumed that the plastic deformation led to no change in volume. Therefore, to the first approximation it was assumed that:

$$\Delta\ell = \Delta A$$

where

$\Delta\ell$ = change in length

ΔA = change in was cross-sectional area

Therefore the following formula was used to determine austenite levels in the plastic region:

$$\%\text{Austenite} = \frac{n}{n_{std}} \times \frac{A_{std}}{A} \times \frac{1}{\Delta\ell}$$

Elastic strains, which were very small, were ignored.

APPENDIX II.

Calculation of Cooling Profiles

Numerical methods were used to calculate the cooling profiles for the slabs of interest.[77] For simplicity, the slabs were assumed to be infinite, thereby allowing the problem to be simplified to a one dimensional problem. The following equation describes the cooling for this condition:

$$\rho Cp \frac{\partial T}{\partial t} = k \frac{\partial^2 T}{\partial x^2}$$

where T is the slab temperature, ρ is the density, Cp is the heat capacity, t is time, x is location in the slab, and k is the thermal conductivity. Because the slab is cooled in a real environment, heat losses at the surface are due to convection as well as radiation. Therefore the following equations describe the boundary conditions:

$$\frac{-k\partial T}{\partial x} = h(T-T_S) + \varepsilon\sigma(T^4 - T_S{}^4) \quad \text{(at surface)} \qquad (1)$$

where h is the heat transfer coefficient, ε is the emissivity, σ is the Stefan-Boltzmann constant, and T_s is the surrounding temperature

$$\frac{\partial T}{\partial x} = 0 \quad \text{at the center of slab} \qquad (2)$$

An implicit numerical method was used to solve this parabolic partial differential equation. In particular, the Crank-Nicolson approach was used.

In considering the heat transfer problem it was also necessary to consider that the heat capacity was temperature dependent, and that with transformtion there was a latent heat given off by the material transformed. The first consideration was dealt with by using a function routine for the heat capacity. In the transformation an adjusted average value was used. Because the equations were solved in a normalized form, this procedure only influenced the time step.

The latent heat term was added to the boundary term. When the transformtion region was approached by the edge, heat was added, which slowed down the cooling rate. A latent heat of 800 cal/g-mole was added. This was adjusted to account for the limited amount of transformation that was taking place during any one time internal. In determining the parameters, the numerically determined cooling profiles were compared to lab data. The best fit parameters were then picked. The values of $h = .00085$ cal-gm/sec-cm^2-°C and $\varepsilon = .9$ gave this fit.

The program follows this explanation. It contains two graphing routines as well as a curve fitting routine for smoothly determining continuous cooling transformation profiles to data points. In determining the cooling profiles the starting values of $\rho = 7.85$ gm/cm^3, $C_p = .149$ (900°C) and $k = .103$ gcal/sec-cm-°C were used for the 4340 and 300-M steels.

```
      PROGRAM KOOL(INPUT,OUTPUT,TAPE1=INPUT,TAPE98,PLOT,TAPE99=PLOT)
      DIMENSION T(1000),X(1000),CNT(1000),F(1000),TKEEP(1000)
      DIMENSION IPRCT(3)
      DIMENSION PERCT(4),N1(4)
      COMMON/PARAM/DENSITY,CP,TK,H,EPSILON,THKNESS,TS,DZETA
      COMMON/ARRAYS/B(201),C(201),D(201),F(201),N,NM1
      COMMON/CCPOOL/XMIN,XMAX,YMIN,YMAX,CCXMIN,CCXMAX,CCYMIN,CCYMAX
      COMMON/CURVES/CRVX(500,4),CRVY(500,4),DP(20,2),COEFF(20,20),Y(20)
      COMMON/NAME1/TITLE(6),XLBL(3),YLBL(3)
      COMMON/NAME2/TTLE2(6),XXLBL(3),YYLBL(3)
      COMMON/CCFACT/FACTOR
      COMMON/LATENL/HTLAT,TTOP
      DATA DLTA/0.0001/
C
C     READ IN LABELS FOR TEMPERATURE PROFILES PLOT- REMOVE IF GRAPHING
C     CARD NO.333 AND SUBROUTINE GRAPH REMOVED
C
      READ 99, XLBL
      READ 99, YLBL
C
C     READ IN LABELS FOR CONTINUOUS COOLING PLOT - REMOVE IF PART 2
C     NOT USED (TAKEN OUT)
C
      READ 99,XXLBL
      READ 99, YYLBL
C
C     PART 1 - CALCULATES NUMERICALLY THE TEMPERATURE PROFILES IN AN
C     INFINITE SLAB USING CRANK - NICHOLSON IMPLICIT METHOD
C             FIRST TITLE EXPERIMENT - THEN READ IN PARAMETERS
C       FIRST CARD READ DENSITY,HEAT CAPACITY,THERMAL CONDUCTIVITY,
C       HEAT TRANSFER COEFF, EMISSIVITY, SLAB HALF THICKNESS, SUR-
C       ROUNDING TEMPERATURE (CGS SYSTEM) 10 SPACES PER QUANTITY.
C       NEXT CARD - READ IN TIME INCREMENT, THICKNESS INCREMENT,
C       FINAL TIME, AND PRINTING INCREMENT - 10 SPACES
C
C                 XXXXX     X        XXXXX    XXXXX        XX
C                 X   X    X X       X   X      X         X X
C                 XXXXX    X X       XXXXX      X           X
C                 X       XXXXX      X  X       X           X
C                 X       X   X      X   X      X           X
C                 X       X   X      X   X      X         XXXXX
C
 1    JT=0
      THOLD=2000.
      HTLAT=0.
      IFIRST=0
      THETA=0.0
      READ 99,TITLE
      READ 100, DENSITY,CP,TK,H,EPSILON,THKNESS,TS
      IF(DENSITY.LE.0.0) GO TO  710
      TFCTR=THKNESS**2*DENSITY*CP/TK
      PRINT 101,DENSITY,CP,TK,H,EPSILON,THKNESS,TFCTR,TS
      READ 100, DTHETA,DZETA,TFINL,TINCR,TTOP
      JTINT=INT(TINCR*TFINL/DTHETA+.5)
      TFINL=TFINL/TFCTR
      DTHETA=DTHETA/TFCTR
       TIME=0.
      RHO=DTHETA/DZETA**2
      PRINT 102, DTHETA,DZETA,RHO
      PRINT 103, TITLE
      BI=DI=RHO
```

```
      CI = 2.0*(1.0+RHO)
      AF1 = RHO
      AF2 = 2.0*(1.0-RHO)
      NM1 = INT(1.0/DZETA + 0.5)
      N = M = NM1+1
      DX = THKNESS*DZETA
      X(1) = 0.0
      DO 2 I=2,N
 2    X(I) = X(I-1)+DX
C
C     SET UP INITIAL CONDITION
C
      CALL IC(T)
C
       TOLD1=T(N)
C     SET UP B, C, AT X = 0.0
C
      CALL BC0
C
C     CALCULATE INTERIOR POINT COEFS. (NOT DEPENDING ON T(X) )
C
222   DO 3 I=2,NM1
      B(I) = BI
      C(I) = CI
      D(I) = DI
 3    CONTINUE
      IKEEP=1
      CNT(1)=T(N)-273.
      E(1)=T(1)-273.
      TKEEP(1)=0.
      GO TO 13
 4    IKEEP=IKEEP+1
      E(IKEEP)=T(M)-273.
      TIME=TIME+TFCTR*DTHETA
      CNT(IKEEP)=T(1)-273.
      TKEEP(IKEEP)=ALOG10(TIME+.0001)
 13   IF(MOD(JT,JTINT).NE. 0) GO TO 12
      PRINT 200, TIME,TS,(X(I),T(I),I=1,N)
C
C      REMOVE CALL GRAPH IF PROFILE PLOTS NOT WANTED
C
      THOLD=T(M)
      IF(TFINL-THETA.LT.DTHETA) GO TO 501
 12   DO 5 I=2,NM1
5      F(I)=AF1*(T(I-1)+T(I+1))+AF2*T(I)
C
C      CALCULATE B.C. AT EDGE BY ITERATION AFTER INITIAL TAYLOR
C      SERIES ESTIMATE
C
       JI=0
 6     CALL BC1(T(M),JT,JI)
      TOLD=T(N)
       CALL THOMAS(T)
      IF(JI.GT.20) GO TO 10
       JI=JI+1
      IF(ABS(T(N)-TOLD).GT.DLTA*T(N)) GO TO 6
7      JT=JT+1
      IFIRST=IFIRST+1
       THETA =THETA+DTHETA
      CP1=HTCAP(T(M),TTOP)
      TFCTR=TFCTR*CP1/CP
      CP=CP1
```

```
      TTHK=DZETA*THKNESS
      HTLAT=-SOURCE(T(N),TOLD1,TTHK)
      TOLD1=T(N)
      PRINT 423,HTLAT,F(N),CP,TOLD1,TTOP
423    FORMAT(5F10.5)
      GO TO 4
C
C     B.C. AT X=XMAX NOT SATISFIED
C
10     REL DIF= ABS(T(N)-TOLD)/T(N)
      PRINT 300, REL DIF
      GO TO 7
 99   FORMAT(8A10)
 100  FORMAT(8F10.0)
 101  FORMAT(1H1,20X*S L A B  P A R A M E T E R S*//
     1        10X*ALL IN C.G.S. UNITS . . .*/
     2     10X*DENSITY = *F6.3,5X*SPECIFIC HEAT = *F6.3,5X*THERMAL *
     3       *CONDUCTIVITY = *F6.4/10X*CONVECTIVE LOSS COEF. = *1PG10.2,
     4        5X*EMISSIVITY = *0PF6.3,5X*THICKNESS = *F7.3
     5            //10X*NATURAL TIME CONSTANT = *F9.3* SECONDS*//
     6              10X *TEMPERATURE OF SURROUNDINGS = *F6.1 * DEG. K*//)
 102  FORMAT(10X*INCREMENTS. . .* 5X*DELTA THETA = *F7.3,5X*DELTA ZETA *
     2        *= *F7.3,5X*RHO = DT/DZ*2H***2 = *1PG10.3//)
 103   FORMAT(5X,6A10 //)
200   FORMAT(*0*15X*TIME = *F9.3* SECONDS*15X*TS = *F10.4//10X*X, T(X)
     X=*/(5(2F10.4,3X)))
 300  FORMAT(2X,5H******W A R N I N G - BC1 NOT CONVERGED - *1PG13.6)
C
C              XXXXX       X       XXXXX     XXXXX      XXXX
C              X   X      X X      X   X       X       X   X
C              XXXXX      X X      XXXXX       X          X
C              X         XXXXX     X X         X         X
C              X         X   X     X  X        X        X
C              X         X   X     X   X       X       XXXXX
C
C      PART 2 USES ARRAYS TKEEP,E,CNT TO GENERATE COOLING PROFILES
C      IT SETS UP A LOG(TIME) VS. TEMPERATURE GRID AND PLOTS PROFILES
C      IT ALSO HAS THE CAPABILITIES OF ADDING PER CENT TRANSFORMED
C      PLOTS WHICH ARE CURVES FITTED TO DATA. READ TITLE FIRST.
C
501    READ 600,TTLE2,MATL
       I11=1
      CALL CNTGRD
      CALL CCPLOT(TKEEP,E,IKEEP,4HJOIN)
      CALL CCPLOT(TKEEP,CNT,IKEEP,4HJOIN)
C
C          CONTINUOUS COOLING TRANSFORMATION CURVES ARE FIT TO DATA POINTS
C      FIRST TIME THROUGH AND SAVED FOR SUBSEQUENT PLOTS IF MATL NOT ZERO
C     FIRST TIME THROUGH (OR IF MATL.NE.0) NO. CCT LINES MUST BE SPEC.
C     AND NO. OF DATA POINTS AND ORDER OF FIT MUST BE SPEC. PER CENT
C     TRANSFORMED ALSO SPECIFIED. THEN DATA POINT PAIRS READ
C
      IF(MATL.EQ.0) GO TO 525
       IF(MATL.EQ.100) GO TO 1
      READ 601,NSET    $ NSET1=NSET
 502  READ 601,NDP,NDPPE
      READ 602, PERCT(I11)
      IF (NDPPE.GT.NDP) GO TO 701
      IF(NDP.GT.20) GO TO  702
      DO 503 I=1,NDP
      READ 603, (DP(I,J),J=1,2)
      DP(I,1)=ALOG10(DP(I,1)     )
```

```
503   CONTINUE
      DO 504 I=1,NDP
      DO 505 JT=1,NDPPE
      EXPO=NDPPE-JT
       COEFF(I,JT)=DP(I,1)**EXPO
505    CONTINUE
      Y(I)=DP(I,2)
504     CONTINUE
      ITEST=0
      CALL DIAG(NDP,NDPPE,ITEST)
      IF(ITEST.NE.0) GO TO  710
      CALL PTCAL(NDP,NDPPE,N1,I11)
      NSET=NSET-1
      I11=I11+1
      IF (NSET.LT.1) GO TO 525
      GO TO 502
525     DO 526 K=1,NSET1
      NHLD=N1(K)
       IF(PERCT(K).GT.100.) GO TO 528
      TRON=90.+CRVY(NHLD,K)
      ENCODE(30,604,IPRCT) PERCT(K)
       CALL CCLTR(1005.,TRON,0,2,IPRCT,30)
528   DO 527 L=1,NHLD
      E(L)=CRVX(L,K)
      CNT(L)=CRVY(L,K)
527    CONTINUE
      CALL CCPLOT(E,CNT,NHLD,4HJOIN)
526     CONTINUE
      GO TO 1
701    PRINT 605
      GO TO 1
702     PRINT 606
      GO TO 1
703    PRINT 607
      GO TO 1
600    FORMAT(6A10,I5)
601   FORMAT(2I5)
602    FORMAT(F10.4)
603   FORMAT(10X,2(F10.5))
604   FORMAT(1X,F5.1,14H PER CT TRANS.      )
605    FORMAT( 2X, * ORDER OF FIT TOO HIGH * )
606   FORMAT(2X, *  TOO MANY DATA POINTS FOR ANALYSIS * )
607   FORMAT(2X, * THE EQUATION CAN NOT BE FIT  * )
710     CALL CCEND
      STOP
      END                                                                    00000
      SUBROUTINE IC(T)
C
C     IC SETS UP THE INITIAL TEMPERATURE DISTRIBUTION OF THE SLAB.
C     THE REASON FOR ARRAY TI IS SO THAT THE INITIAL TEMPERATURE DIST.
C     MAY BE MADE A FUNCTION OF X.
C
      COMMON /ARRAYS/ B(201),C(201),D(201),F(201),N,NM1
      DIMENSION T(500),TI(500)
       DATA TI/250*1173./
      DO 1 I=1,N
1      T(I)=1143.
      RETURN
      END
      SUBROUTINE BCO
C
C     BCO SETS THE BOUNDARY CONDITION AT ZERO.
```

```
C
      COMMON /ARRAYS/ B(201),C(201),D(201),F(201),N,NM1
      B(1) = 0.0
      C(1) = 1.0
      D(1) = -1.0
      F(1) = 0.0
      RETURN
      END
      SUBROUTINE GRAPH(X,Y,M,TIME,IFIRST,TS,THOLD)
      COMMON/CCPOOL/XMIN,XMAX,YMIN,YMAX,CCXMIN,CCXMAX,CCYMIN,CCYMAX
      COMMON/NAME1/TITLE(6),XLBL(3),YLBL(3)
      DIMENSION X(100),Y(100)    ,ITIME(3)
      DATA PART,TRAP/10., 9./
      CCXMIN=100.$CCXMAX=600.$CCYMIN=100.$CCYMAX=1000.
      XMIN=.0
      XMAX=X(M)
      YMIN=300.
      YMAX=1200.
      TCHCK=Y(M)-TS
      IF(TCHCK.LE.10.) RETURN
      IF(IFIRST.GE.1)   GO TO 32
      CALL CCNEXT
      CALL CCGRID(1,IFIX(PART),6HNOLBLS,1,IFIX(TRAP))
      CALL CCLBL(IFIX(PART),IFIX(TRAP))
      CALL CCLTR(260.,10.,0,1,XLBL,30)
      CALL CCLTR(10.,550.,1,1,YLBL,10)
      CALLCCLTR(100.,1020.,0,2,TITLE,60)
 32    CALLCCPLOT(X,Y,M)
      CCY=Y(M)-200.
      ENCODE(30,50,ITIME) TIME
 50   FORMAT( 4H T = , G7.1, 4H SEC )
      IF(THOLD-Y(M).LT.12.) RETURN
      CALL CCLTR(620.,CCY,0,1,ITIME,30)
      RETURN
      END
      SUBROUTINE BC1(TT,JT,JI)
      COMMON/LATENL/HTLAT,TTOP
C
C      BC1 CALCULATES THE BOUNDARY CONDITION COEFFICIENTS AT ZETA EQUAL
C     TO ONE BY FIRST MAKING A TAYLOR SERIES APPROXIMATION AND THEN
C     ITERATING UNTIL THERE IS NO FURTHER CHANGE IN T(N).
C
      COMMON /ARRAYS/ B(201),C(201),D(201),F(201),N,NM1
      COMMON /PARAM/ DENSITY, CP, TK, H, EPSILON, THKNESS, TS, DZETA
      DATA SIGMA /1.355E-12/
      T = TT
      IF (JT .GT. 0) GO TO 1
      B(N) = -1.0
      D(N) = 0.0
      DX BY TK = DZETA*THKNESS/TK
      AF1 = DX BY TK * H
      AC1 = AF1+1.0
      AF1 = AF1*TS
      AC2 = DX BY TK * EPSILON*SIGMA
      AC3 = 4.0*AC2
      AF2 = AC2*TS**4
      AF3 = 3.0*AC2
      FN = AF1+AF2
 1    IF (JI .GT. 0) GO TO 2
      TM3 = T**3
      C(N) = AC1 + AC3*TM3
      F(N) = FN + AF3*TM3*T    -HTLAT
```

```
      RETURN
2     F(N)=FN-HTLAT
      C(N) = AC1 + AC2*T**3
      RETURN
      END
      SUBROUTINE THOMAS(U)
      COMMON /ARRAYS/ B(201),C(201),D(201),F(201),N,NM1
      DIMENSION ALFA(201), BETA(201),U(201)
C
C     NOTE - DIVISION TAKES ABOUT FOUR TIMES AS LONG AS MULTIPLICATION.
C
      CINV = 1.0/C(1)
      ALFA(1) = -D(1)*CINV
      BETA(1) = F(1)*CINV
      DO 15 I=2,NM1
      IM1 = I-1
      DENO = 1.0/(B(I)*ALFA(IM1) + C(I))
      ALFA(I) = -D(I)*DENO
      BETA(I) = (F(I)-B(I)*BETA(IM1))*DENO
 15   CONTINUE
      U(N) = (F(N) - B(N)*BETA(NM1))/(C(N) + B(N)*ALFA(NM1))
      DO 25 J=1,NM1
      I = N-J
      U(I) = ALFA(I)*U(I+1) + BETA(I)
 25   CONTINUE
      RETURN
      END
      SUBROUTINE DIAG(NROW,NCOL,ITEST)
      COMMON/CURVES/CRVX(500,4),CRVY(500,4),DP(20,2),A(20,20),B(20)
      DIMENSION EQMAT(20,20),CONST(20)
      NEQMAX=NROW-NCOL+1
      DO 50 NEQ=1,NEQMAX
      DO 20 I=1,NCOL
      DO 10 J=1,NCOL
   10 EQMAT(I,J)=A(NEQ+I-1,J)
   20 CONST(I)=B(NEQ+I-1)
      KMAX=NCOL-1
      DO 30 K=1,KMAX
      PIVOT=EQMAT(K,K)
      IF(ABS(PIVOT).LT.1E-50) GO TO 60
      IMIN=K+1
      DO 30 I=IMIN,NCOL
      F=EQMAT(I,K)/PIVOT
      CONST(I)=CONST(I)-F*CONST(K)
      DO 30 J=K,NCOL
      EQMAT(I,J)=EQMAT(I,J)-F*EQMAT(K,J)
   30 CONTINUE
      DO 40 KT=2,NCOL
      K=NCOL+2-KT
      PIVOT=EQMAT(K,K)
      IF(ABS(PIVOT).LT.1E-50) GO TO 60
      IMAX=K-1
      DO 40 IT=1,IMAX
      I=K-IT
      F=EQMAT(I,K)/PIVOT
      CONST(I)=CONST(I)-F*CONST(K)
      DO 40 JT=I,K
      J=K+I-JT
      EQMAT(I,J)=EQMAT(I,J)-F*EQMAT(K,J)
   40 CONTINUE
      DO 50 I=1,NCOL
      A(NEQ,I)=CONST(I)/EQMAT(I,I)
```

```
   50 CONTINUE                                                          00000
      RETURN                                                            00000
   60 PRINT 1000
 1000 FORMAT(/15X,50H***** UNABLE TO DETERMINE FITTING EQUATIONS. *****)
      ITEST=1
      RETURN
      END                                                               00000
       SUBROUTINE PTCAL(NDP,NDPPE,N1,ILL)
      COMMON/CCPOOL/XMIN,XMAX,YMIN,YMAX,CCXMIN,CCXMAX,CCYMIN,CCYMAX
      COMMON/CURVES/CRVX(500,4),CRVY(500,4),DP(20,2),COEFF(20,20),Y(20)
      DIMENSION N1(4)
      N=0  $ PI=3.141592654
      TFCT=(DP(NDP,1)-DP(1,1))/400.
      XKEEP=DP(1,1)
      DO 80 ITEMP=1,400
      N=N+1
      I=ITEMP-1
      TEMP=FLOAT(I)*TFCT+XKEEP
      IF(TEMP.GT.DP(1,1)) GO TO 11
      CRVX(N,ILL)=TEMP
      CRVY(N,ILL)=DP(1,2)
      GO TO 80
 11   IF(TEMP.GT.DP(NDP,1)) GO TO 90
      CRVX(N,ILL)=TEMP
      IMAX=NDP-1
      DO 10 I=1,IMAX
      IPLUS1=I+1
      IF(TEMP.LT.DP(I,1).OR.TEMP.GT.DP(IPLUS1,1)) GO TO 10
      IREGION=I
      GO TO 20
   10 CONTINUE
   20 TIMEAVE=0.  $ K=NDPPE-1  $ J=IREGION-NDPPE+2  $ SNORM=0.
   30 IF(J.GT.0) GO TO 40
      K=K-1  $ J=J+1
      GO TO 30
   40 DO 60 I=J,IREGION
      IF(I.GT.(NDP-NDPPE+1)) GO TO 50
      IFI=NDPPE+I-1
      S=(SIN(PI*(TEMP-DP(I,1))/(DP(IFI,1)-DP(I,1))))**2
      SNORM=SNORM+S  $ TIMEAVE=TIMEAVE+S*FQ(TEMP,COEFF,I,NDPPE)
      GO TO 60
   50 K=K-1
   60 CONTINUE
      IF(TIMEAVE.EQ.0.0.AND.SNORM.EQ.0.0) SNORM=1.0
      TIMEAVE=TIMEAVE/SNORM
      CRVY(N,ILL)=TIMEAVE
      IF (TIMEAVE.GE.YMIN) GO TO 70
       CRVY(N,ILL)=YMIN
      GO TO 80
 70   IF (TIMEAVE.LT.YMAX) GO TO 80
       CRVY(N,ILL)=YMAX
   80 CONTINUE
  106  FORMAT(3X,I5,5X,F10.4,5X,F10.4)
90     N1(ILL)=N
       RETURN
      END
      SUBROUTINE CNTGRD
      COMMON/NAME2/TTLE2(6),XXLBL(3),YYLBL(3)
        COMMON/CCPOOL/XMIN,XMAX,YMIN,YMAX,CCXMIN,CCXMAX,CCYMIN,CCYMAX
      COMMON/PARAM/DENSITY,CP,TK,H,EPSILON,THKNESS,TS,DZETA
      DIMENSION ILABEL(3)
      COMMON/CCFACT/FACTOR
```

0 00 01 00 01 47 70 04 07 85 74 1


```
      XMIN=0.
      XMAX=5.
      YMIN=0.
      YMAX=900.
      FACTOR=1.
      CCXMIN=100.
      CCXMAX=1000.
      CCYMIN=100.
      CCYMAX=1000.
      CALL CCNEXT
      CALL CCGRID(5,1,6HNOLBLS,9,10)
      CALL CCLTR(200.,1020.,0,2,TTLE2,60)
      CALL CCLTR(400.,20.,0,2,XXLBL,30)
      CALL CCLTR(25.,400.,1,2,YYLBL,30)
      CALL CCLTR(50.,100.,0,2,1H0,1)
      CALL CCLTR(50.,400.,0,2,3H300,3)
      CALL CCLTR(50.,700.,0,2,3H600,3)
      CALL CCLTR(50.,1000.,0,2,3H900,3)
      CALL CCLTR(100.,70.,0,2,1H1,1)
      ENCODE(30,11,ILABEL) H
      CALL CCLTR(700.,950.,0,1,ILABEL,30)
      THK2=THKNESS*2.
      ENCODE(30,12,ILABEL) THK2
      CALL CCLTR(700.,920.,0,1,ILABEL,30)
      ENCODE(30,13,ILABEL) EPSILON
      CALL CCLTR(700.,890.,0,1,ILABEL,30)
      RETURN
11    FORMAT(1X,20H HEAT TRANS COEF =   ,F10.6)
12    FORMAT(1X,12H THICKNESS = F8.4,8H  CM.      )
13    FORMAT(1X,13H EMISSIVITY =    ,F6.2)
      END
      FUNCTION EQ(X,COEFF,I,NDPPE)
      DIMENSION COEFF(20,20)
      EQ=0.0
      DO 10 J=1,NDPPE
      JT=NDPPE-J
   10 EQ=EQ+COEFF(I,J)*(X**(JT))
      RETURN
      END
      FUNCTION HTCAP(T,TTOP)
      IF(T.LT.TTOP) GO TO 1
       HTCAP=(4.85+.003*T)/56.
      RETURN
1     IF(T.LE.473.) GO TO 2
      A1=(T-473.)/200.
      HTCAP=(A1*(4.85+.003*T)+(1.-A1)*(3.37+.0071*T+43000.0/T**2))/56.
      RETURN
2     HTCAP=(3.37+.0071*T+43000.0/T**2)/56.
      RETURN
      END
      FUNCTION SOURCE(T,TOLD,THKNESS)
      COMMON/LATENL/HTLAT,TTOP
      A1=.8
      IF(T.GT.TTOP) GO TO 3
       IF(T.LE.473.)      GO TO 1
      SOURCE=A1*THKNESS*(TTOP-T)
      TTOP=T
      RETURN
1     IF(TOLD.LE.473.) GO TO 3
      SOURCE=A1*(TOLD-473.     ) *THKNESS
      TTOP=0.
      RETURN
3     SOURCE=0.
      RETURN
      END
```

REFERENCES

1. A. J. Baker, F. T. Lauta, and R. P. Wei, Structure and Properties of Ultrahigh-Strength Steel, ASTM STP 370, The American Society for Testing and Materials, 1965, p.3.
2. G. Kohn, D. Eng. Thesis (to be published).
3. M. S. Bhat, D. Eng. Thesis, (To be published).
4. A. M. Hall, Introduction to Today's Ultrahigh-Strength Structural Steels, ASTM STP 498, American Society for Testing and Materials, 1971.
5. W. A. Backoften and M. L. Ebner, Metallurgical Aspects of Fracture of High Strength Steels, Final Tech. Report, Watertown Arsenal Lab., (1963).
6. K. J. Irvine, Steel Strengthening Mechanisms, Climax Molybdenum Co., 1965, p.55.
7. W. E. Wood, Eng. Fract. Mech. 7, 219 (1975).
8. M. F. Carlson, B. V. N. Rao, R. O. Ritchie, and G. Thomas, LBL-5111, Lawrence Berkeley Laboratory, University of California, Berkeley, April 1976.
9. G. Y. Lai, W. E. Wood, R. Clark, V. F. Zackay and E. R. Parker, Met. Trans. 5, 1663 (1974).
10. C. J. Altstetter, M. Cohen, and B. L. Averbach, Trans. ASM 55, 287 (1962).
11. J. Vajda, J. J. Hauser and C. Wells, Trans. ASM 49, 517 (1957).
12. C. E. Ericsson, M. S. Thesis, University of California, Berkeley, Dec. 1973 (LBL-2279).

13. J. L. Yuen, M. S. Thesis, University of California, Berkeley, July 1974 (LBL-3103).

14. B. de Miramon, M. S. Thesis, University of California, Berkeley Sept. 1967 (UCRL-17849).

15. B. D. Cullity, Elements of X-Ray Diffraction, Addison-Wesley Publishing Co. Inc., 1959, p. 391.

16. D. Webster, Summary Report D6-25220, The Boeing Co., Seattle, Wash., ARPA Contract N00014-6G-C-0365, April 1970.

17. A. W. Gunderson and C. L. Harmsworth, Test Memo No. MAAE70-5 AFML, Wright Patterson AFB, Sept. 1970.

18. P. B. Hirsch, A. Howie, R. B. Nicholson, D. W. Pashley, and M. J. Whelan, Electron Microscopy of Thin Crystals, Butterworth & Co., Ltd., London, (1969).

19. G. Kurdjamov and G. Sachs, Z. Physik 64, 325 (1930).

20. G. K. Manning and C. H. Lory, Metals Technology, p. 442-466, 1946.

21. J. W. Cahn, Acta. Met. 4, 572 (1956).

22. Isothermal Transformation Diagrams, United States Steel, Pittsburgh, PA, 1963.

23. E. G. Bain and H. W. Paxton, Alloying Elements in Steel, American Society for Metals, Metals Park, Ohio, (1966).

24. R. D. Chapman and W. E. Jominy, Trans. ASM 47, 869 (1955).

25. B. N. P. Babu, D. Eng. Thesis, University of California, Berkeley, Aug. 1974 (LBL-2772).

26. W. W. Cias, Climax Molybdenum Report L-291-07-01, February 24, 1972.

27. S. K. Das and G. Thomas, Trans. ASM 62, 659 (1969).

28. D. H. Huang and G. Thomas, Met. Trans. 2, 1587 (1971).

29. D. H. Huang, Ph. D. Thesis, University of California, Berkeley, May 1975 (LBL-3713).

30. A. G. Allten and P. Payson, Trans. ASM 45, 498 (1953).

31. W. S. Owen, Trans. ASM 46, 812 (1954).

32. B. G. Reisdorf, Trans. AIME 227, 1334 (1963).

33. G. R. Speich, Trans. AIME 245, 2555 (1969).

34. G. R. Speich and W. C. Leslie, Met. Trans. 3, 1043 (1972).

35. E. Tekin and P. M. Kelly, AIME report, 1965, p. 173.

36. G. Y. Lai, Met. Trans. 6A, 1469 (1975).

37. R. F. Hehemann, K. R. Kinsman, and H. I. Aaronson, Met. Trans. 3, 1077 (1972).

38. M. Cohen, Trans. ASM 41, 35 (1949).

39. L. C. Castleman, B. L. Averbach, and M. Cohen, Trans. ASM 44, 263 (1952).

40. B. L. Averbach and M. Cohen, Trans. ASM 41, 1024-1060 (1949).

41. D. Webster, Trans. ASM 61, 816 (1968).

42. C. A. Pampillo and H. W. Paxton, Met. Trans. 3, 2895 (1972).

43. S. Jin, S. K. Hwang, and J. W. Morris, Jr., Met. Trans. 6A (1975).

44. S. Jin, D. Huang, and J. W. Morris, Jr., Met. Trans. 7A, 637 (1976).

45. B. Francis, Ph.D. Thesis, University of California, Berkeley, May 1975, (LBL-3124).

46. H. J. Elmendorf, Trans. ASM 33, 236 (1944).

47. R. W. Balciffe, B. L. Averbach, and M. Cohen, Trans. ASM 43, (1951).

48. G. E. Pellissier, Eng. Fract. Mech. 1, 55 (1968).

0 0 0 0 4 7 4 0 7 0 6 6 7 3

49. R. T. Ault, G. M. Waid, and R. B. Bertolo, AFML-TR-71-27, Feb. 1971, AFML, Wright-Patterson Air Force Base.

50. E. A. Stergerwald and C. Vishnevsky, AMMRC CR-67-13(F), Feb. 1968, TRW Inc. Cleveland, Ohio.

51. L. F. Porter, Met. Eng. Quarterly 6, 17 (1966).

52. T. B. Cox and J. R. Low, Jr., Met. Trans. 5, 1457 (1974).

53. P. A. Blanchard and A. R. Triano, WADC-TN-58-176, Sept. 1958.

54. T. Litchenberg, unpublished research.

55. R. D. Goolsby, Ph.D. Thesis, University of California, Berkeley, Nov. 1971, (LBL-405).

56. E. S. Davenport, J. of Matls. 677 (May 1957).

57. K. J. Irvine and F. B. Pickering, JISI 201, 518 (1963).

58. W. E. Duckworth, Met. Reviews, p. 145 (1968).

59. M. E. Buch and P. M. Kelly, Acta Met. 19, 1363 (1971).

60. W. C. Leslie, Met. Trans. 3, 5 (1972).

61. E. B. Kula and A. A. Anctil, J. of Matls. 4, 817 (1969).

62. B. R. Banerjee, JISI 203, 166 (1965).

63. C. H. Shih, B. L. Averbach, and M. Cohen, Trans. ASM 48, 86 (1956).

64. D. Bhandarkar, V. F. Zackay, and E. R. Parker, Met. Trans. 3, 2619 (1972).

65. M. A. Grossman, Trans. AIME 167, 39 (1946).

66. L. J. Klinger, et al., Trans. ASM 46, 1557 (1954).

67. R. P. Wei, Fracture Toughness Testing and Its Applications, ASTM STP 381, American Society for Testing and Materials, 196, 279, (1965).

68. B. S. Lement, B. L. Averbach, and M. Cahn, Trans. ASM, 46, 851, (1954).

69. Y. H. Liu, Trans. ASM 62, 55 (1969).

70. J. M. Capus and G. Mayer, Metallurgica 62, 133 (1960).

71. C. J. McMahon, Temper Embrittlement in Steels, ASTM STP 407, American Society for Testing and Mateirals, 1968, pp. 127.

72. D. Fahr, Met. Trans. 2, 1883 (1971).

73. W. W. Gerberich, P. L. Hemmings, and V. F. Zackay, Met. Trans. 2, 2243 (1971).

74. S. S. Strunk, A. W. Pense, and R. D. Stout, WRC Bulletin No. 120, (Feb. 1967).

75. R. O. Ritchie, B. Francis, and W. L. Server, Met. Trans. 7A, 831 (1976).

76. R. O. Ritchie, R. M. Horn, and E. R. Parker, unpublished results.

77. R. L. Ketter and S. P. Prawel, Modern Methods of Engineering Computation, McGraw Hill Book Co., 1969, p. 395.

0 00 07 00 04 47 70 04 07 86 77 4

Table I. Chemical Composition of Alloys (wt%).

Alloy	C	Mn	Cr	Ni	Mo	S	P	Si	Cu	V
4340*	.41	.80	.79	1.75	.23	.004	.006	.23	.06	-
300-M*	.42	.76	.76	1.76	.41	.002	.007	1.59	-	.1

*Vacuum are remelted.

Table II. Tensile Properties - Round Specimens.

Cooling Treatment	Tempering (°C) Temperature	.2% Yield Strength (ksi)	Ultimate Tensile Strength (ksi)	Elongation (%)	Reduction in Area (%)
Oil Quenched 300-M	100*	215	335	9.3	25.0
	300	245	286	12.1	40.4
	350	245	283	-	-
	400	244	272	13.1	49.7
	470	217	244	12.1	50.0
	500	203	231	11.5	50.8
	650	156	172	18.1	55.6
2.5 cm-Air Cool 4340	AC**	167	220	11.0	47.2
	200	176	215	13.9	59.7
	275	181	214	15.2	65.4
	350	176	206	15.5	64.3
	450	162	180	16.2	62.3
	650	107	132	22.0	69.0

*Wood[7]
**As-cooled

Table III. Tensile Properties - Round Specimens.

Cooling Treatment	Tempering (°C) Temperature	.2% Yield Strength (ksi)	Ultimate Tensile Strength (ksi)	Elongation (%)	Reduction in Area (%)
2.5 cm Air Cool-300-M	AC	210	312	9.2	20.4
	300	250	297	12.1	32.7
	350	254	291	10.0	35.2
	400	244	280	10.6	37.2
	450	212	260	11.8	32.0
	450*	227	258	10.6	32.7
	470	200	250	10.2	31.3
	470*	216	251	10.4	31.2
	470**	225	250	11.1	33.9
	650	157	175	18.4	50.1

*Double Tempered
**Triple Tempered

0008047 0047 8578

Table IV. Tensile Properties - Round Specimens

Cooling Treatment	Tempering (°C) Temperature	.2% Yield Strength (ksi)	Ultimate Tensile Strength (ksi)	Elongation (%)	Reduction in Area (%)
5.0 cm Air cooled 300-M	AC	181	264	12.3	29.0
	300	218	254	10.7	42.5
	350	214	249	12.3	44.1
	400	210	244	12.7	41.2
	450	185	240	11.6	31.8
	450*	200	234	7.4	31.3
	470	166	231	12.3	34.4
	470*	199	234	10.8	32.0
	470**	198	228	11.1	32.8
	630	166	189	20.5	45.6

*Double tempered

**Triple tempered

Table V. Tensile Properties - Round Specimens

Cooling Treatment	Tempering (°C) Temperature	.2% Yield Strength (ksi)	Ultimate Tensile Strength (ksi)	Elongation (%)	Reduction in Area (%)
10 cm Air Cooled 300-M	AC	161	209	16.3	45.1
	300	165	214	18.2	54.3
	350	172	206	17.7	55.4
	400	173	203	21.3	56.6
	450	157	225	14.7	36.4
	650	144	173	17.2	51.3
15 cm Air Cooled 300-M	AC	142	200	17.3	38.4
	300	157	195	21.3	53.3
	350	156	194	23.1	51.9
	400	153	190	26.8	48.4
	450	132	216	11.6	18.8
	650	144	179	15.7	47.0

00000004/70004/87/66/96

Table VI. Retained Austenite, Tensile Properties.

Cooling Treatment	Tempering Temperature	Austenite (unloaded) (%)	Austenite (at Yield) (%)	Austenite (2% Strain) (%)	Yield Strength (ksi)	Ultimate Tensile Strength (ksi)
Oil Quenched 300-M	AQ	5.8	0.8	0.0	238	335
	300	3.8	2.4	1.4	256	294
	350	3.7	2.6	1.7	252	289
	400	3.1	1.8	0.2	242	271
	470	0.6	0.0	0.0	205	244
	550	0.0	0.0	0.0	204	226
2.5 cm Air Cooled-4340	AC	4.5	2.0	0.0	141	190
	200	4.4	2.8	0.7	152	197
	275	.9	0.0	0.0	153	190
	350	0.0	0.0	0.0	153	188
	450	-	-	-	147	174
	550	-	-	-	134	163
	650	-	-	-	116	143

Table VII. Retained Austenite, Tensile Properties

Cooling Treatment	Tempering Temperature	Austenite (unloaded) (%)	Austenite (at Yield) (%)	Austenite (2% Strain) (%)	Yield Strength (ksi)	Ultimate Tensile Strength (ksi)
2.5 cm Air Cool 300-M	AC	14.4	8.8	5.5	199	262
	300	10.5	9.0	7.4	210	251
	300*	11.1	9.8	-	212	253
	350	11.4	10.0	8.2	208	246
	350*	11.7	10.4	-	205	244
	400	12.4	10.7	8.3	205	243
	400*	12.2	10.5	7.4	194	240
	425	11.7	9.4	5.1	182	241
	425*	11.2	8.1	3.4	172	239
	450	9.9	5.8	1.1	164	242
	450*	7.6	3.8	0.0	172	245
	470	6.6	3.1	0.0	180	241
	470*	3.8	1.0	0.0	180	238

*Double Tempered

00 00 41 00 47 00 40 78 77 00

Table VIII. Retained Austenite, Tensile Properties

Cooling Treatment	Tempering Temperature	Austenite (unloaded) (%)	Austenite (at Yield) (%)	Austenite (2% Strain) (%)	Yield Strength (ksi)	Ultimate Tensile Strength (ksi)
5.0 cm Air Cool 300-M	AC	17.6	13.8	10.4	176	242
	300	13.8	12.5	11.5	203	235
	300*	12.5	11.2	-	198	238
	350	14.6	13.7	12.4	192	227
	350*	14.7	13.4	-	200	231
	400	15.3	14.0	12.1	194	228
	400*	14.6	13.1	10.4	185	228
	425	15.1	13.3	9.4	174	220
	425*	10.3	7.0	2.6	171	234
	450	10.2	6.0	1.4	167	238
	450*	8.7	5.4	1.0	167	235
	470	8.0	4.7	1.1	173	240
	470*	4.4	1.5	0.0	176	232

*Double Tempered

Table IX. Retained Austenite, Tensile Properties

Cooling Treatment	Tempering Temperature	Austenite (unloaded) (%)	Austenite (at Yield) (%)	Austenite (2% Strain) (%)	Yield Strength (ksi)	Ultimate Tensile Strength (ksi)
10 cm Air Cooled 300-M	AC	29.3	26.6	20.9	134	212
	300	24.3	23.1	21.3	156	196
	350	24.4	23.3	21.9	158	195
	400	26.9	25.6	23.3	153	199
	450	14.8	11.3	5.1	141	226
	550	-	-	-	162	236
	650	-	-	-	144	184
15 cm Air Cooled 300-M	AC	30.2	25.6	20.2	128	205
	300	23.1	22.0	20.5	155	191
	350	25.0	24.1	22.8	156	188
	400	27.7	26.4	24.3	149	192
	450	22.1	17.9	9.7	120	212
	550	-	-	-	153	223
	650	-	-	-	144	184

0000004770040787 19

Table X. Fracture Toughness, Charpy V-notch.

Cooling Treatment	Tempering (°C) Temperature	K_{Ic} (ksi-in$^{1/2}$)	K_{Ic} (MPa$\sqrt{m}$)	C_y (ft-lb)	C_y (Joules)
Oil Quenched 300-M	AQ	31	33.9	[9.5	[12.9
	(200)	(57.5)	(63.8)	10.25	13.9
	300	59.5	65.0	18.75	25.4
				16.75	22.7
	350	-	-	16.6	22.5
				16.75	22.7
	400	55	60.1	12.8	17.4
				11.9	16.1
	470	62.5	68.3	12.5	17.0
				12.25	16.6
	550	80	87.4		
	650			42.0	56.9
				39.0	52.9
2.5 cm Air Cool - 4340	AC	44.9	49.1	10.5	14.2
				-	-
	200	83.4	91.1	15.5	21.0
				15.4	20.9
	275	79.2	86.6	12.4	16.8
				10.2	30.7
	350	82.0	89.6	15.8	21.5
				15.4	20.9
	450	95.2*	104*	-	-
				-	-
	650			49.3	66.9
				56.9	77.3

*Not valid

Table XI. Fracture Toughness, Charpy Energy.

Cooling Treatment	Tempering (°C) Temperature	K_{Ic}(ksi-in$^{1/2}$)	K_{Ic}(MPa$\sqrt{m}$)	C_y(ft-lb)	C_y(Joules)
2.5 cm Air Cool - 300-M	AC	43.7	47.8	4.8	6.5
				12.4	16.8
	300	63.2	69.1	11.8	16.0
				16.4	22.3
	350	57.3	62.6	15.8	21.5
				17.1	23.2
	400	68.5	74.9	12.3	16.7
				6.6	9.0
	450	38.9	42.5	7.6	70.3
				5.3	7.2
	450**	35.5	38.8	-	
	470	42.9	46.9	-	
	470**	36.5	39.9	-	
	470†	34.2	37.4	-	
	650	106.2*	116.1*	20.3	27.6
				13.2	17.9

*Not valid, **Double Tempered, †Triple Tempered.

0000004477 00447 0877 29

Table XII. Fracture Toughness, Charpy Energy.

Cooling Treatment	Tempering (°C) Temperature	K_{Ic} (ksi-in$^{1/2}$)	K_{Ic} (MPa$\sqrt{m}$)	C_y (ft-lb)	C_y (Joules)
5.0 cm Air Cool - 300-M	AC	58.7	64.2	11.3**	15.3
				19.6**	26.6
	300	80.9	88.4	15.0	20.4
				-	-
	350	51.3	56.1	14.7	20.0
				-	-
	450	59.7	65.2	17.6	23.9
				12.6	17.1
	450	39.0	42.6	8.3	11.3
				13.2	17.9
	450†	32.0	34.9	-	-
	470	46.0	50.3	-	-
	470†	30.6	33.4	-	-
	470‡	31.1	34.0	-	-
	650	119.8*	130.9*	33.4	45.4
				34.4	46.7

*Not valid
**Radius off
†Double Tempered
‡Triple Tempered

Table XIII. Fracture Toughness, Charpy Energy.

Cooling Treatment	Tempering (°C) Temperature	K_{Ic} (ksi-in$^{1/2}$)	K_{Ic} (MPa$\sqrt{m}$)	C_y (ft-lb)	C_y (Joules)
10 cm Air Cool - 300-M	AC	80.4	87.9	25.0	33.9
				26.4	35.8
	300	100.4	109.7	32.9	44.7
				30.8	41.8
	350	87.5	95.6	19.9	27.0
				18.5	25.1
	400	86.1	94.1	20.7	28.1
				21.3	28.9
	450	35.8	39.1	4.6	6.2
				-	-
	650	80.4	87.9	11.3	15.3
				11.3	15.3
15 cm Air Cooled 300-M	AC	61.5	67.2	12.6	17.1
				12.3	16.7
	300	78.0	85.2	19.0	25.8
				20.5	27.8
	350	80.0	87.4	18.9	25.7
				19.2	26.1
	400	75.7	82.7	17.6	23.9
				18.5	25.1
	450	38.7	42.3	5.8	7.9
				5.4	7.3
	650	62.0	67.8	11.5	15.6
				11.2	15.2

0 0 0 4 7 0 4 2 3

Table XIV. X-ray Data for 300-M Material.

Treatment	Temperature	%Austenite (220_γ:211_α)	%Austenite (311_γ:211_α)	$a_o(211_\alpha)$	$a_o(311_\gamma)$	$a_o(220_\gamma)$
5.0 cm Air Cool	300°C	14.8%	11.6%	2.866Å	3.627Å	3.628Å
	400°C	14.5%	14.7%	2.867	3.611Å	3.616Å
	470°C	3.9%	2.5%	2.868	3.598Å	3.598Å
10 cm Air Cool	300°C	20.0%	17.4%	2.867	3.622Å	3.631Å
	470°C	9.3%	14.8%	2.867	3.599Å	3.592Å

00 00 00 00 41 77 00 43 78 78 41

FIGURE CAPTIONS

Fig. 1. Heat treating molds for increasing thickness of tensile specimens.

Fig. 2. Dimensions for (a) standard Charpy V-notch specimen and (b) standard round tensile specimen.

Fig. 3. Flat tensile specimens used for magnetic measurements.

Fig. 4. Schematic of standard ASTM impact tension specimen.

Fig. 5. Continuous cooling transformation diagram for 300-M, determined using dilatometry. Rate 1 is equivalent to oil quenching, while rates 3 through 6 are equivalent to air cooling of 2.5 cm to 15 cm slabs.

Fig. 6. Comparison of laboratory and numerically determined cooling profile for 2 cm thick slab, air cooled.

Fig. 7. Numerically determined cooling profiles for 2.5 cm and 5.0 cm thick slabs, air cooled. Edge and center profile shown where ε and h are assumed to be 0.9 and 0.00085, respectively.

Fig. 8. Numerically determined profiles for 10 cm and 15 cm air cooled slabs ($\varepsilon = 0.9$ and $h = 0.00085$).

Fig. 9. Tensile properties as a function of tempering temperature for oil quenched 300-M (Data averaged).

Fig. 10. Tensile properties as a function of tempering temperature for 2.5 cm air cooled 300-M (Data averaged).

Fig. 11. Tensile properties as a function of tempering temperature for 5.0 cm air cooled 300-M (Data averaged).

Fig. 12. Tensile properties as a function of tempering temperature for 10 cm air cooled 300-M (Data averaged).

Fig. 13. Tensile properties as a function of tempering temperature for 15 cm air cooled 300-M (Data averaged).

Fig. 14. Tensile properties as a function of tempering temperature for 2.5 cm air cooled 4340 (Data averaged).

Fig. 15. Ductility parameters displayed as a function of tempering temperature for oil quenched 300-M.

Fig. 16. Reduction in area, elongation as a function of tempering for 2.5 cm air cooled 300-M.

Fig. 17. Ductility parameters as a function of tempering temperature for air cooled 300-M, 5.0 cm thick.

Fig. 18. Reduction in area, elongation for 10 cm air cooled, 300-M, as a function of tempering temperature.

Fig. 19. Ductility parameters as a function of tempering temperature for 15 cm air cooled 300-M.

Fig. 20. Elongation, reduction in area as a function of tempering temperature for 2.5 cm air cooled 4340.

Fig. 21. Fracture toughness vs. tempering temperature for oil quenched 300-M.

Fig. 22. Fracture toughness vs. tempering temperature for 2.5 thick air cooled 300-M.

Fig. 23. Fracture toughness vs. tempering temperature for 5.0 cm thick air cooled 300-M.

Fig. 24. Fracture toughness vs. tempering temperature for 10 cm thick air cooled 300-M.

0 0 0 0 4 7 0 4 3 3 2

Fig. 25. Fracture toughness vs. tempering temperature for 15 cm thick air cooled 300-M.

Fig. 26. Fracture toughness vs. tempering temperature for 2.5 cm thick air cooled 4340.

Fig. 27. Charpy impact energy vs. tempering temperature for 300-M in air cooled and oil quenched conditions. (Data averaged).

Fig. 28. Charpy impact energy vs. tempering temperature for air cooled 300-M and air cooled 4340 (Data averaged).

Fig. 29. Charpy impact energy vs. testing temperature for 2.5 cm air cooled 300-M in several temper conditions.

Fig. 30. Fractographs of oil quenched 300-M. (a) As-quenched, (b) tempered at 300°C, (c) tempered at 400°C, and (d) tempered at 650°C.

Fig. 31. Fractograph of 2.5 cm air cooled 300-M. (a) As cooled, (b) tempered at 300°C, (c) tempered at 400°C, and (d) tempered at 450°C.

Fig. 32. Fractographs of 5.0 cm air cooled 300-M. (a) Tempered at 300°C and (b) tempered at 470°C.

Fig. 33. Fractographs of 10 cm air cooled 300-M. (a) As cooled, (b) tempered at 300°C, (c) tempered at 450°C and (d) tempered at 650°C.

Fig. 34. Fractographs of 15 cm air cooled 300-M. (a) As-cooled, (b) tempered at 300°C, (c) tempered at 450°C, and (d) tempered at 650°C.

Fig. 35. Fractographs of 2.5 cm air cooled 4340. (a) Tempered at 200°C, and (b) tempered at 275°C.

Fig. 36. Retained austenite level with and without load vs. tempering temperature for oil quenched 300-M.

Fig. 37. Retained austenite level with and without load vs. tempering temperature for 2.5 cm thick air cooled 300-M.

Fig. 38. Retained austenite level with and without load vs. tempering temperature for 5.0 cm thick air cooled 300-M.

Fig. 39. Retained austenite level with and without load vs. tempering temperature for 10 cm thick air cooled 300-M.

Fig. 40. Retained austenite level with and without load vs. tempering temperature for 15 cm thick air cooled 300-M.

Fig. 41. Retained austenite level with and without load vs. tempering temperature for 2.5 cm air cooled 4340.

Fig. 42. Generalized stress-strain behavior for lower strength austenite containing material. Austenite level vs. strain is also shown.

Fig. 43. Comparison of stress-strain behavior, and of austenite vs. strain behavior for the 400°C and 470°C tempered 5.0 cm thick air cooled 300-M.

Fig. 44. Optical micrographs of oil quenched 300-M (a) As-quenched, (b) tempered at 470°C, and (c) tempered at 650°C.

Fig. 45. Optical micrographs of 2.5 cm thick air cooled 300-M. (a) As cooled, (b) double tempered at 470°C, and (c) tempered at 650°C.

Fig. 46. Optical micrographs of 5.0 cm air cooled 300-M. (a) As-cooled, (b) tempered at 300°C, and (c) tempered at 470°C.

0 0 0 0 4 7 0 4 8 8 8

Fig. 47. Optical micrographs of 10 cm air cooled 300-M. (a) As-cooled, (b) tempered at 300°C, (c) tempered at 450°C, and (d) tempered at 650°C.

Fig. 48. Optical micrographs of 15 cm air cooled 300-M. (a) As cooled and (b) tempered at 650°C.

Fig. 49. Optical micrographs of 2.5 cm air cooled 300-M. (a) As cooled and (b) tempered at 650°C.

Fig. 50. Transmission electron microscopy showing oil quenched 300-M structure. (a) Bright field image showing dislocated lath structure. (b) Dark field image revealing lath boundary films of austenite; $[111]_\gamma \parallel [110]_\alpha$.

Fig. 51. Transmission electron micrograph (a) revealing precipitation in a lath with heavy dislocation tangles also revealed, and (b) showing evidence of twinning.

Fig. 52. Transmission electron micrograph revealing the structure of the 2.5 cm air cooled material. (a) Bright field image revealing mixed microstructure. (b) Dark field image reveals austenite morphology. Associated SAD shows austenite-ferrite pattern; $[111]_\gamma \parallel [110]_\alpha$.

Fig. 53. Transmission electron microscopy revealing the structure of 300-M, 2.5 cm thick, air cooled (a) Bright field image reveals mixed microstructure including twinned areas. (b) Dark field image reveals wavy austenite retained after cooling.

Fig. 54. Microstructure of 5.0 cm thick air cooled 300-M as revealed by TEM. (a) Bright field image (b) Dark field image of austenite retained after cooling.

Fig. 55. Transmission electron microscopy of 10 cm air cooled 300-M. (a) Bright field image showing structure (b) Dark field image revealing austenite; $[111]_\gamma \parallel [110]_\alpha$.

Fig. 56. Transmission electron microscopy of air cooled 300-M with (a) bright field image of 10 cm thickness and (b) bright field image of 15 cm thickness.

Fig. 57. Structure of 15 cm thick air cooled 300-M revealed by TEM. (a) Bright field image and (b) dark field image of austenite.

Fig. 58. Transmission electron microscopy showing (a) internal precipitation in oil quenched 300-M tempered at 300°C, and (b) lath boundary precipitation in oil quenched 300-M tempered at 470°C.

Fig. 59. Transmission electron microscopy revealing structural features in 5.0 cm thick air cooled 300-M tempered at 300°C. (a) Bright field image and (b) dark field image revealing retained austenite, still present after tempering; $[111]_\gamma \parallel [110]_\alpha$.

Fig. 60. Transmission electron microscopy showing structure in 5.0 cm cooled 300-M tempered at 470°C. (a) Bright field image and (b) dark field image of austenite; $[111]_\gamma$, $[011]_\alpha$, $[01\bar{2}]_{Fe_3C}$ zones.

0 0 0 0 4 7 0 4 8 8 4

Fig. 61. Transmission electron microscopy of 470°C temper structure in 5.0 cm thick air cool 300-M; $(1\bar{1}1)_\alpha$ orientation.

Fig. 62. Normalized yield strength and fracture toughness vs. cooling rate. All material in 300°C temper condition.

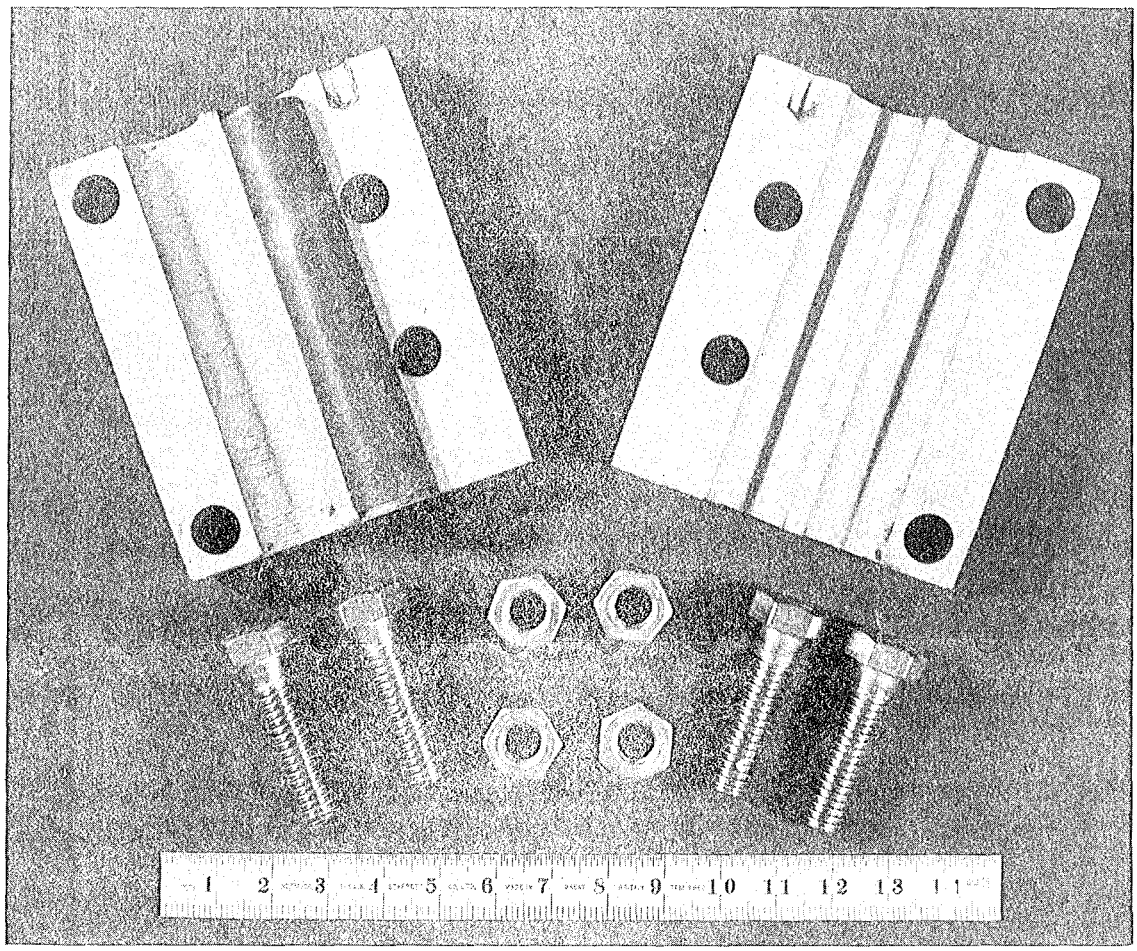

XBB 760-10001

Fig. 1.

0 0 0 0 4 7 0 4 7 8 5

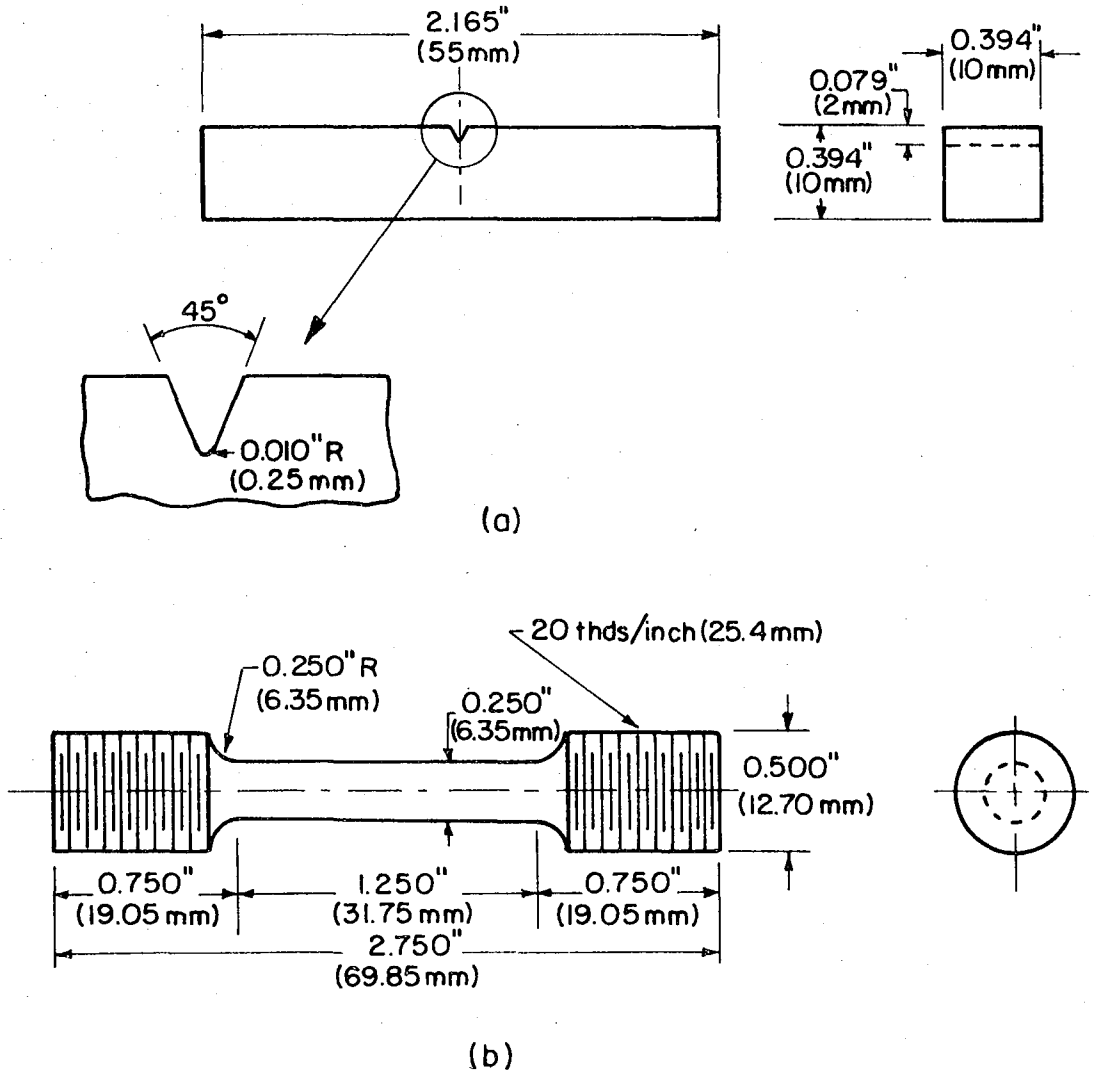

XBL 736-6280

Fig. 2.

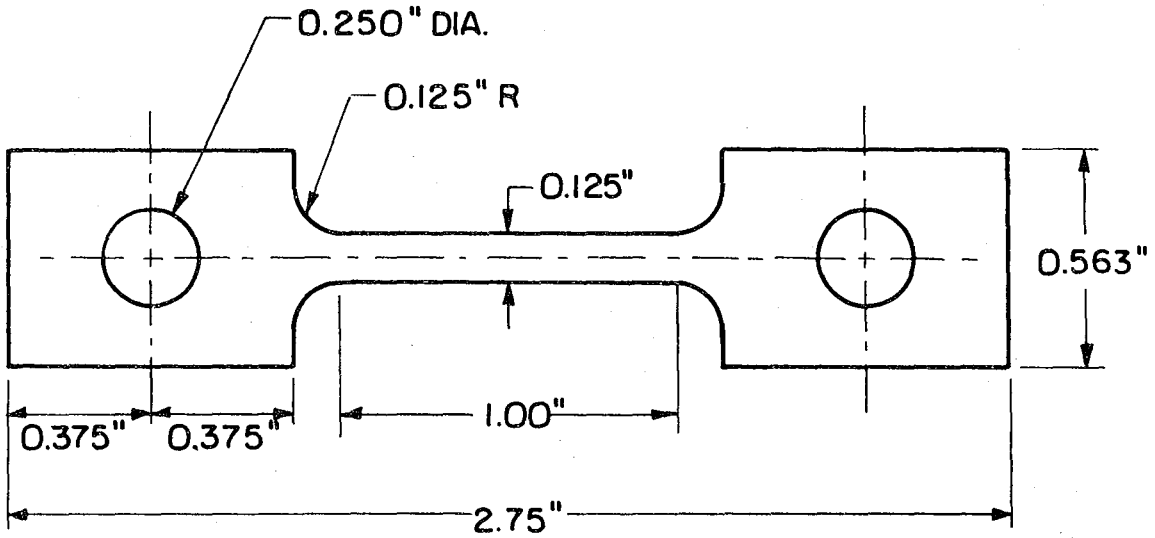

XBL737-6444

Fig. 3.

8 0 0 0 4 7 0 4 8 9 9

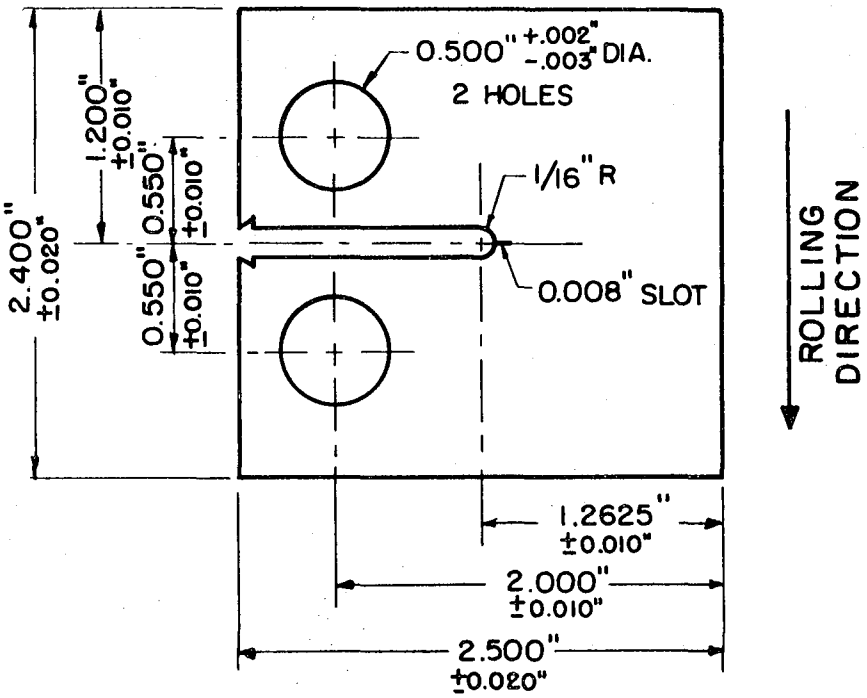

FRACTURE TOUGHNESS SPECIMEN

XBL 737-6465

Fig. 4.

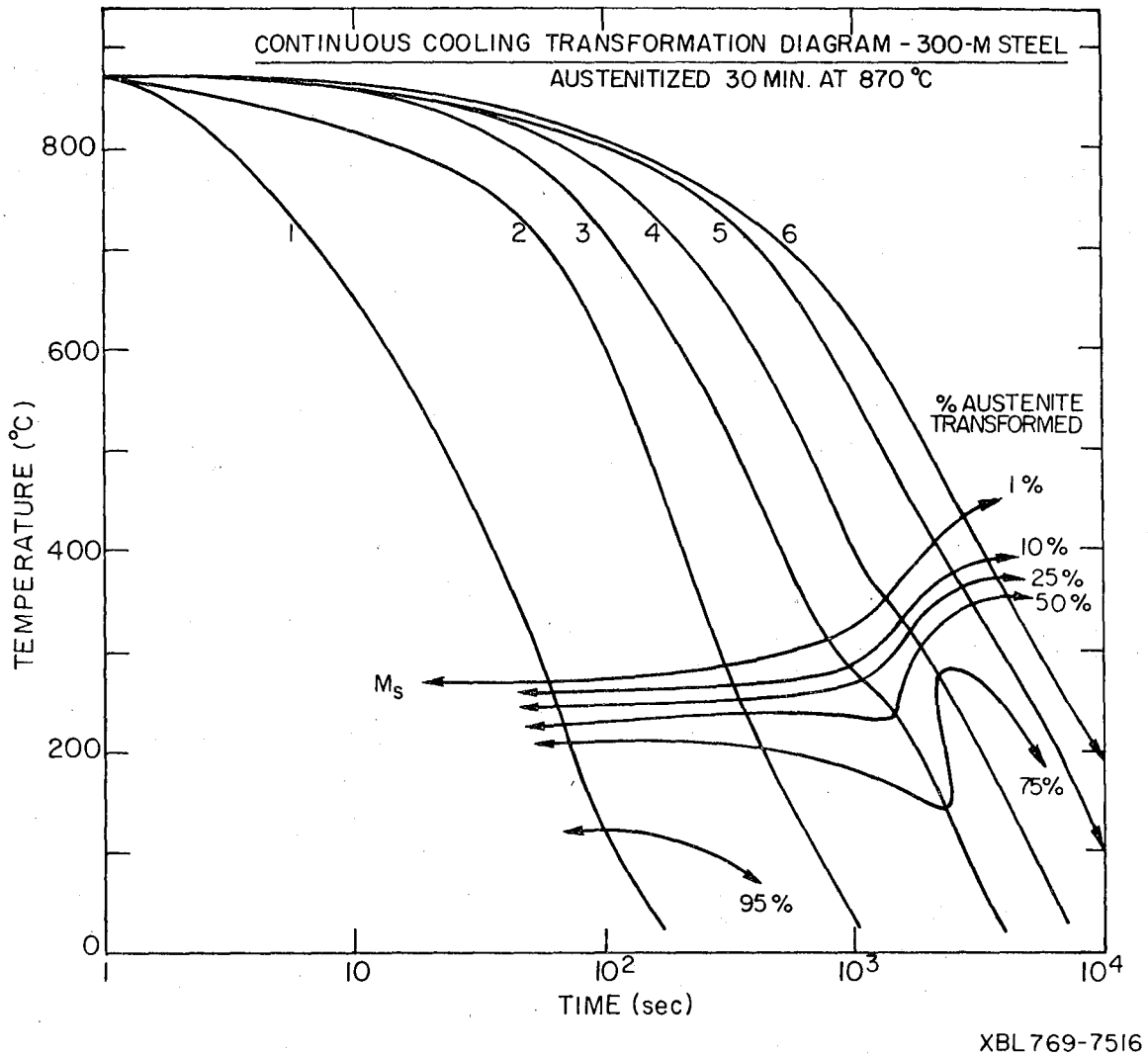
CONTINUOUS COOLING TRANSFORMATION DIAGRAM - 300-M STEEL
AUSTENITIZED 30 MIN. AT 870 °C
TEMPERATURE (°C)
800
600
400
200
0
1
10
10^2
10^3
10^4
TIME (sec)
1
2
3
4
5
6
% AUSTENITE TRANSFORMED
1%
10%
25%
50%
75%
95%
M_s
XBL 769-7516

Fig. 5.

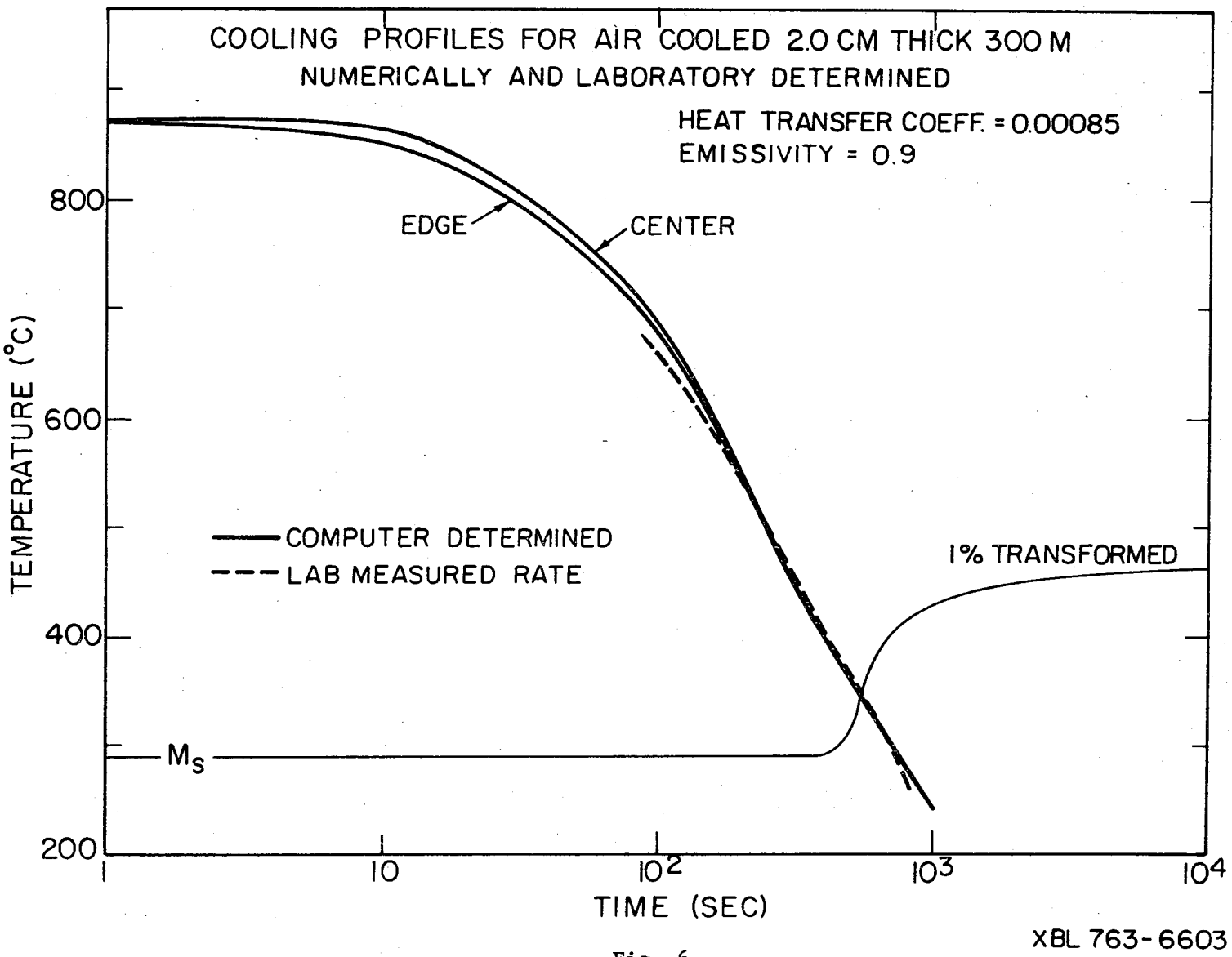

XBL 763-6603

Fig. 6.

0 0 0 4 7 0 8 8 8

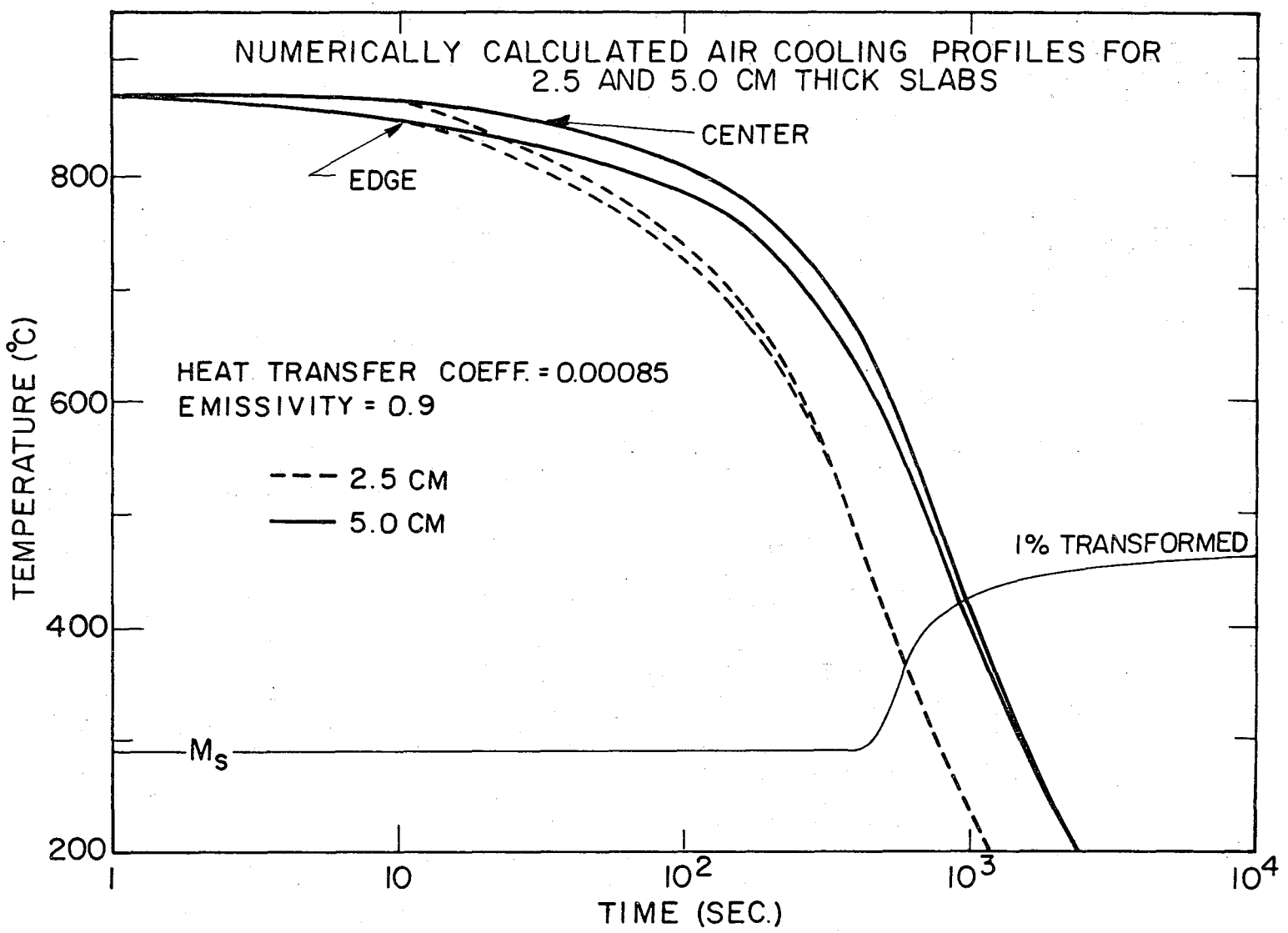

XBL 763-6605

Fig. 7.

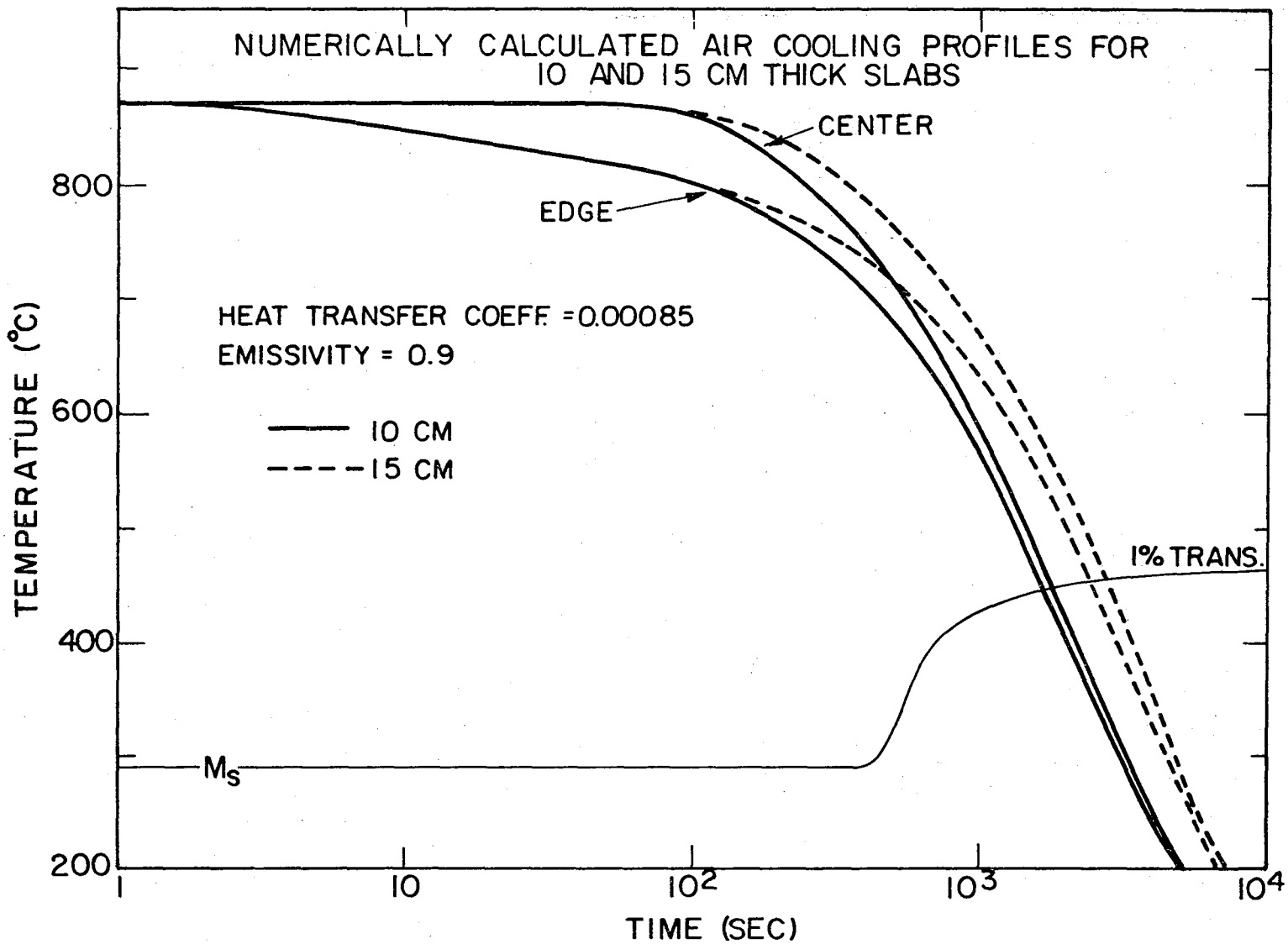

XBL 763-6604

Fig. 8.

0 0 0 0 4 7 7 0 0 4 8 7 9 9 8 1

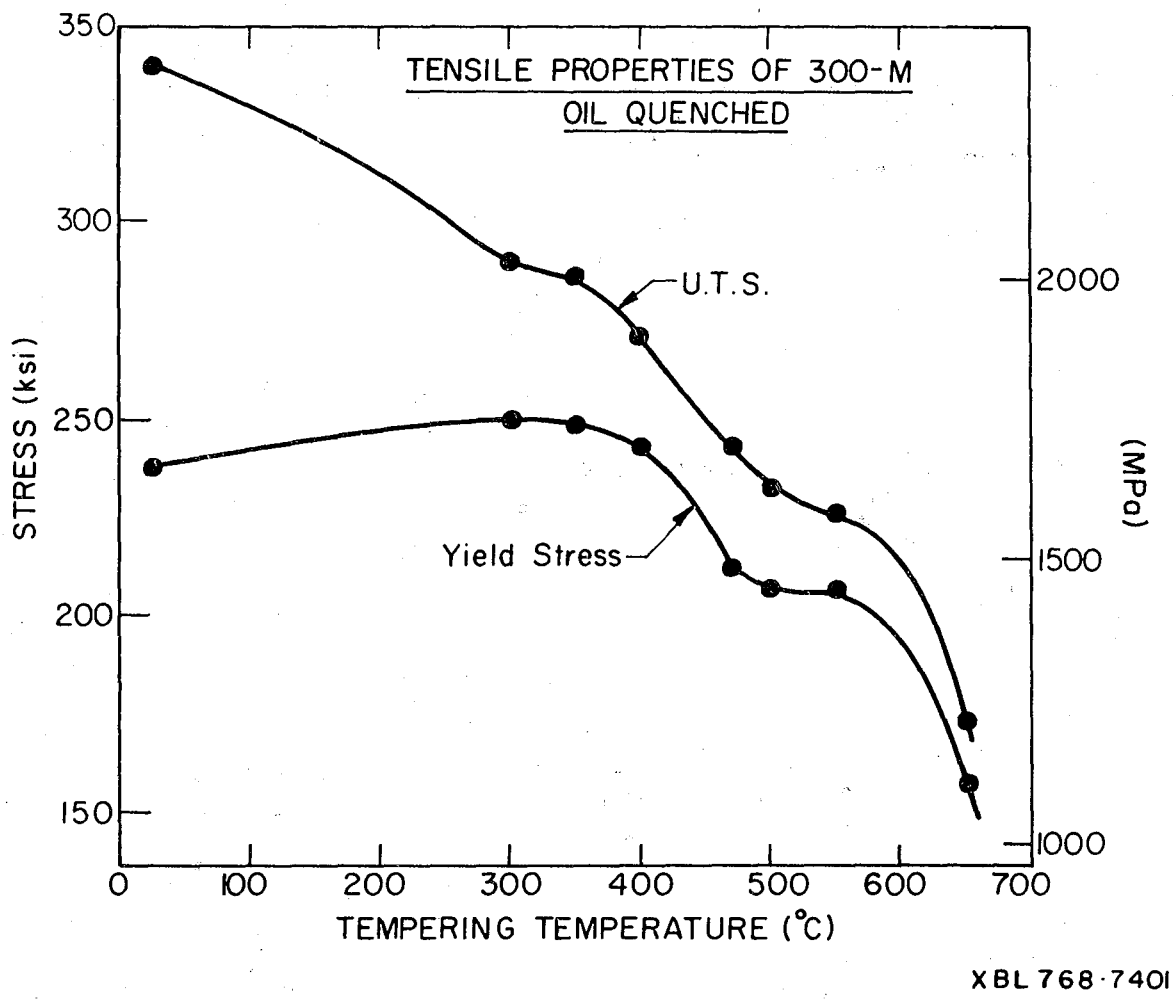
TENSILE PROPERTIES OF 300-M
OIL QUENCHED
U.T.S.
Yield Stress
STRESS (ksi)
(MPa)
350
300
250
200
150
2000
1500
1000
0
100
200
300
400
500
600
700
TEMPERING TEMPERATURE (°C)
XBL 768-7401

Fig. 9.

0 0 0 0 4 7 0 0 1 0 8 2

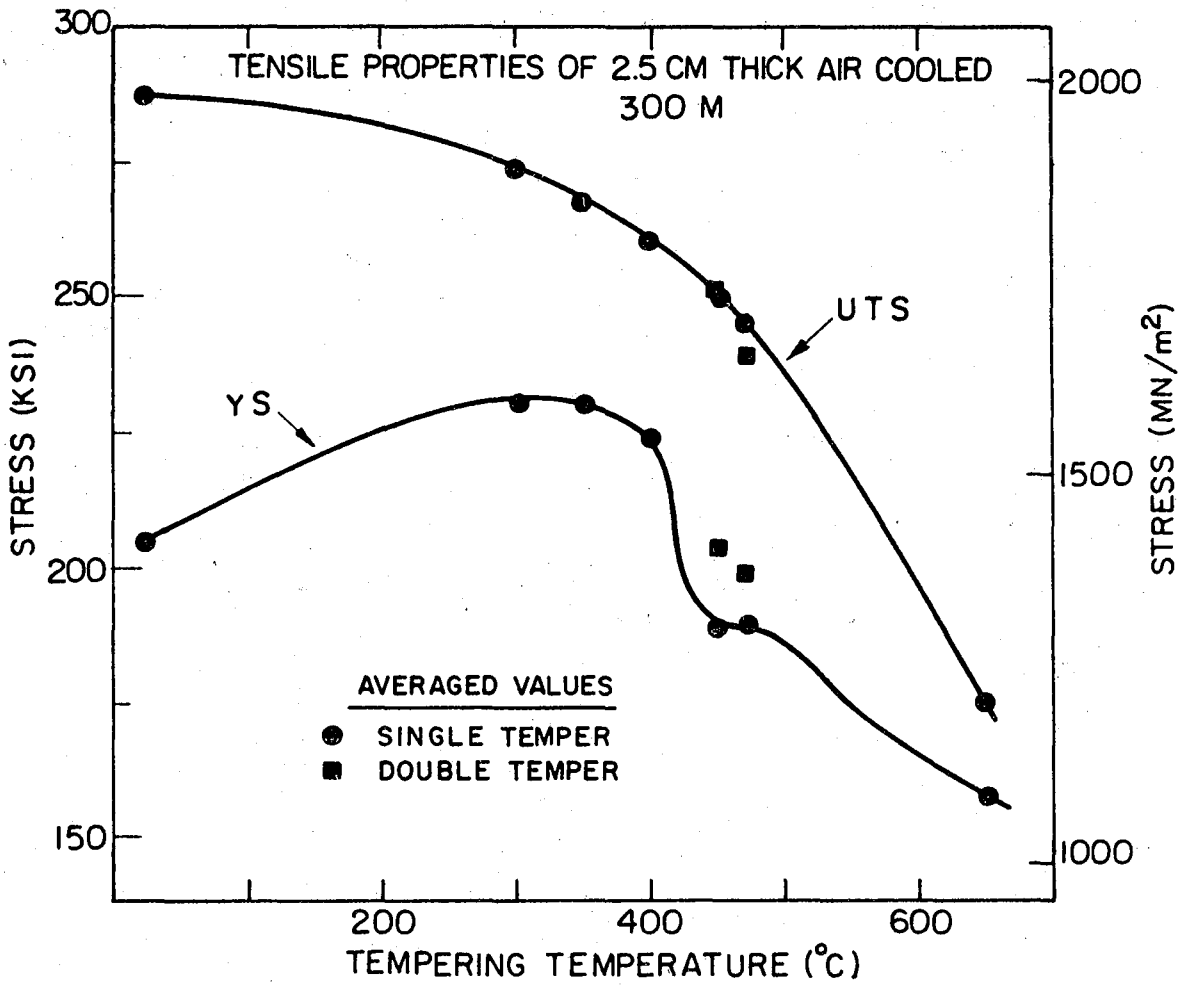

XBL 763-6613 A

Fig. 10.

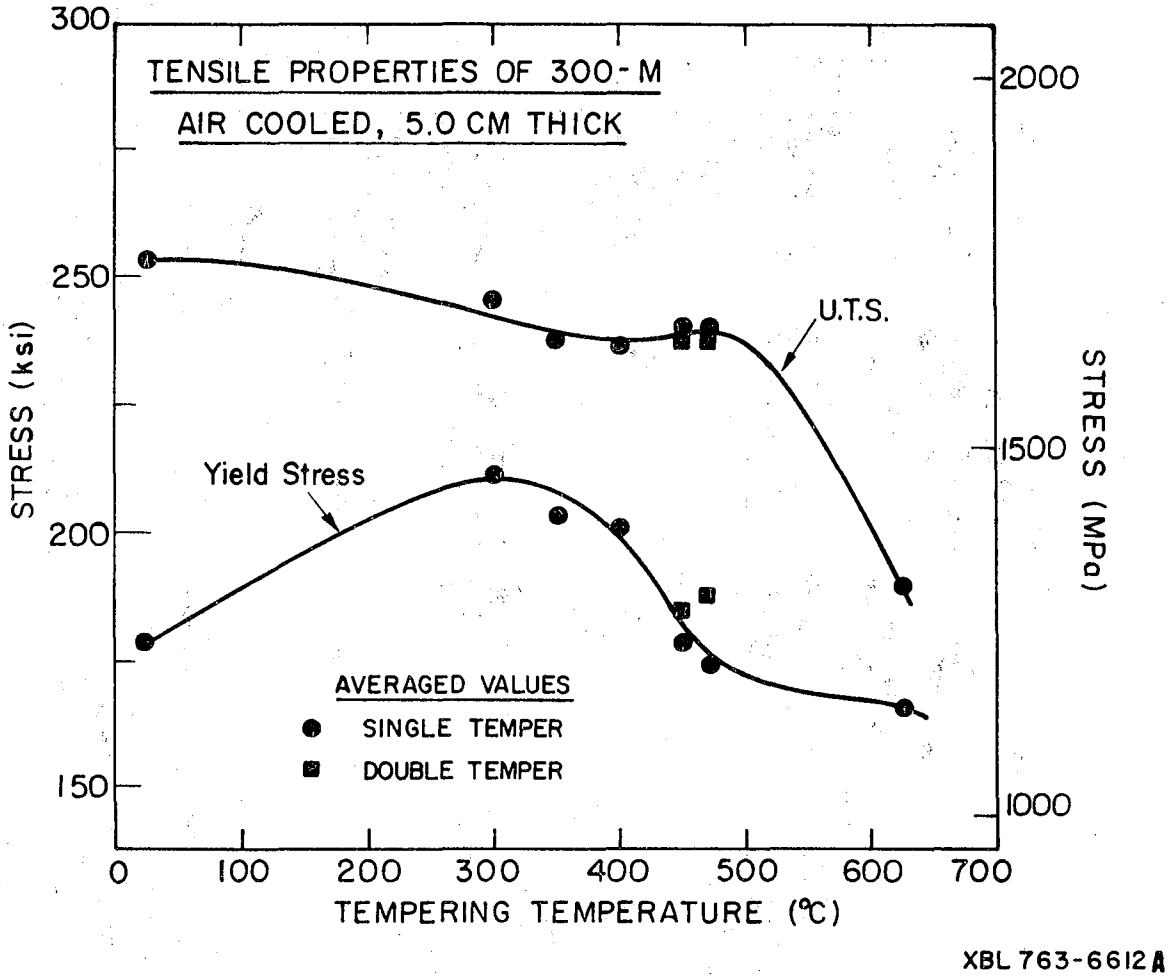
TENSILE PROPERTIES OF 300-M
AIR COOLED, 5.0 CM THICK
U.T.S.
Yield Stress
AVERAGED VALUES
SINGLE TEMPER
DOUBLE TEMPER
STRESS (ksi)
STRESS (MPa)
TEMPERING TEMPERATURE (°C)
300
250
200
150
2000
1500
1000
0
100
200
300
400
500
600
700
XBL 763-6612A

Fig. 11.

0 0 0 0 4 7 0 0 1 8 8

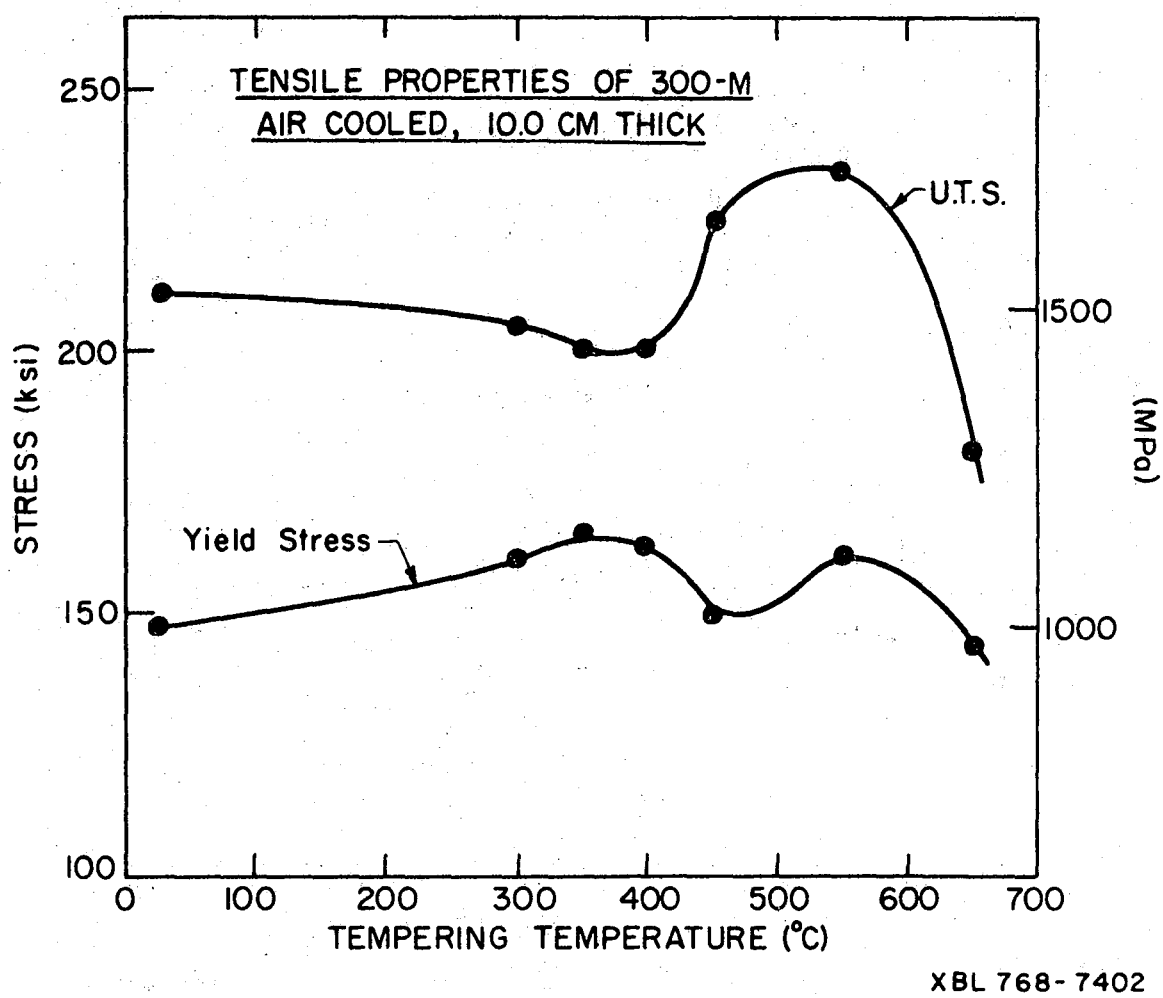

Fig. 12.

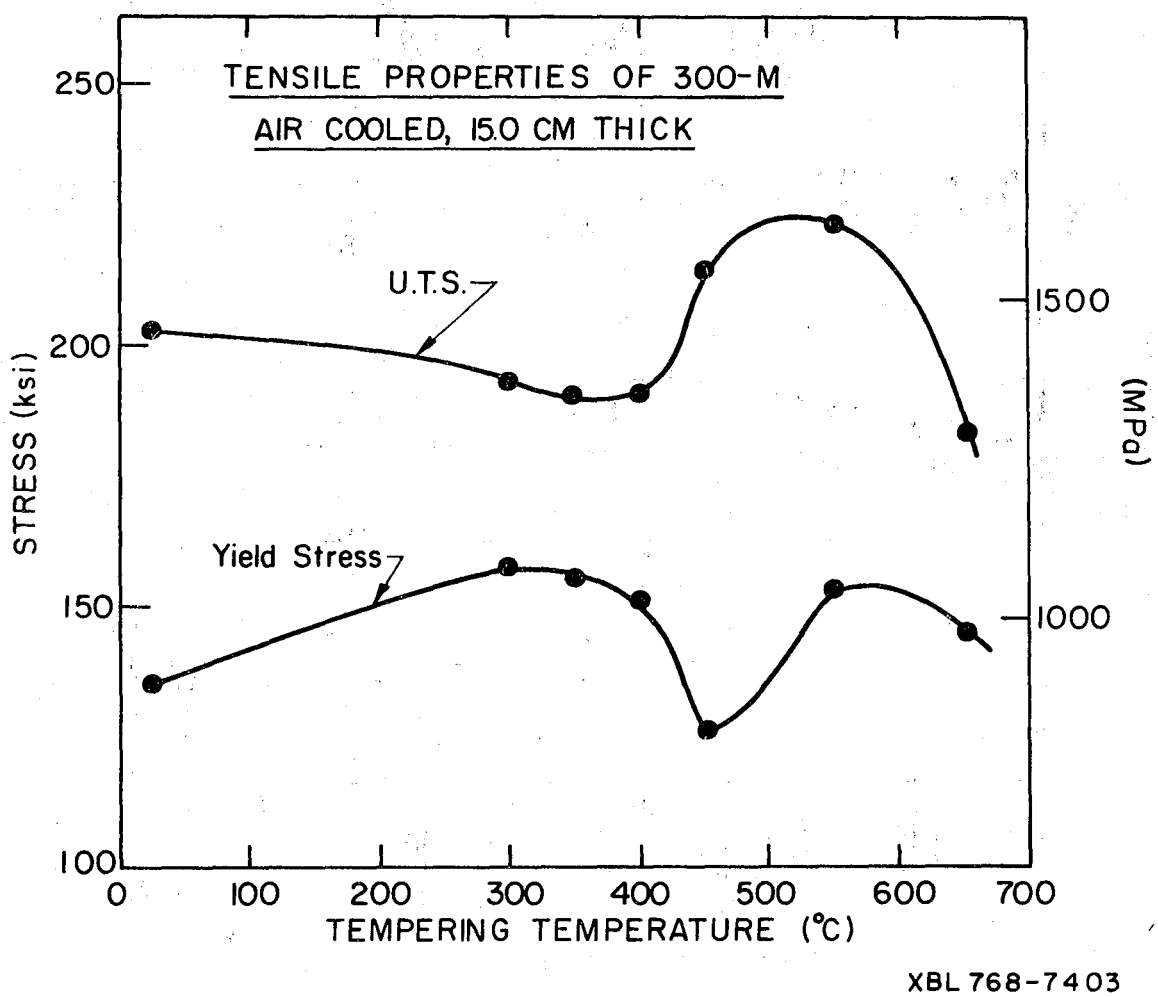
TENSILE PROPERTIES OF 300-M
AIR COOLED, 15.0 CM THICK
U.T.S.
Yield Stress
STRESS (ksi)
(MPa)
250
200
150
100
1500
1000
0
100
200
300
400
500
600
700
TEMPERING TEMPERATURE (°C)
XBL 768-7403

Fig. 13.

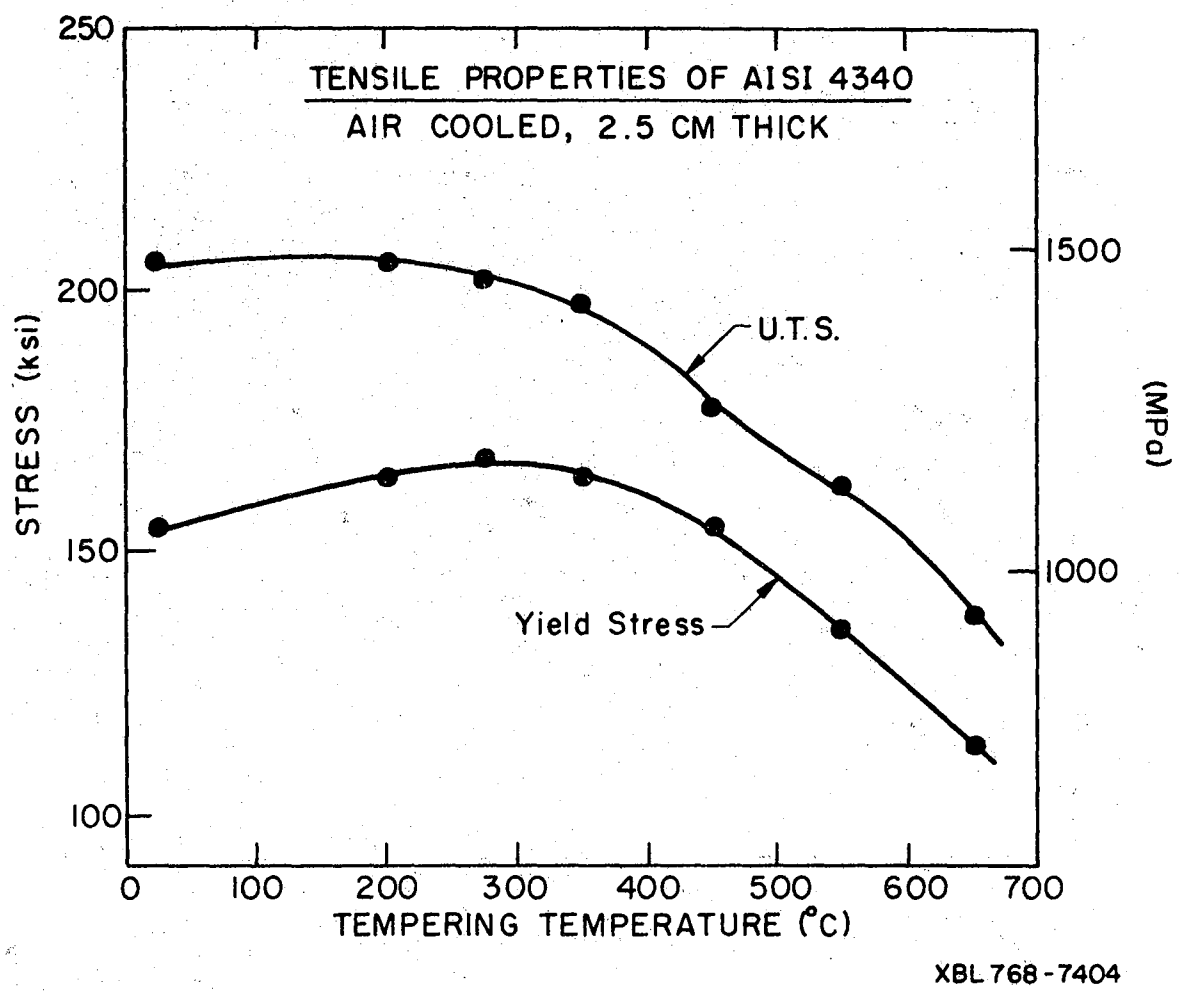
TENSILE PROPERTIES OF AISI 4340
AIR COOLED, 2.5 CM THICK
250
200
150
100
STRESS (ksi)
1500
1000
(MPa)
U.T.S.
Yield Stress
0
100
200
300
400
500
600
700
TEMPERING TEMPERATURE (°C)
XBL 768-7404

Fig. 14.

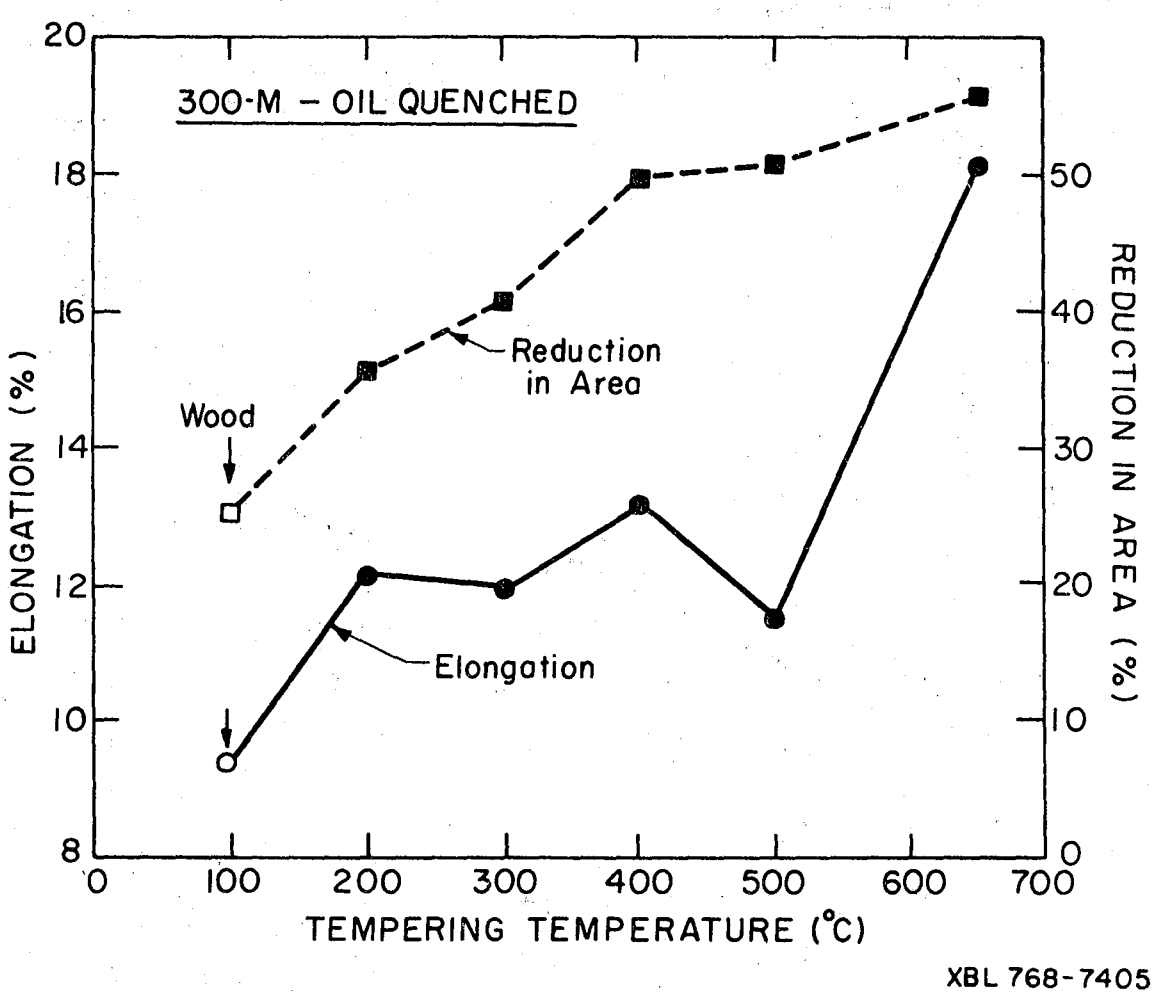
300-M – OIL QUENCHED
Reduction in Area
Wood
Elongation
ELONGATION (%)
REDUCTION IN AREA (%)
TEMPERING TEMPERATURE (°C)
20
18
16
14
12
10
8
50
40
30
20
10
0
0
100
200
300
400
500
600
700
XBL 768-7405

Fig. 15.

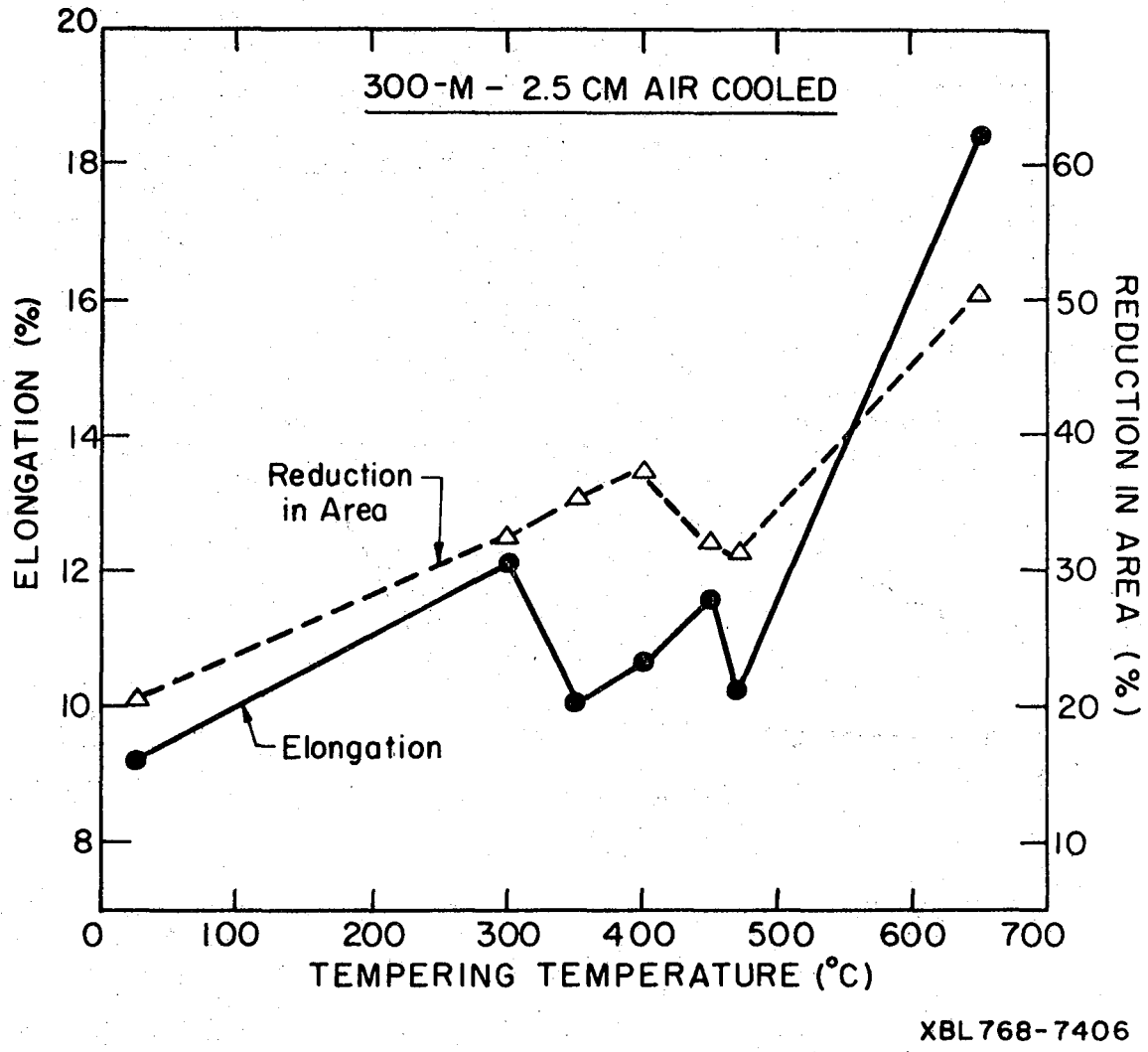
300-M - 2.5 CM AIR COOLED
ELONGATION (%)
REDUCTION IN AREA (%)
TEMPERING TEMPERATURE (°C)
Reduction in Area
Elongation
20
18
16
14
12
10
8
60
50
40
30
20
10
0
100
200
300
400
500
600
700
XBL 768-7406

Fig. 16.

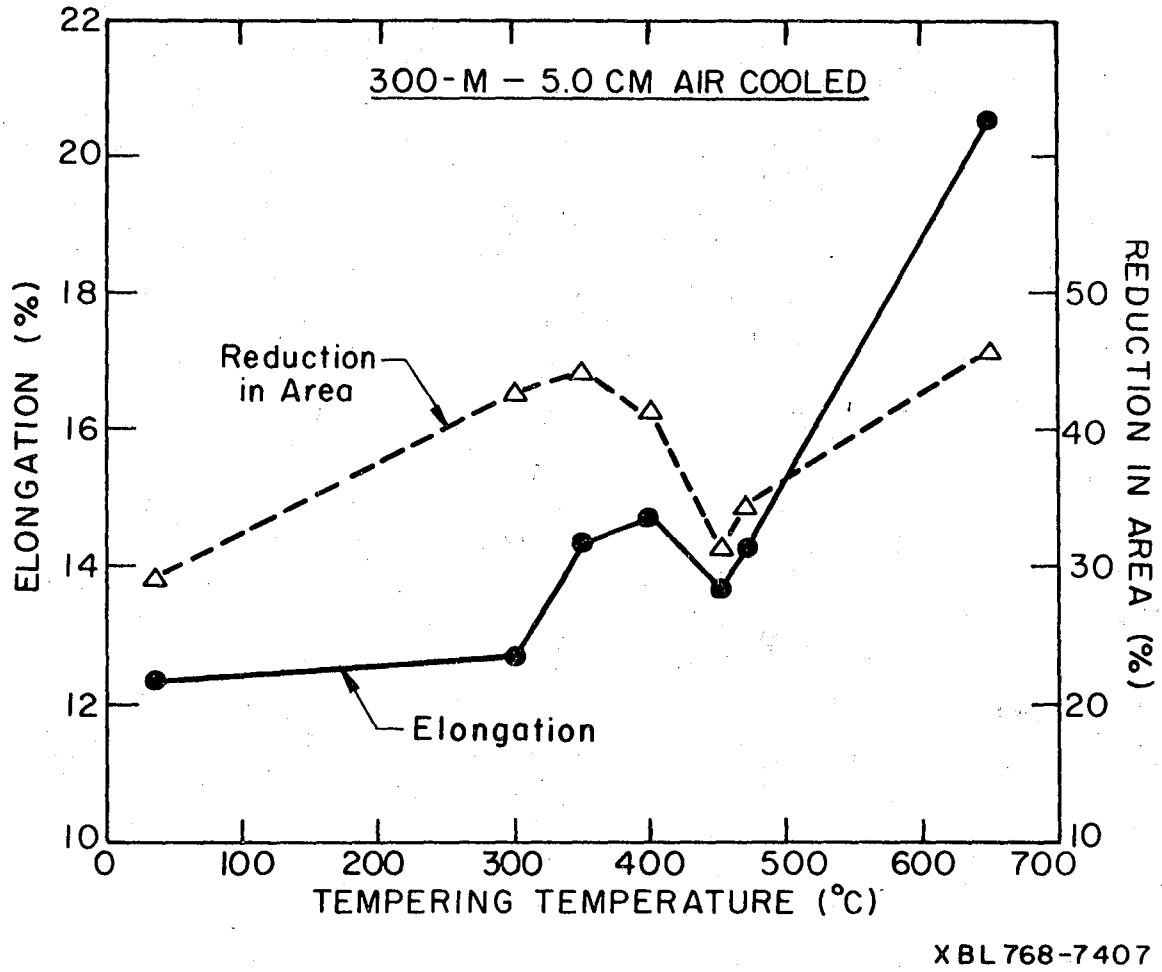
300-M – 5.0 CM AIR COOLED
ELONGATION (%)
REDUCTION IN AREA (%)
TEMPERING TEMPERATURE (°C)
Reduction in Area
Elongation
22
20
18
16
14
12
10
50
40
30
20
10
0
100
200
300
400
500
600
700
XBL768-7407

Fig. 17.

0 0 0 0 4 7 0 0 4 8 9 3

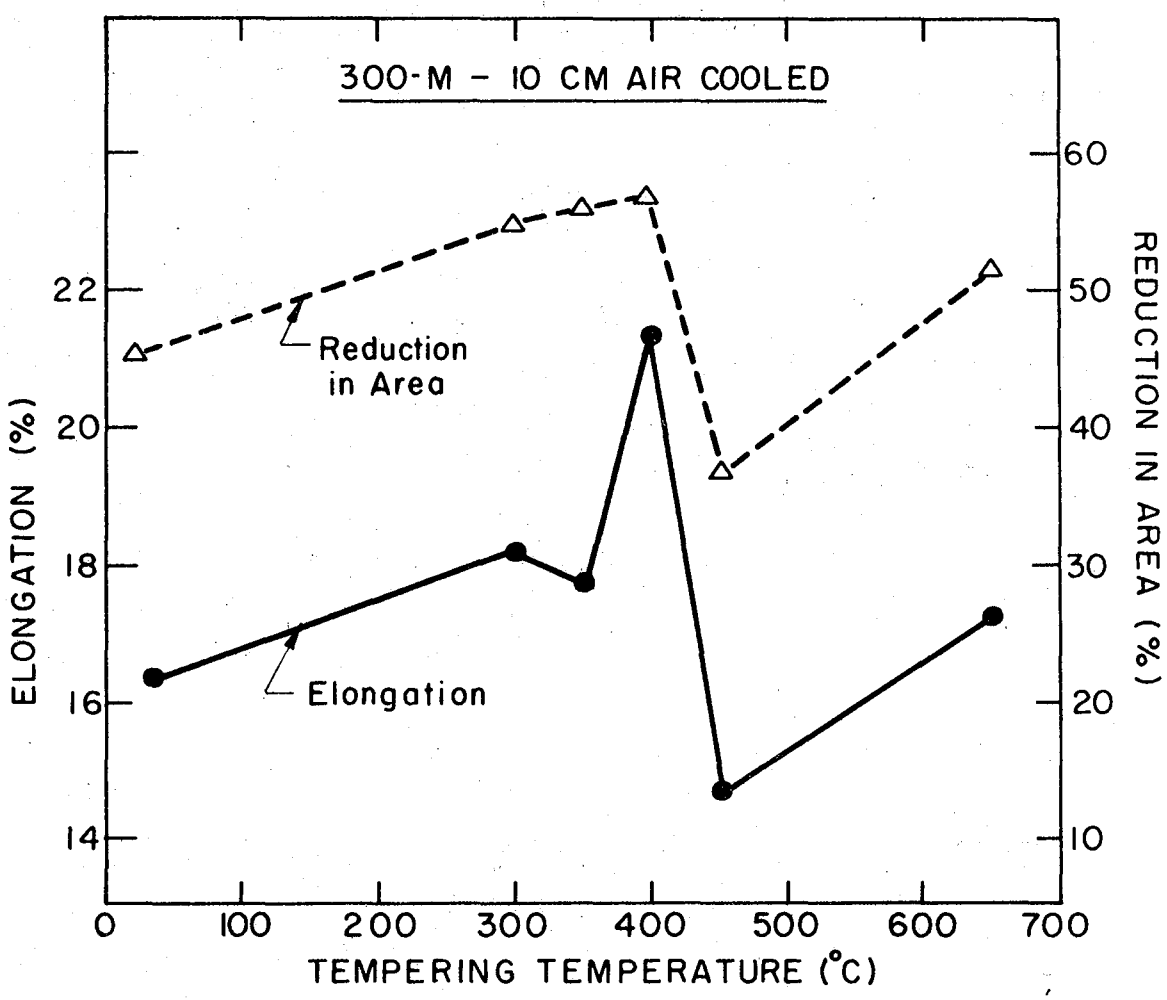

XBL768-7462

Fig. 18.

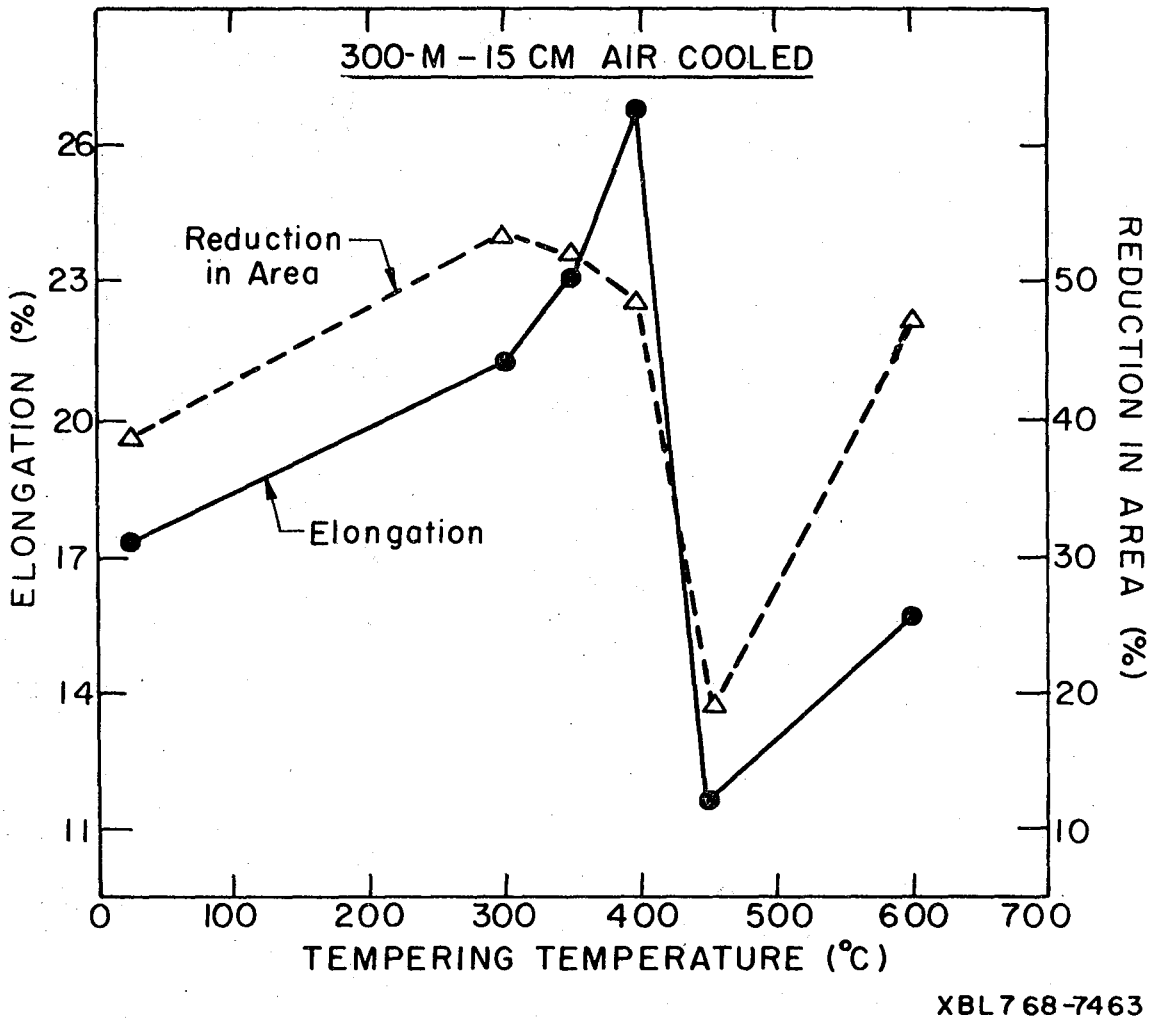
300-M - 15 CM AIR COOLED
Reduction in Area
Elongation
ELONGATION (%)
REDUCTION IN AREA (%)
TEMPERING TEMPERATURE (°C)
26
23
20
17
14
11
50
40
30
20
10
0
100
200
300
400
500
600
700
XBL768-7463

Fig. 19.

0 0 0 0 4 7 0 0 0 8 4

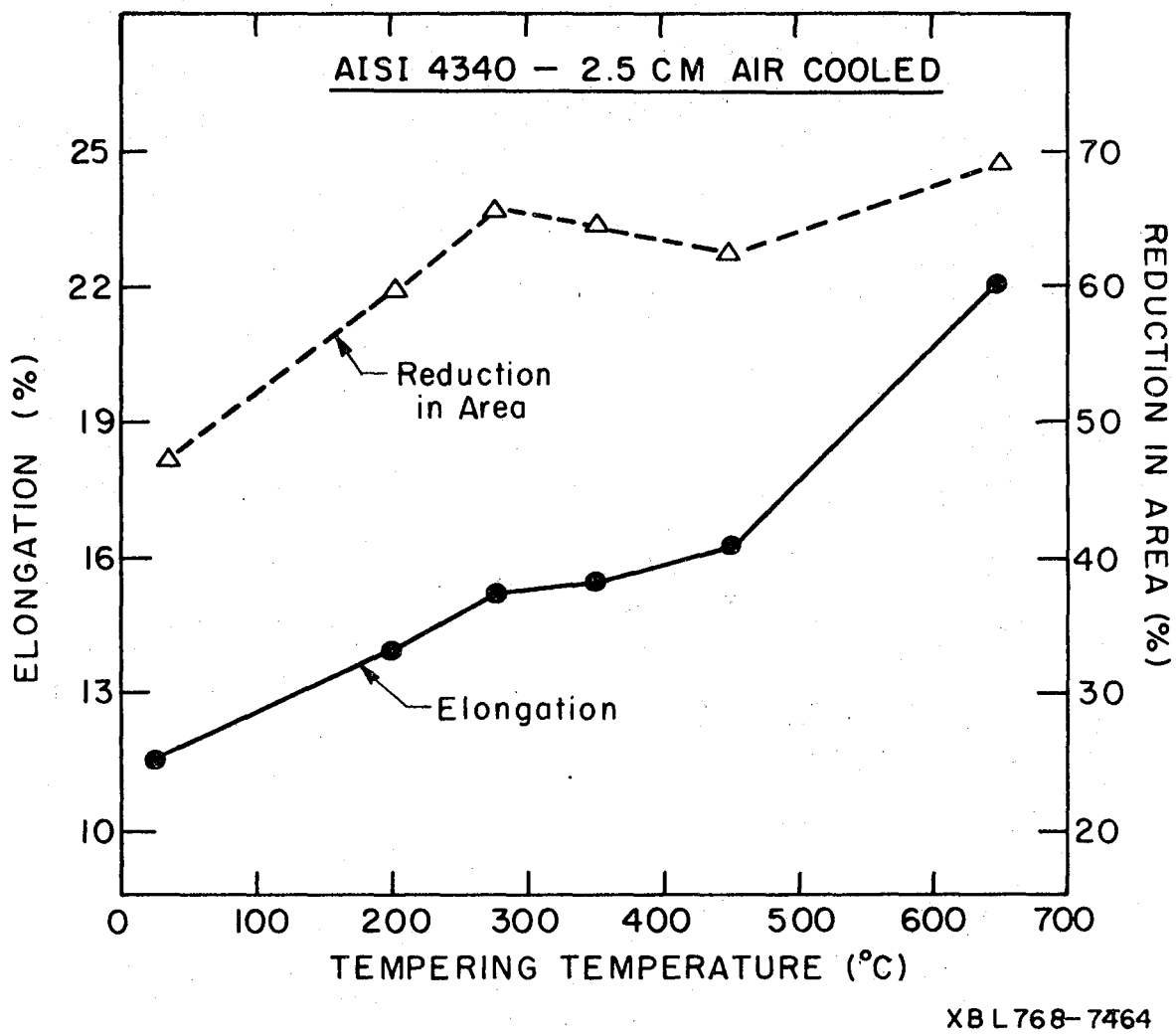

Fig. 20.

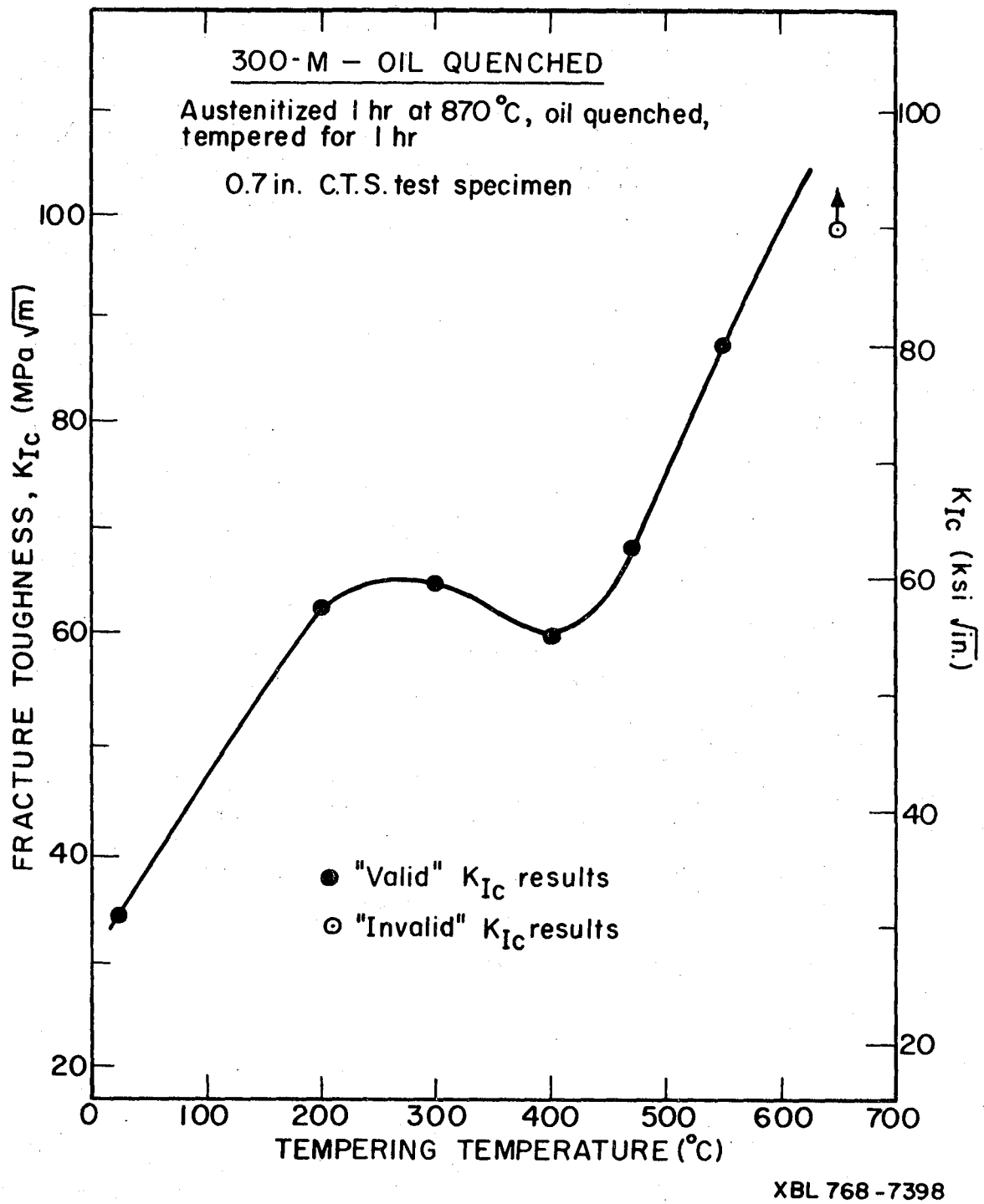
300-M – OIL QUENCHED
Austenitized 1 hr at 870 °C, oil quenched, tempered for 1 hr
0.7 in. C.T.S. test specimen
FRACTURE TOUGHNESS, K_{Ic} (MPa $\sqrt{m}$)
K_{Ic} (ksi $\sqrt{in.}$)
TEMPERING TEMPERATURE (°C)
"Valid" K_{Ic} results
"Invalid" K_{Ic} results
XBL 768-7398

Fig. 21.

0 0 0 0 0 4 7 0 0 8 9 5

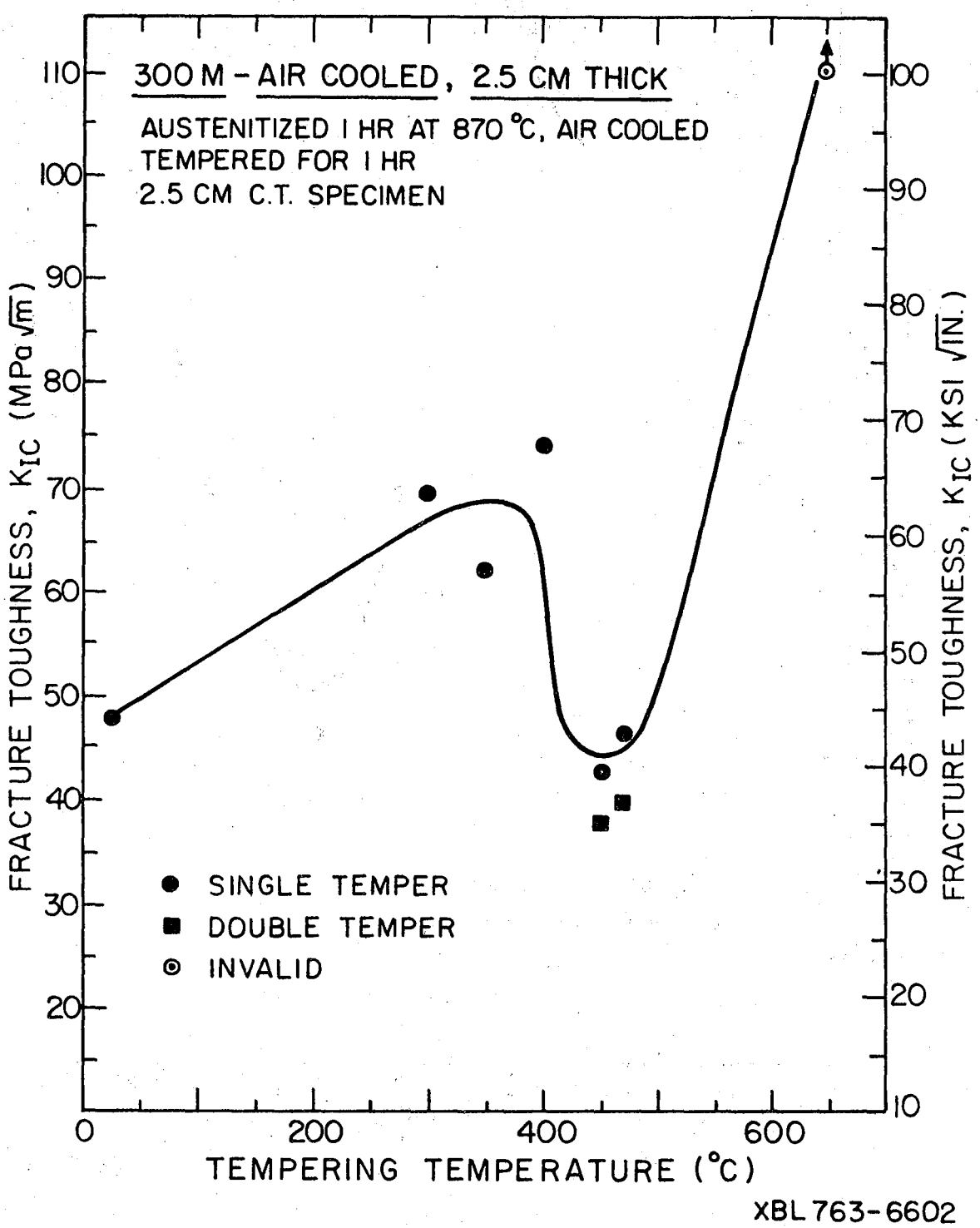

Fig. 22.

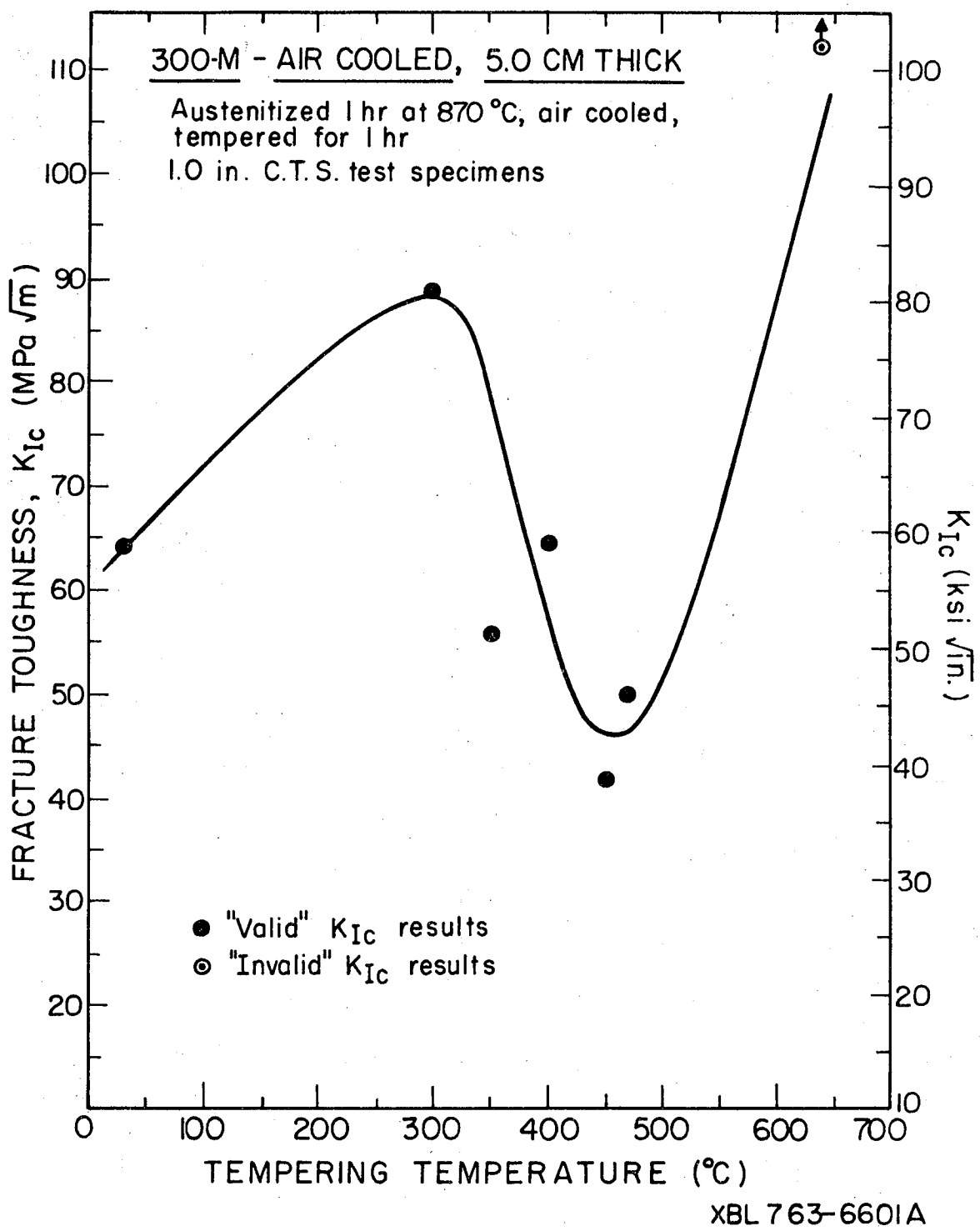
300-M - AIR COOLED, 5.0 CM THICK
Austenitized 1 hr at 870 °C, air cooled, tempered for 1 hr
1.0 in. C.T.S. test specimens
FRACTURE TOUGHNESS, K_{Ic} (MPa $\sqrt{m}$)
K_{Ic} (ksi $\sqrt{in.}$)
TEMPERING TEMPERATURE (°C)
"Valid" K_{Ic} results
"Invalid" K_{Ic} results
XBL 763-6601A

Fig. 23.

0 0 0 0 0 4 7 0 4 7 8 9
0 0 0 0 0 4 7 0 0 8 9 6

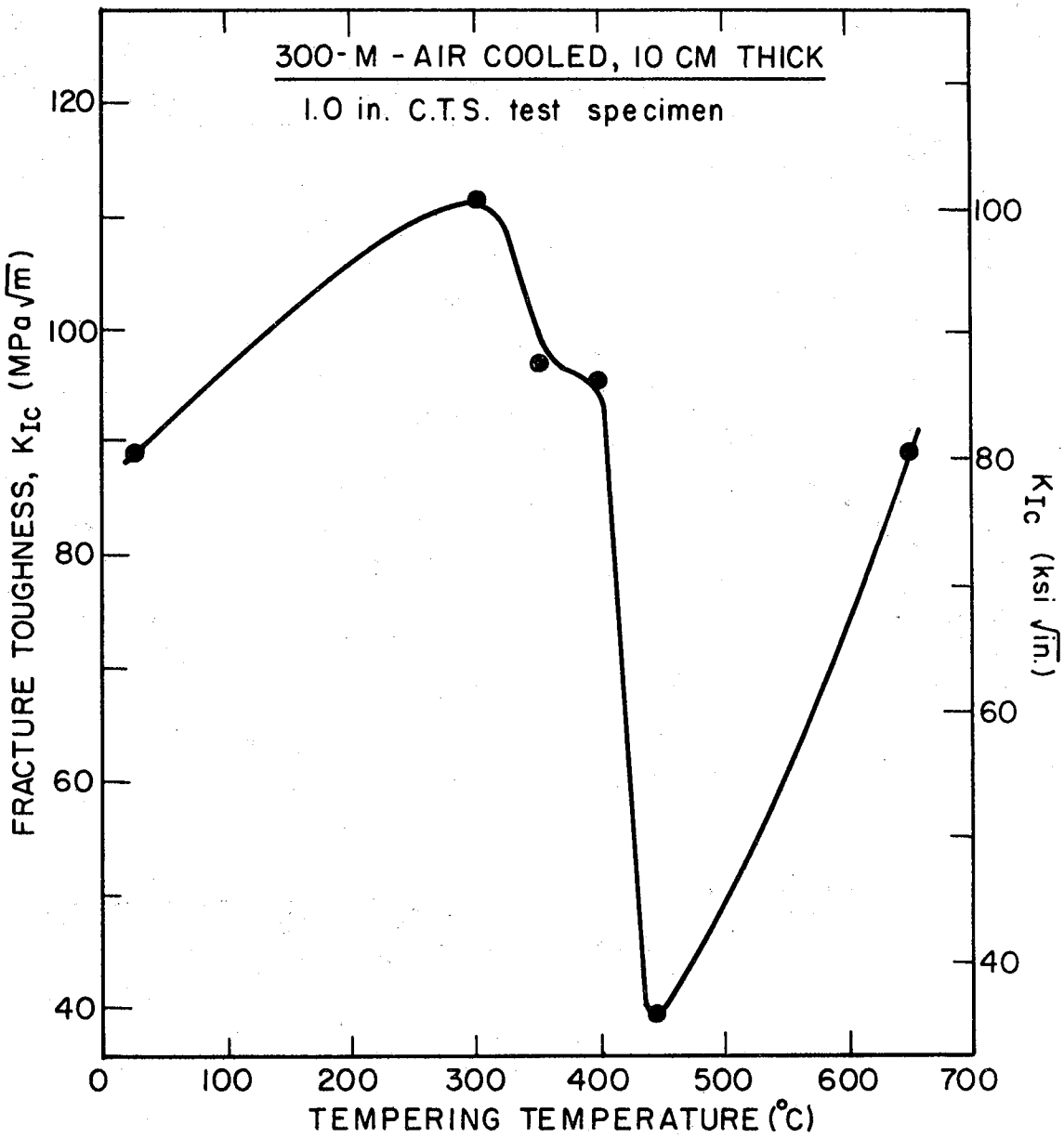

XBL 768-7399

Fig. 24.

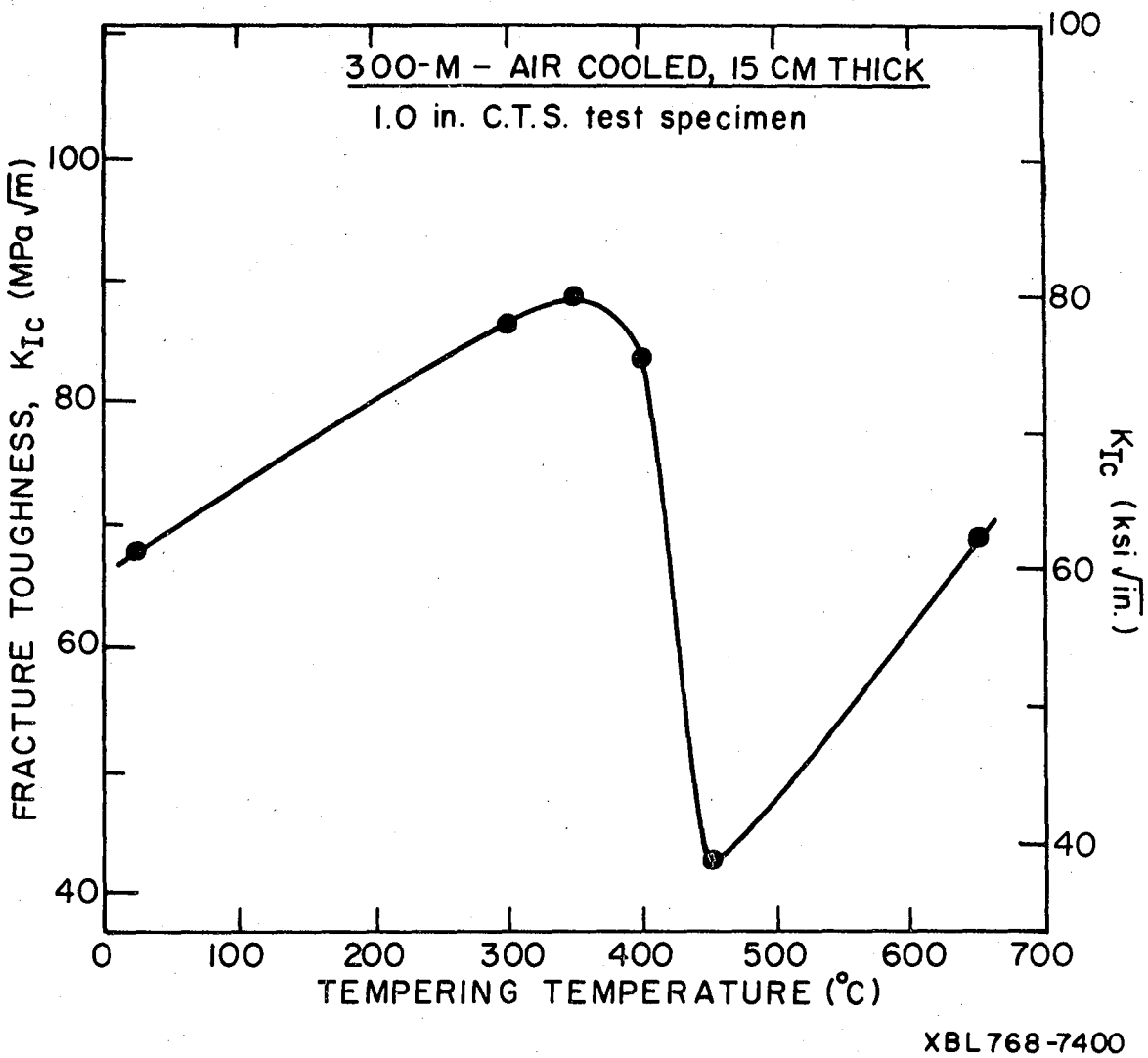
300-M - AIR COOLED, 15 CM THICK
1.0 in. C.T.S. test specimen
FRACTURE TOUGHNESS, K_{Ic} (MPa $\sqrt{m}$)
K_{Ic} (ksi $\sqrt{in.}$)
100
80
60
40
0
100
200
300
400
500
600
700
TEMPERING TEMPERATURE (°C)
XBL 768-7400

Fig. 25.

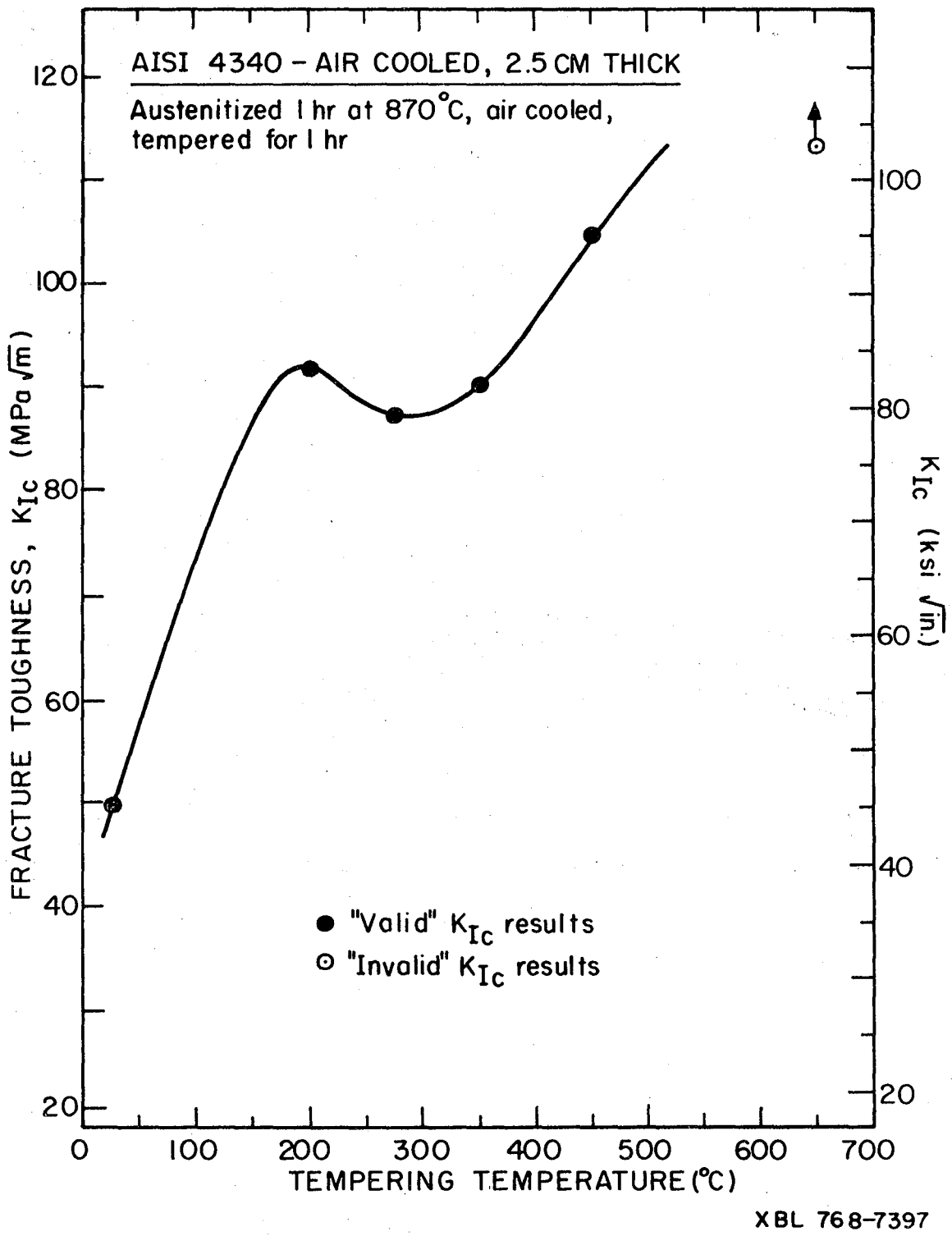
AISI 4340 - AIR COOLED, 2.5 CM THICK
Austenitized 1 hr at 870°C, air cooled, tempered for 1 hr
FRACTURE TOUGHNESS, K_{Ic} (MPa $\sqrt{m}$)
K_{Ic} (ksi $\sqrt{in.}$)
TEMPERING TEMPERATURE (°C)
"Valid" K_{Ic} results
"Invalid" K_{Ic} results
120
100
80
60
40
20
0
100
200
300
400
500
600
700
XBL 768-7397

Fig. 26.

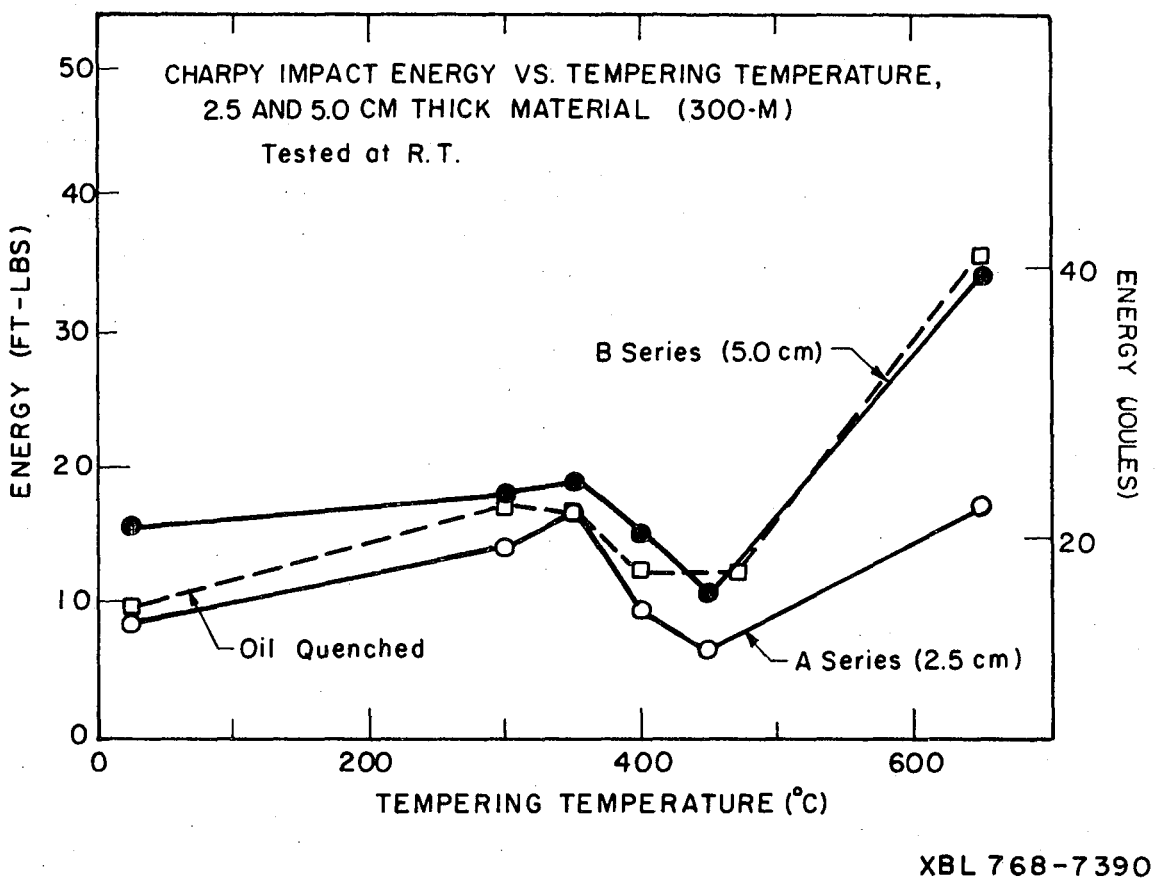
CHARPY IMPACT ENERGY VS. TEMPERING TEMPERATURE,
2.5 AND 5.0 CM THICK MATERIAL (300-M)
Tested at R.T.
ENERGY (FT-LBS)
ENERGY (JOULES)
B Series (5.0 cm)
Oil Quenched
A Series (2.5 cm)
TEMPERING TEMPERATURE (°C)
0
10
20
30
40
50
0
200
400
600
20
40
XBL 768-7390

Fig. 27.

0 0 0 0 4 7 0 0 8 9 8

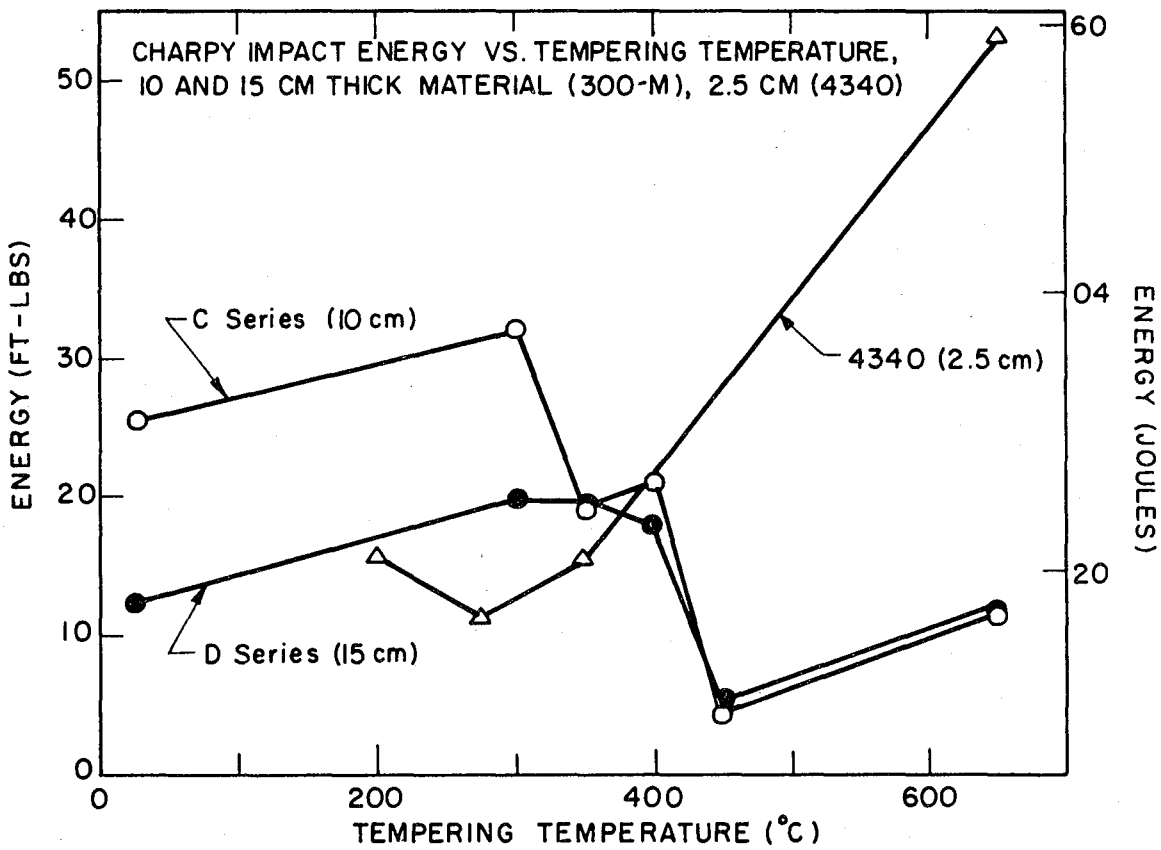

XBL 768-7391

Fig. 28.

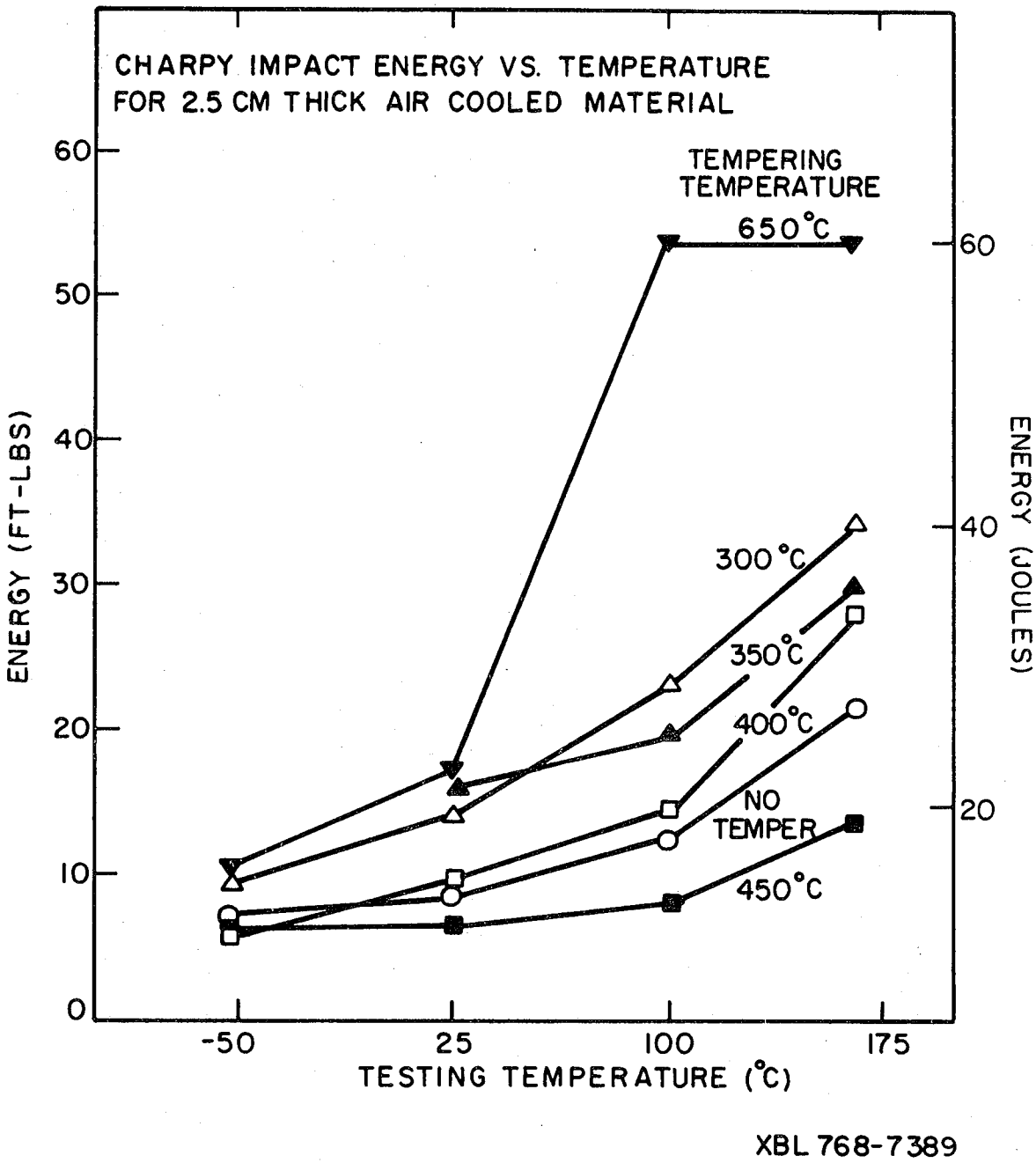
CHARPY IMPACT ENERGY VS. TEMPERATURE
FOR 2.5 CM THICK AIR COOLED MATERIAL
TEMPERING
TEMPERATURE
650°C
300°C
350°C
400°C
NO
TEMPER
450°C
ENERGY (FT-LBS)
ENERGY (JOULES)
TESTING TEMPERATURE (°C)
0
10
20
30
40
50
60
-50
25
100
175
20
40
60
XBL 768-7389

Fig. 29.

0 0 0 0 4 7 0 0 8 9 9

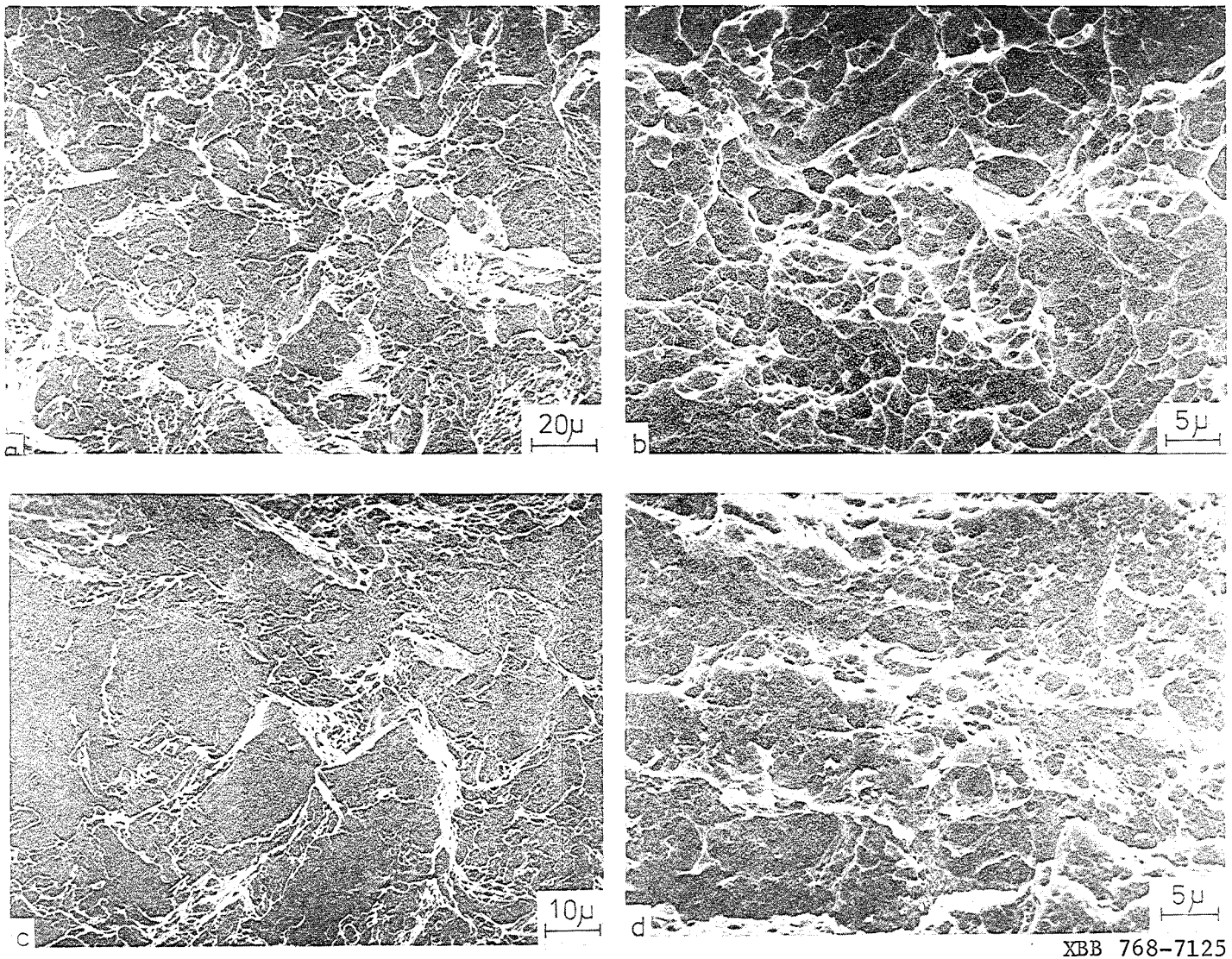

XBB 768-7125

Fig. 30.

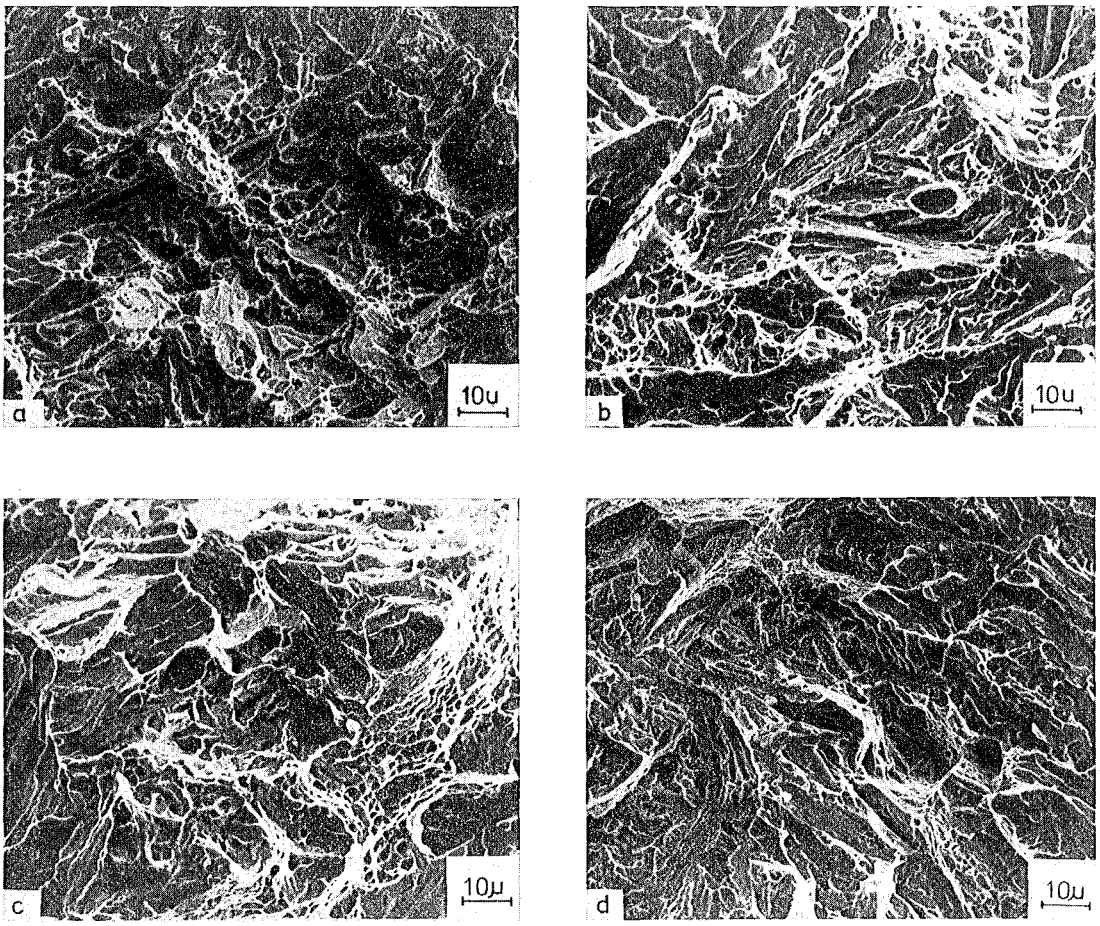

XBB 768-7625

Fig. 31.

0 0 0 0 4 7 0 4 7 8 0

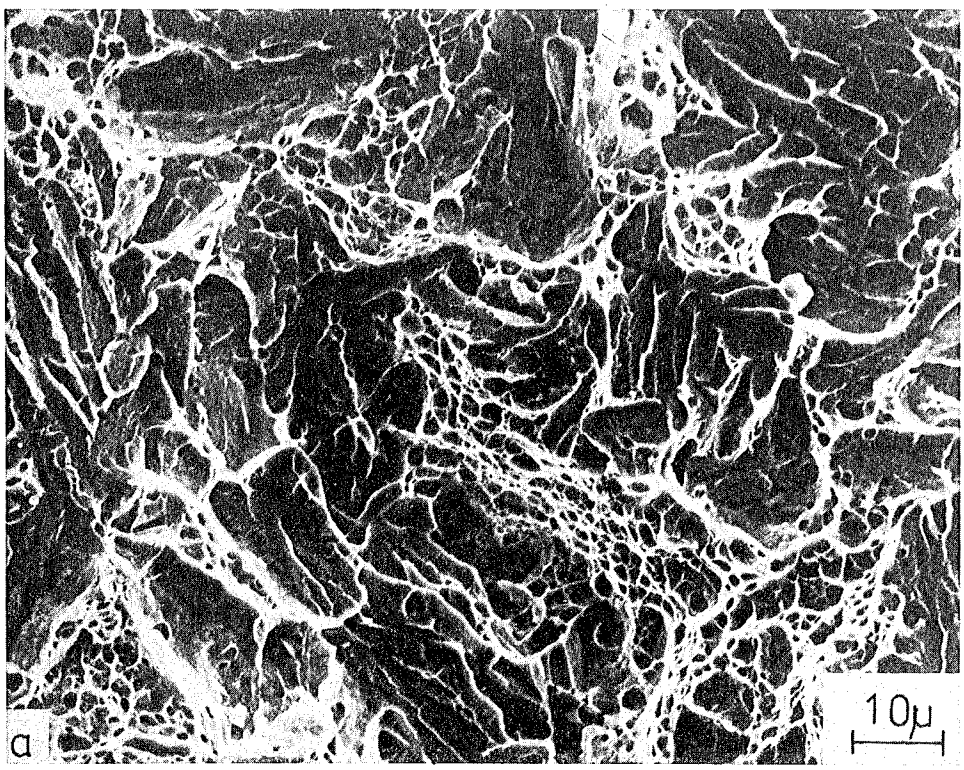

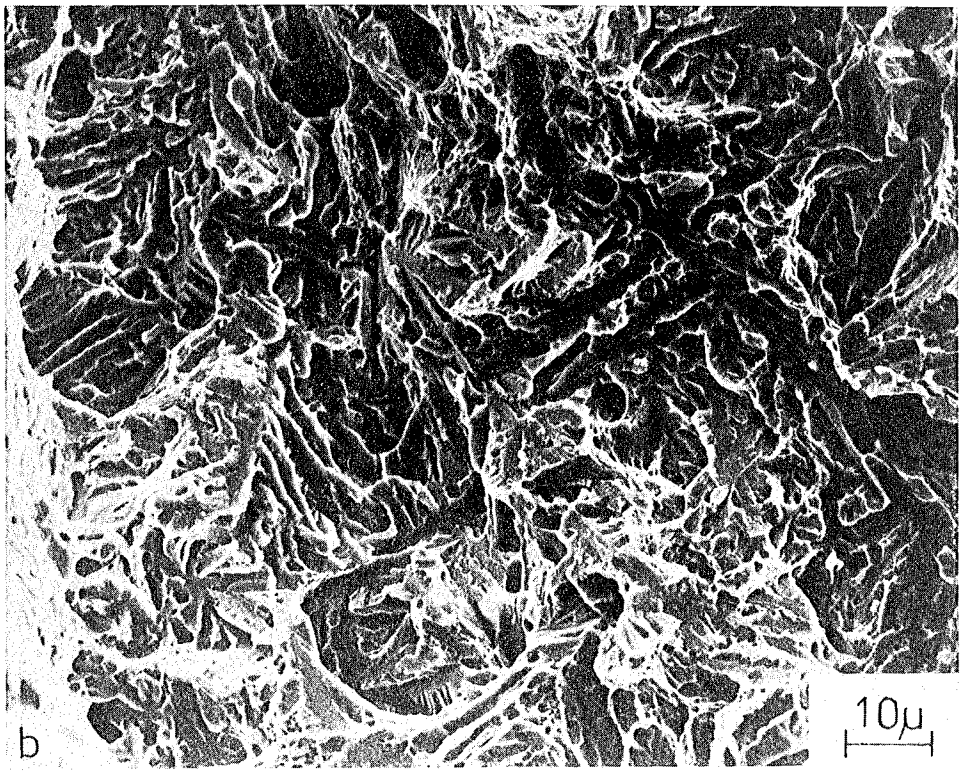

XBB 768-7124

Fig. 32.

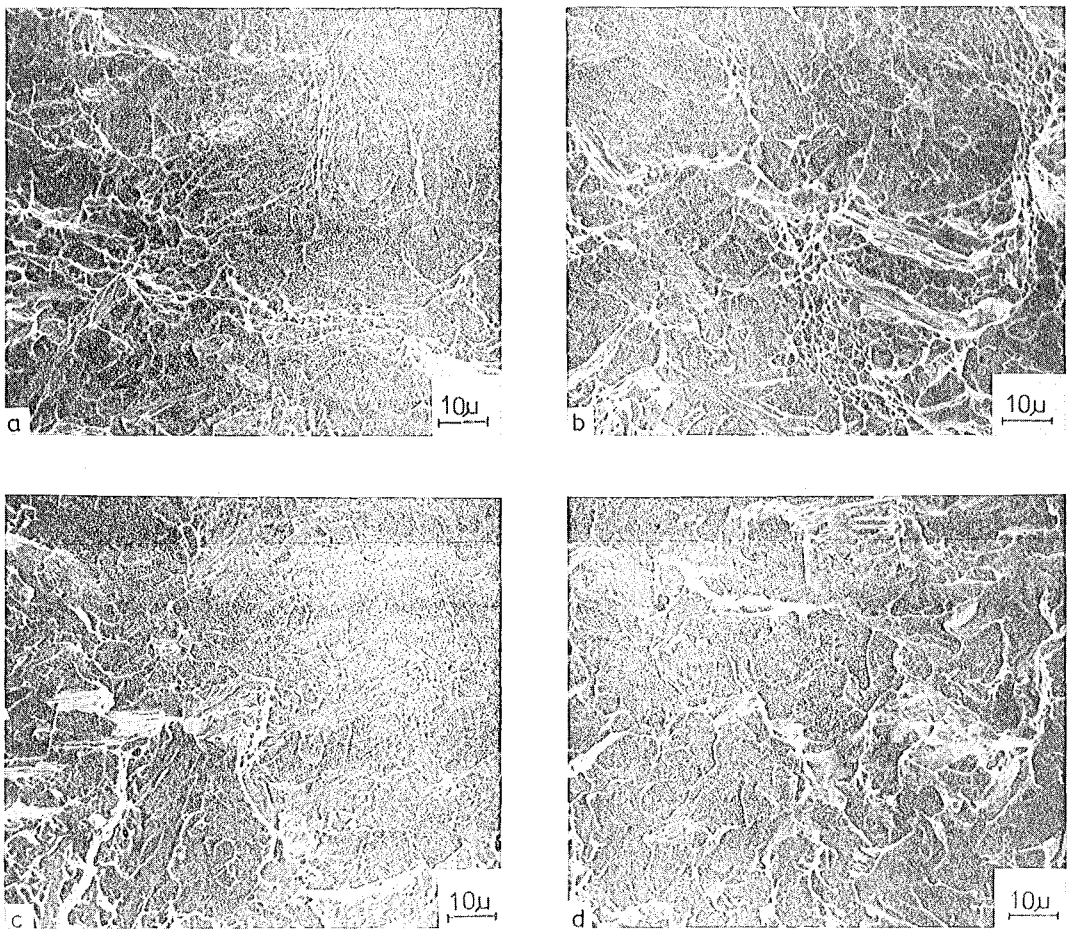

XBB 768-7624

Fig. 33.

0 0 0 0 4 7 0 0 7 0 1

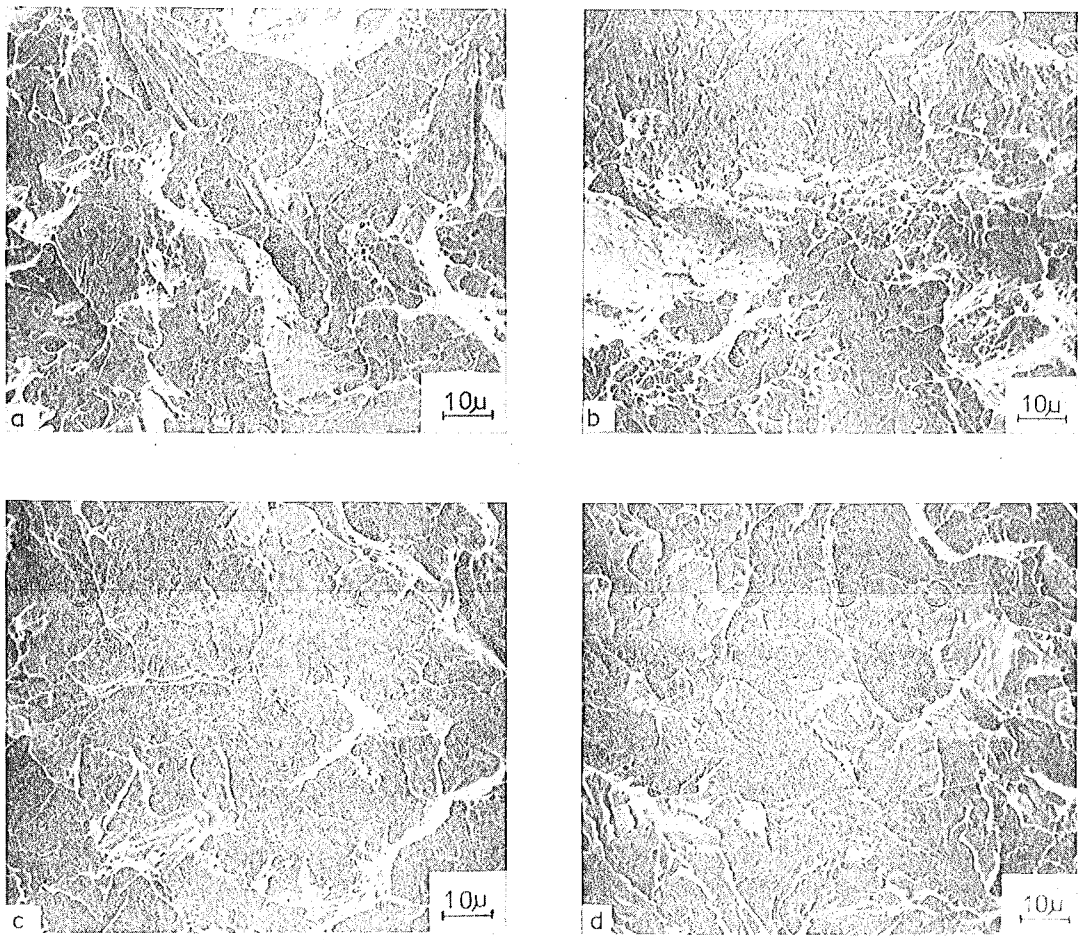

XBB 768-7623

Fig. 34.

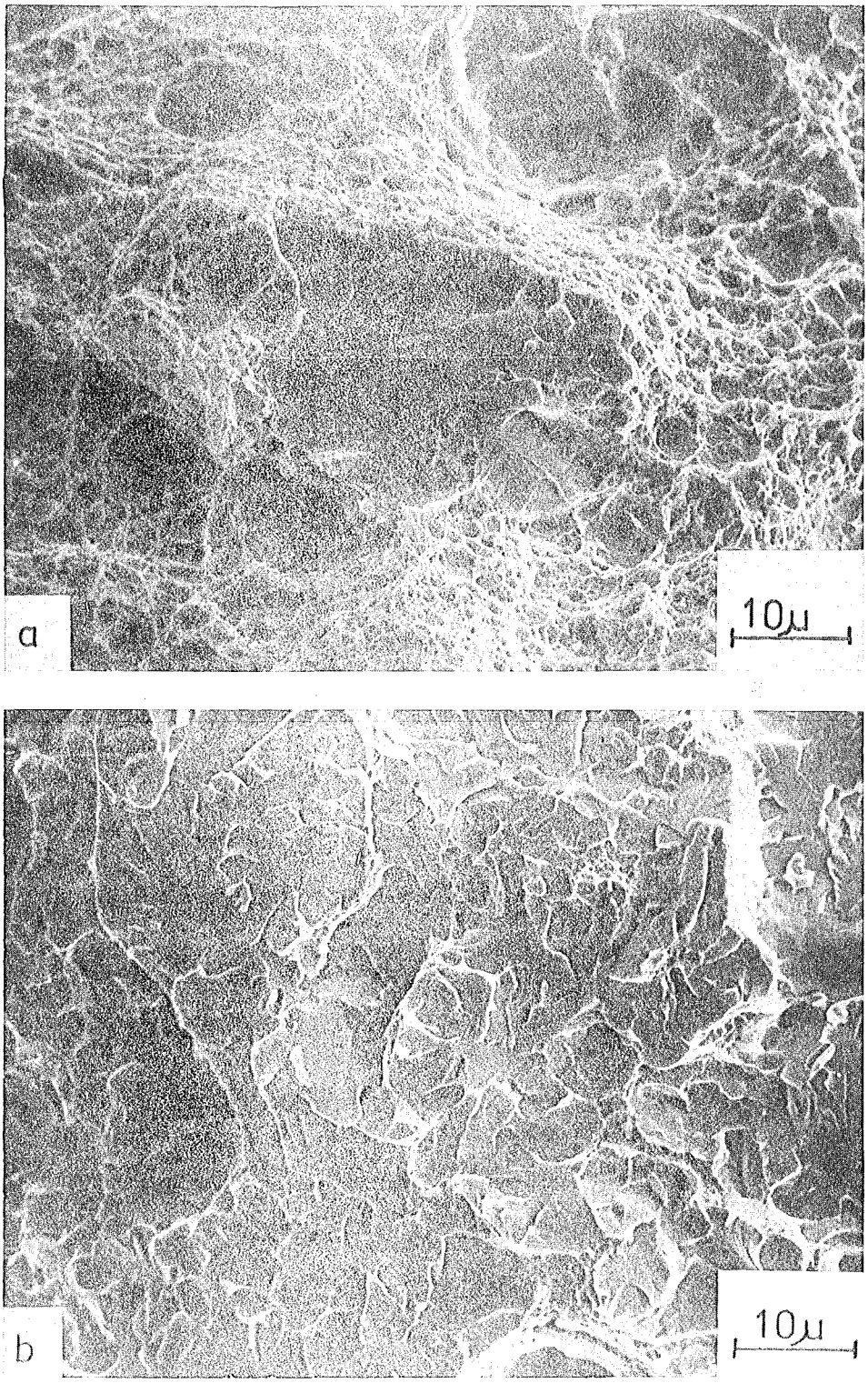

XBB 769-8123

Fig. 35.

0 0 0 0 4 7 0 4 7 9 2

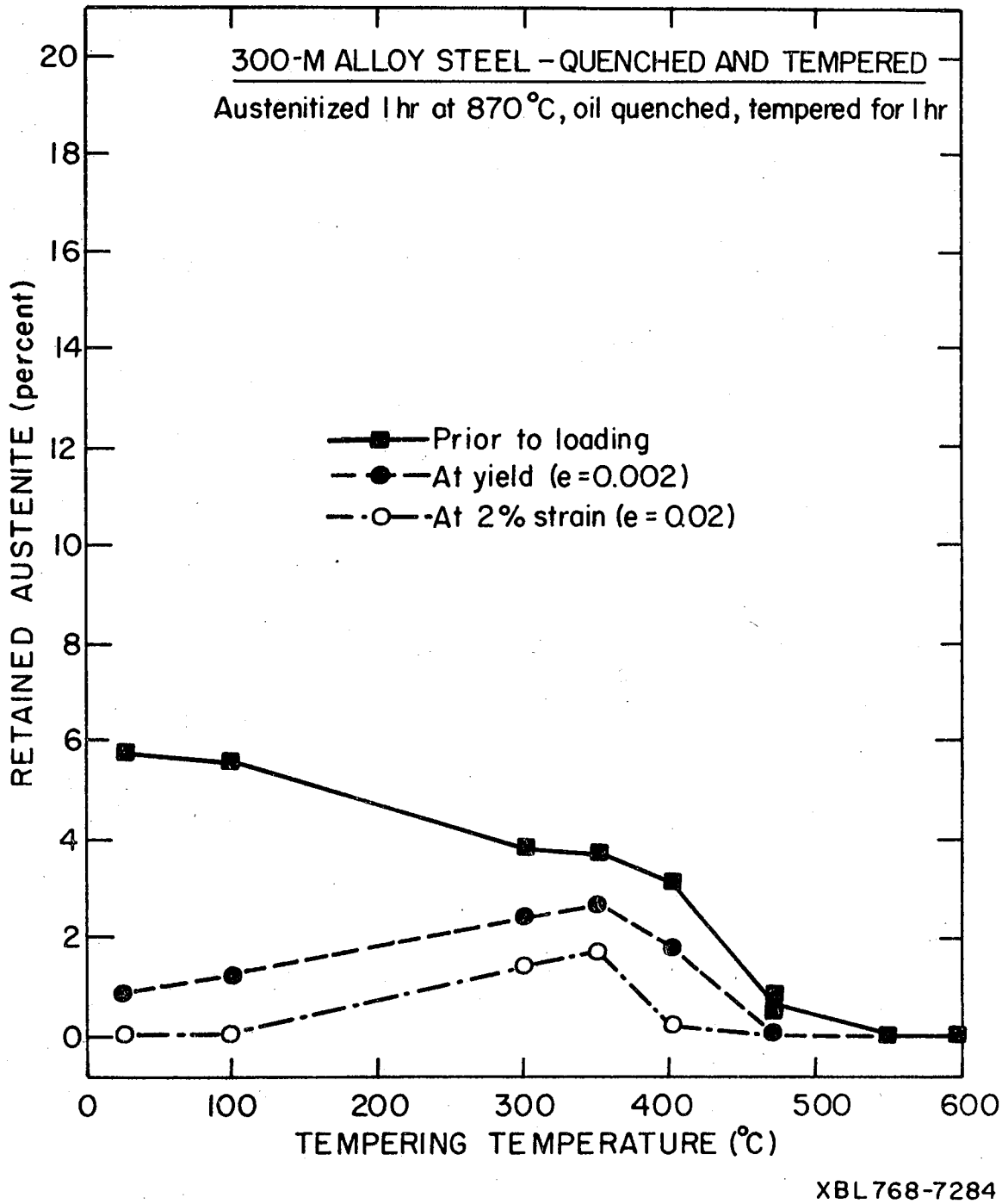

Fig. 36.

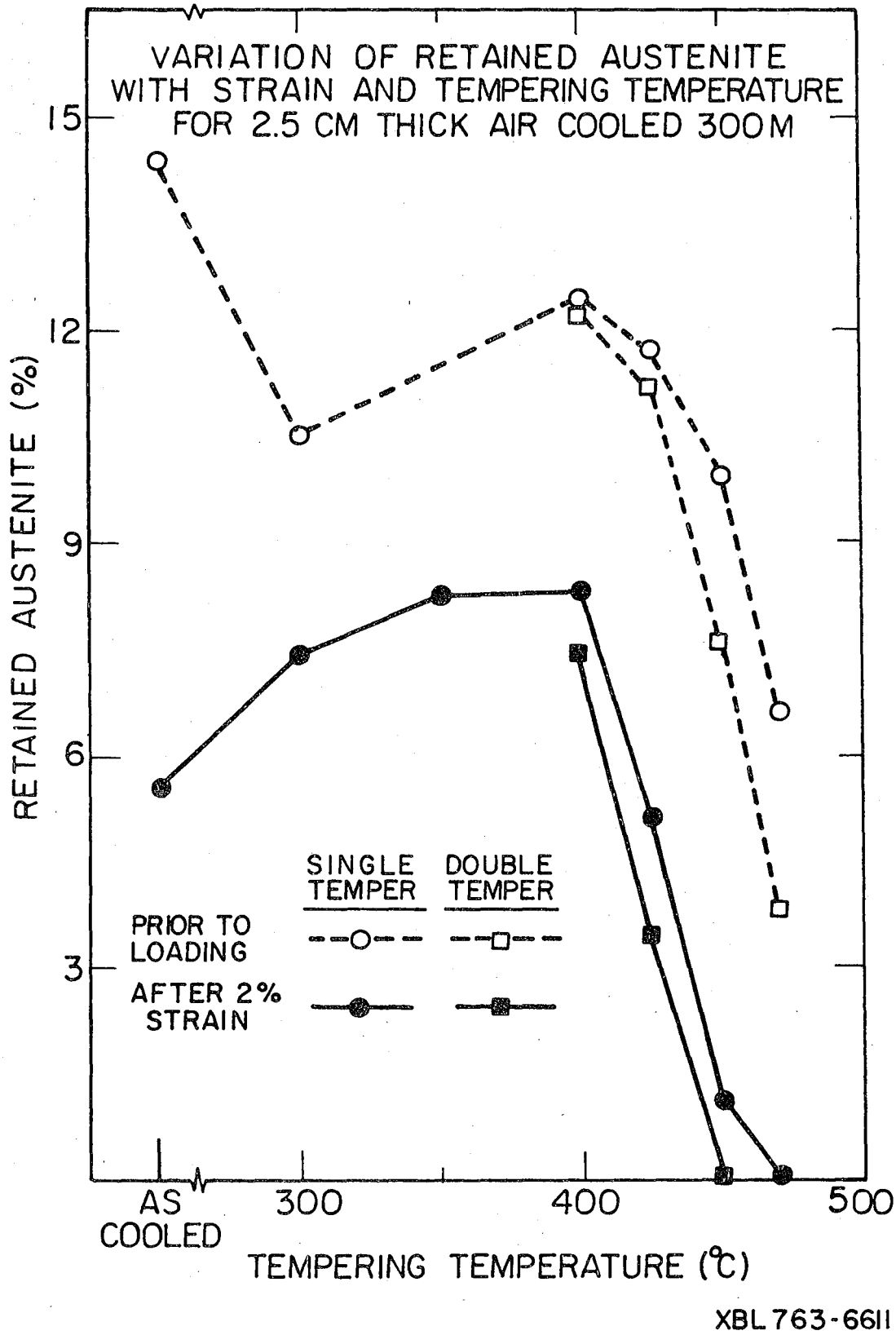
VARIATION OF RETAINED AUSTENITE
WITH STRAIN AND TEMPERING TEMPERATURE
FOR 2.5 CM THICK AIR COOLED 300M
RETAINED AUSTENITE (%)
15
12
9
6
3
SINGLE TEMPER
DOUBLE TEMPER
PRIOR TO LOADING
AFTER 2% STRAIN
AS COOLED
300
400
500
TEMPERING TEMPERATURE (°C)
XBL 763-6611

Fig. 37.

0 0 0 0 4 7 0 0 7 0 3

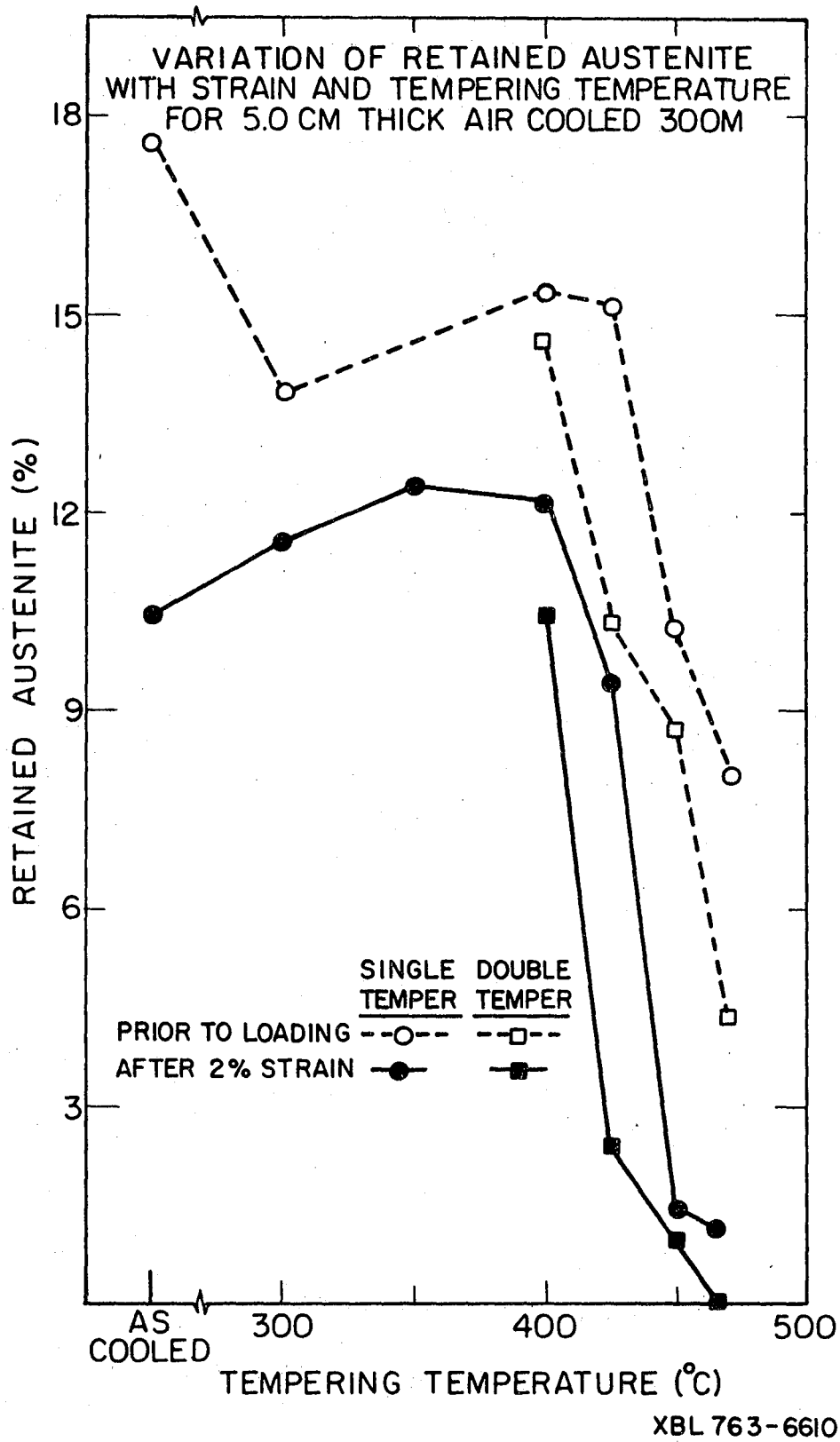

Fig. 38.

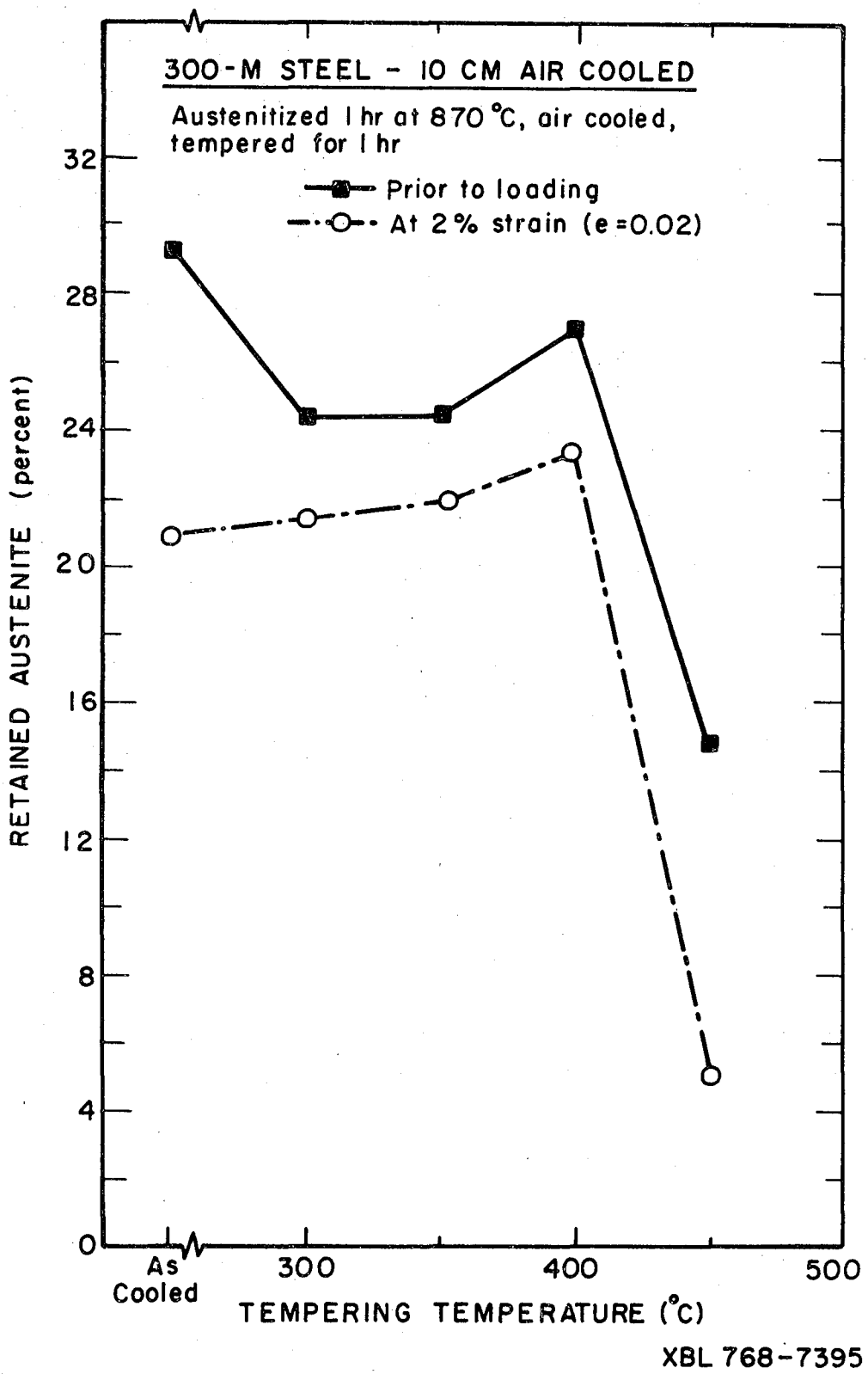
300-M STEEL - 10 CM AIR COOLED
Austenitized 1 hr at 870 °C, air cooled, tempered for 1 hr
Prior to loading
At 2% strain (e=0.02)
RETAINED AUSTENITE (percent)
0
4
8
12
16
20
24
28
32
As Cooled
300
400
500
TEMPERING TEMPERATURE (°C)
XBL 768-7395

Fig. 39.

0 0 0 0 4 7 0 4 7 9 4

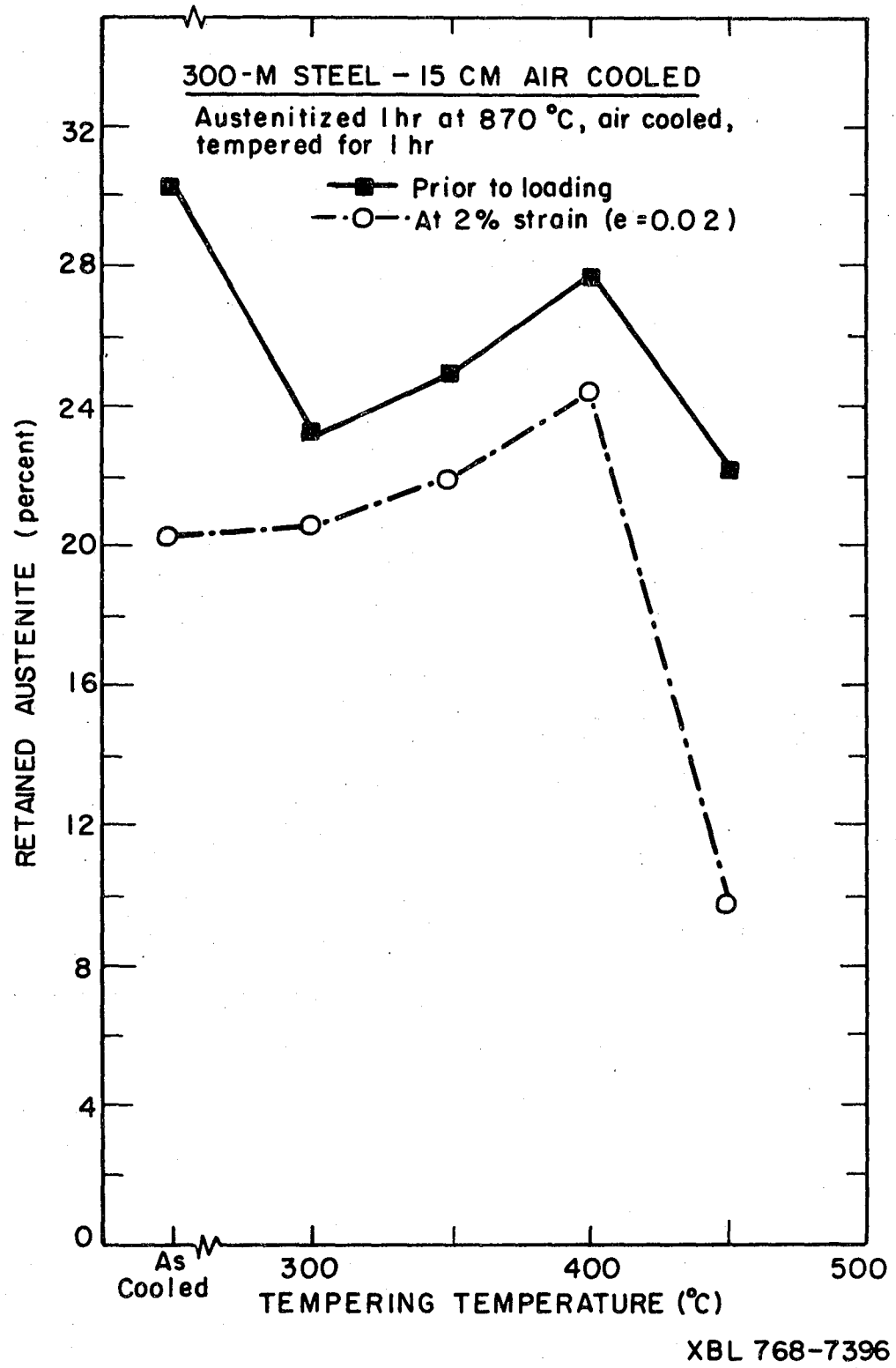

Fig. 40.

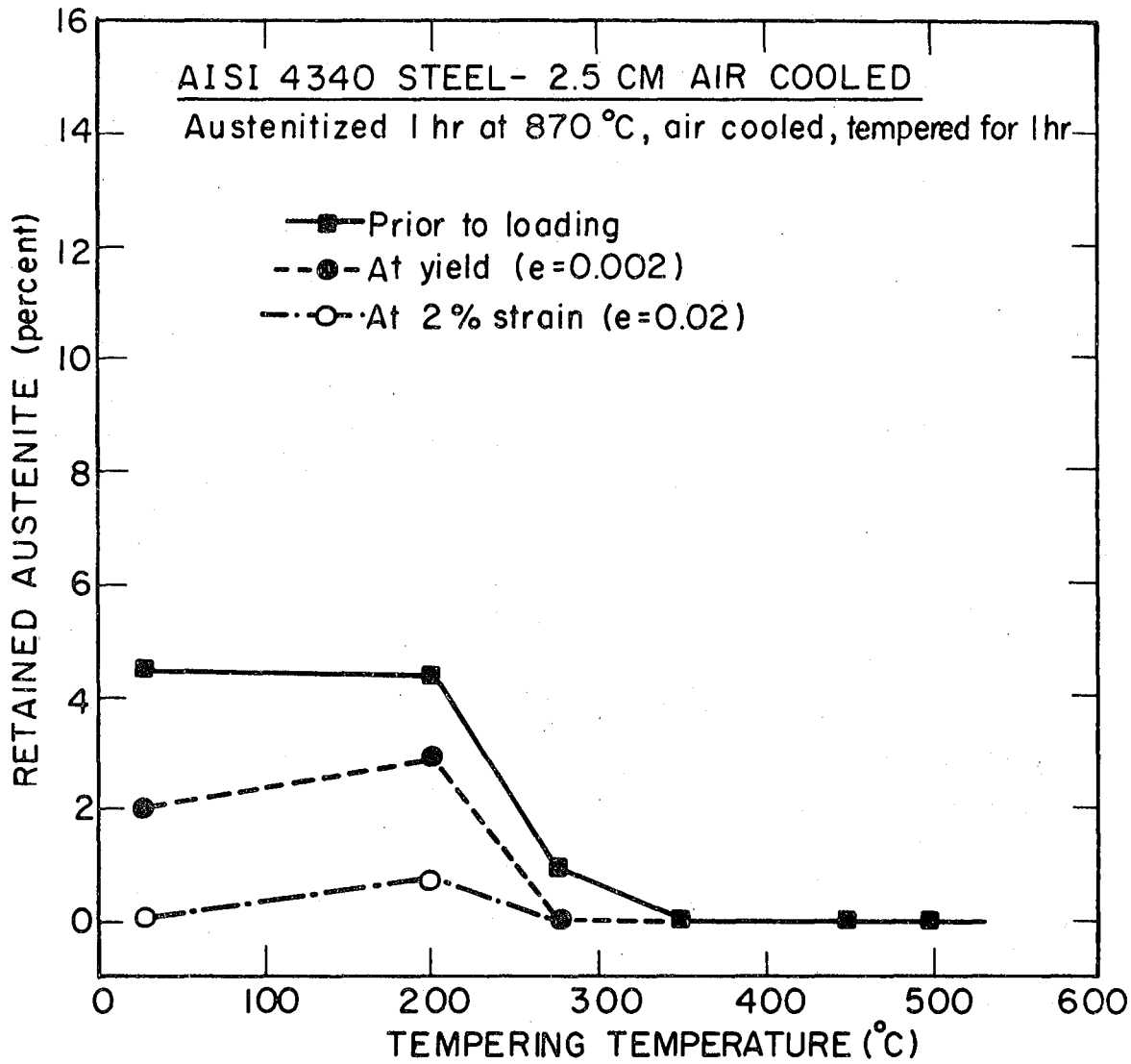

XBL 768-7394

Fig. 41.

0 0 0 0 4 7 0 4 7 9 5

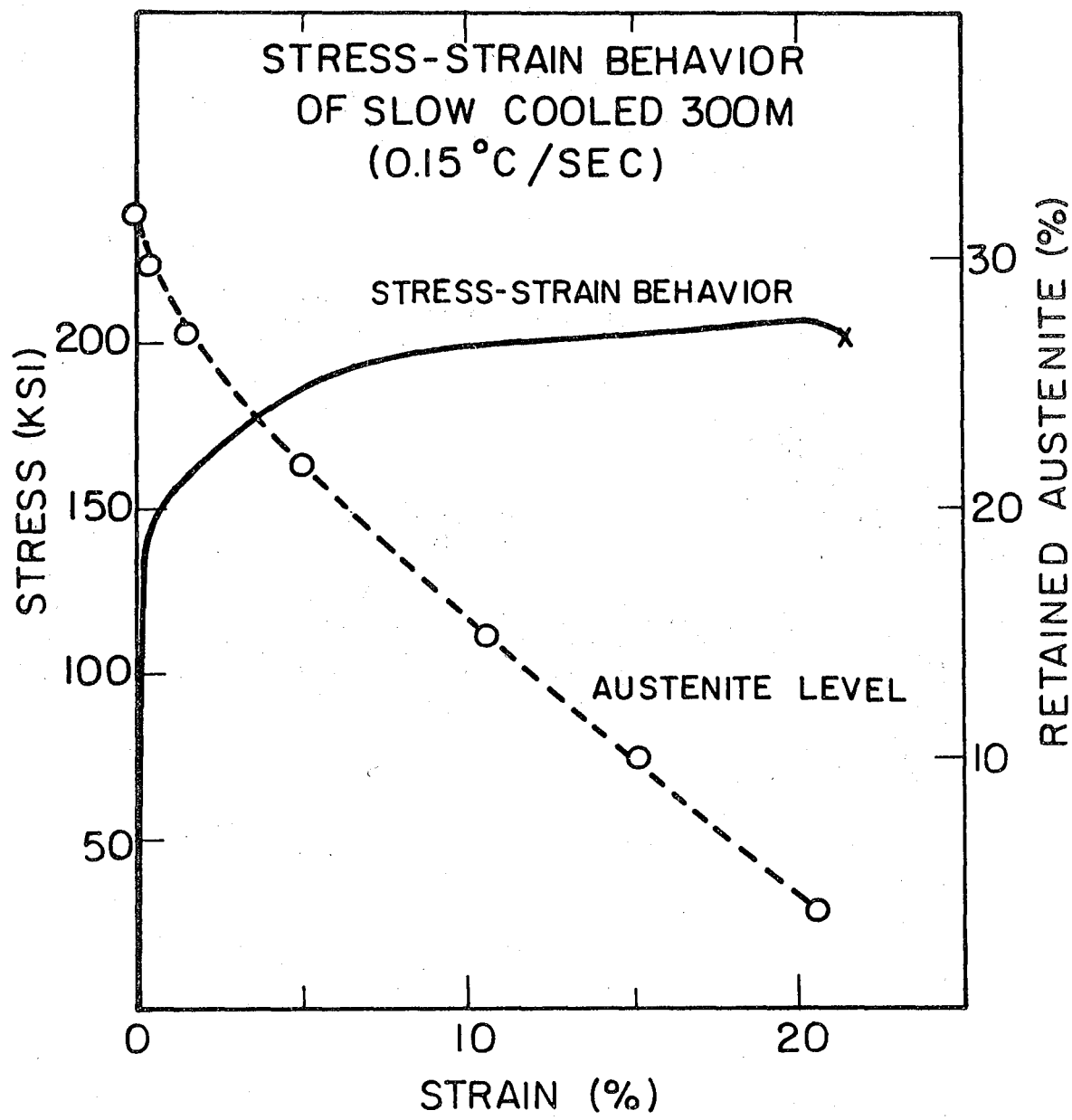

XBL 763-6609

Fig. 42.

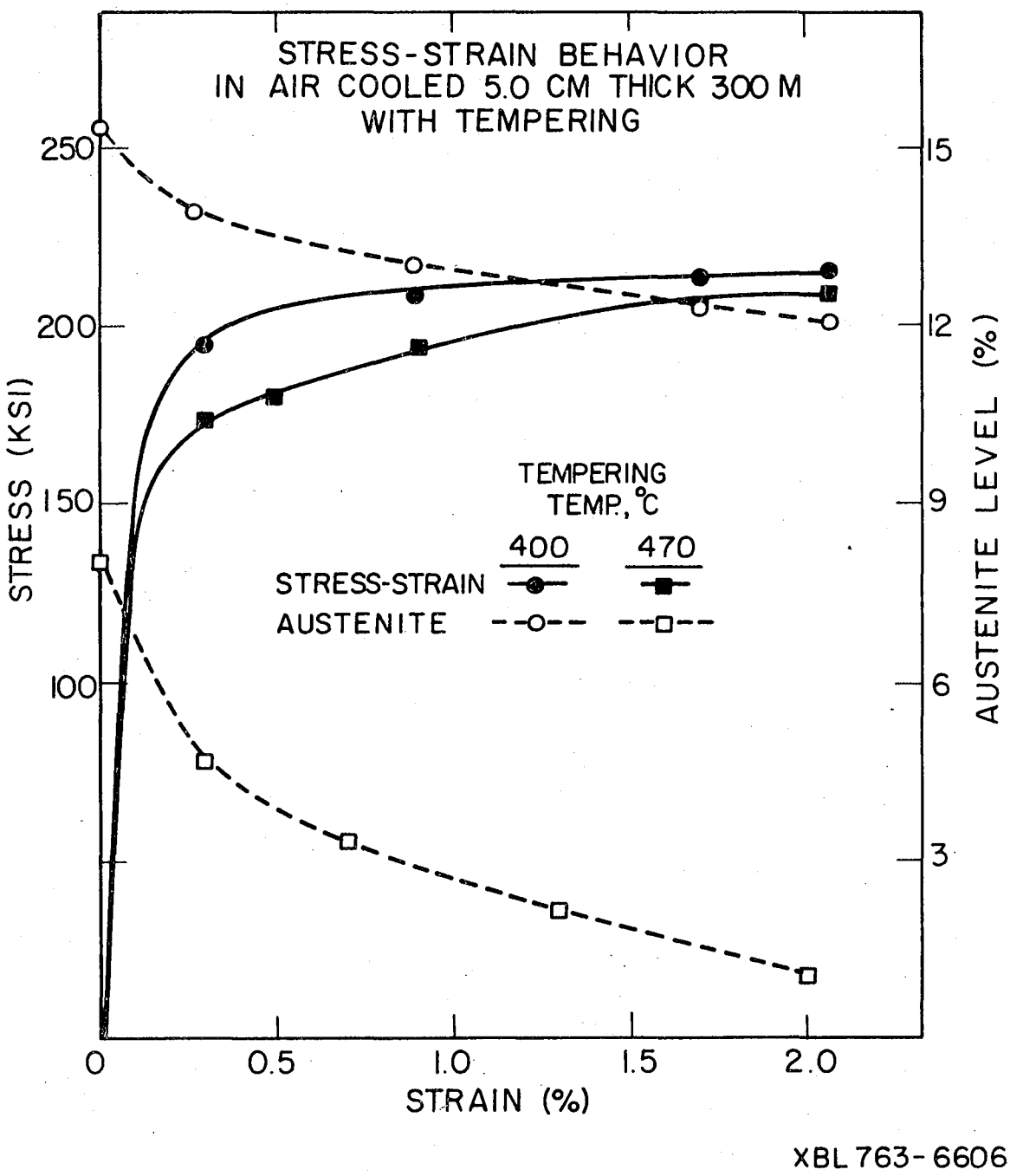
STRESS-STRAIN BEHAVIOR
IN AIR COOLED 5.0 CM THICK 300 M
WITH TEMPERING
STRESS (KSI)
250
200
150
100
AUSTENITE LEVEL (%)
15
12
9
6
3
TEMPERING
TEMP., °C
400
470
STRESS-STRAIN
AUSTENITE
0
0.5
1.0
1.5
2.0
STRAIN (%)
XBL 763-6606

Fig. 43.

0 0 0 0 4 7 0 0 7 9 8

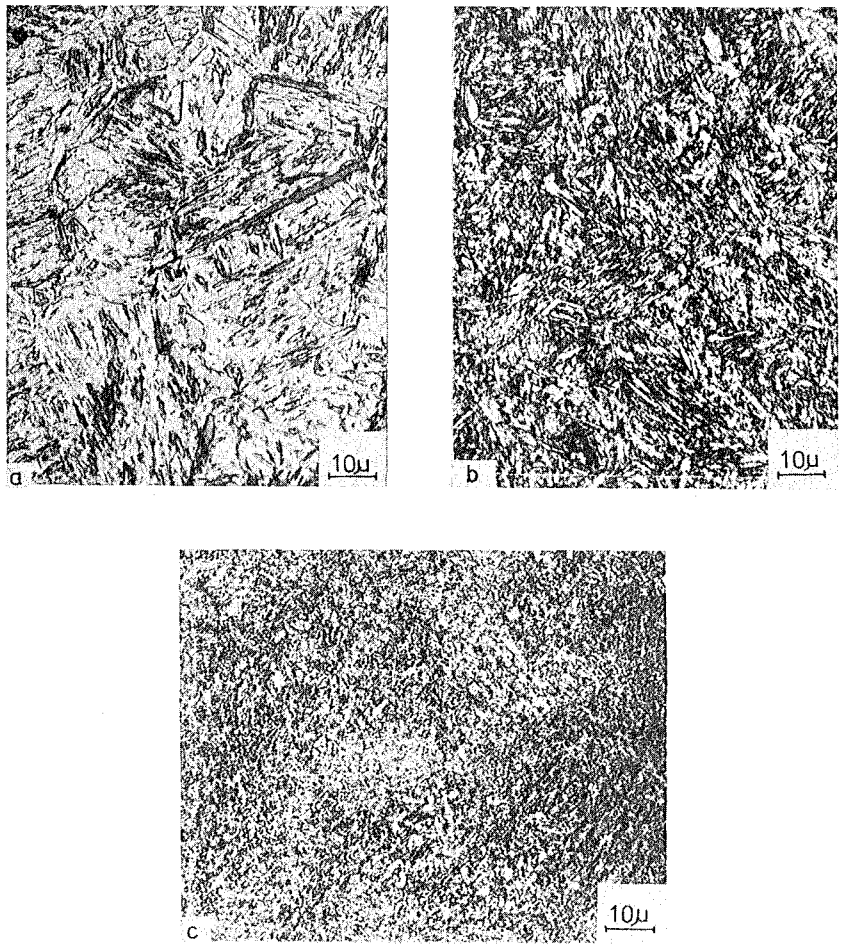

XBB 768-7619

Fig. 44.

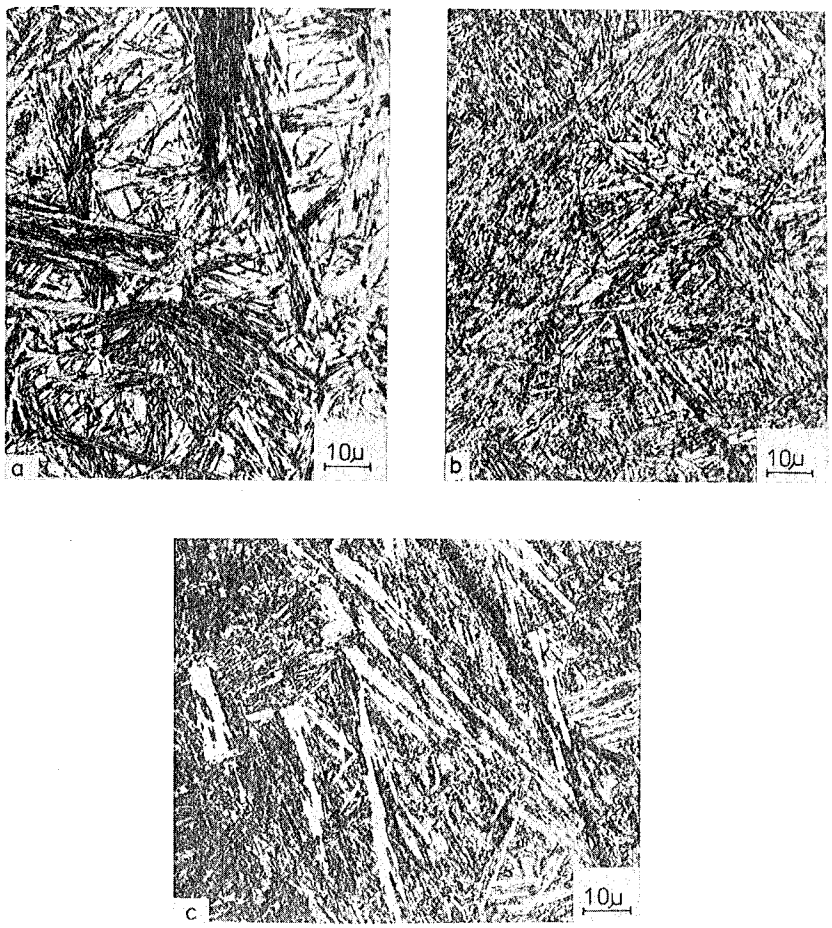

XBB 768-7621

Fig. 45.

0 0 0 0 4 7 0 0 3 8 7

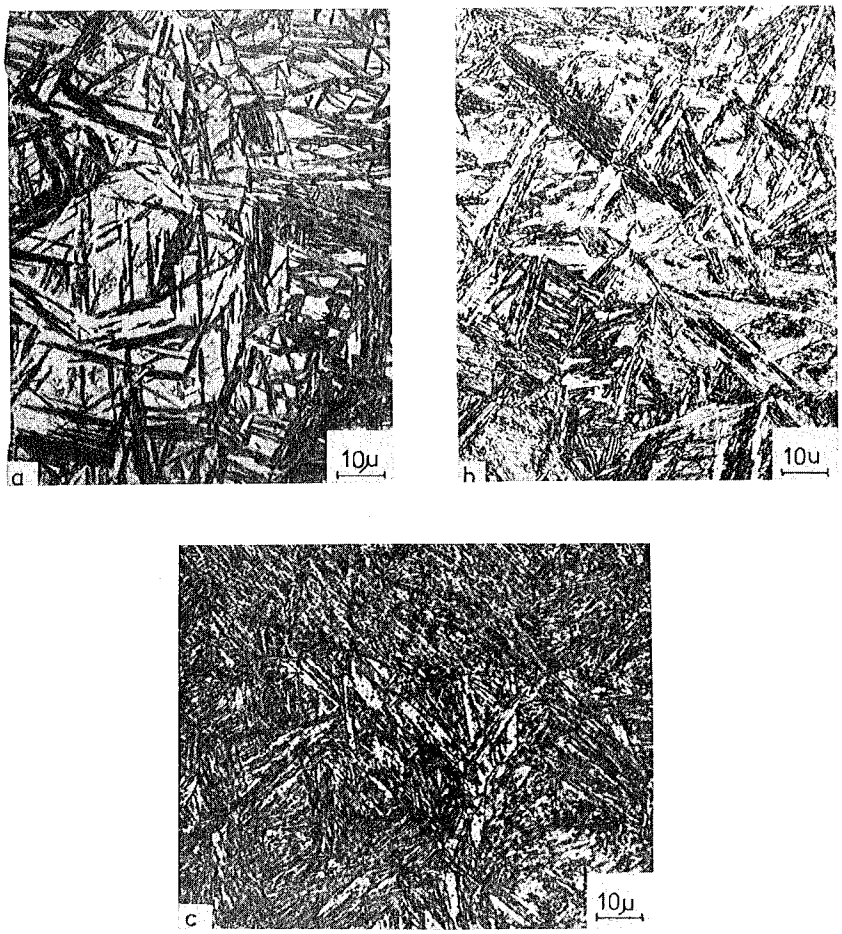

XBB 768-7620

Fig. 46.

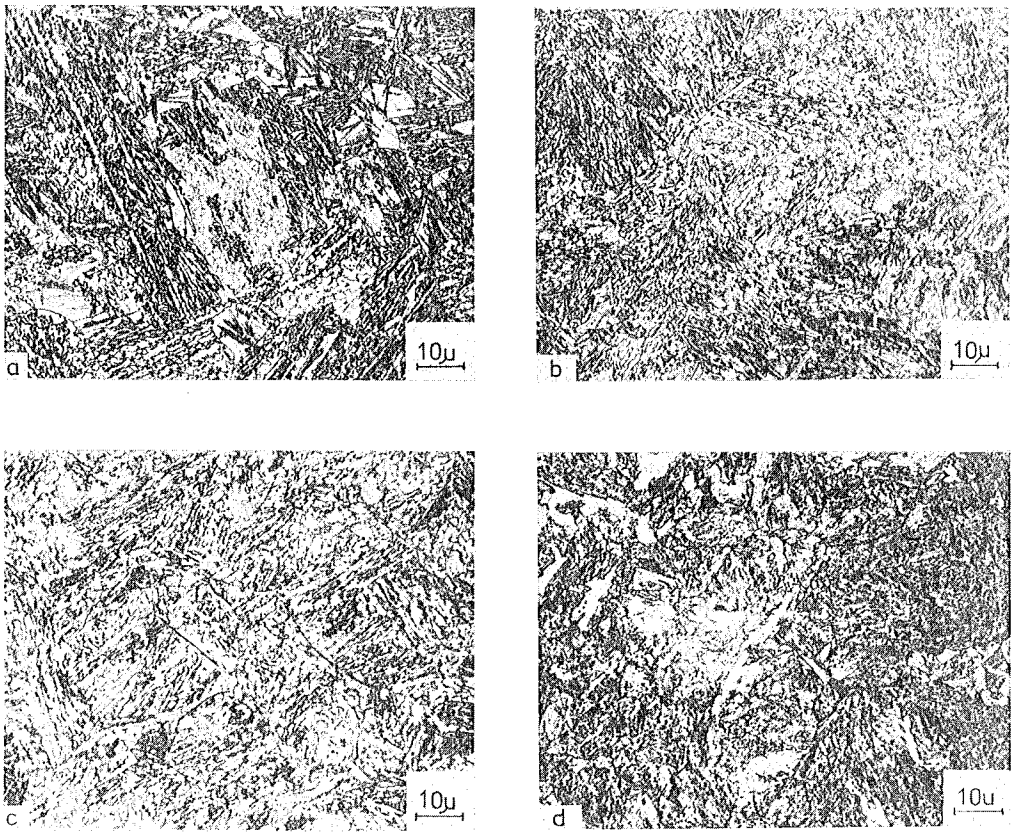

XBB 768-7622

Fig. 47.

0 0 0 0 4 7 0 0 7 0 0

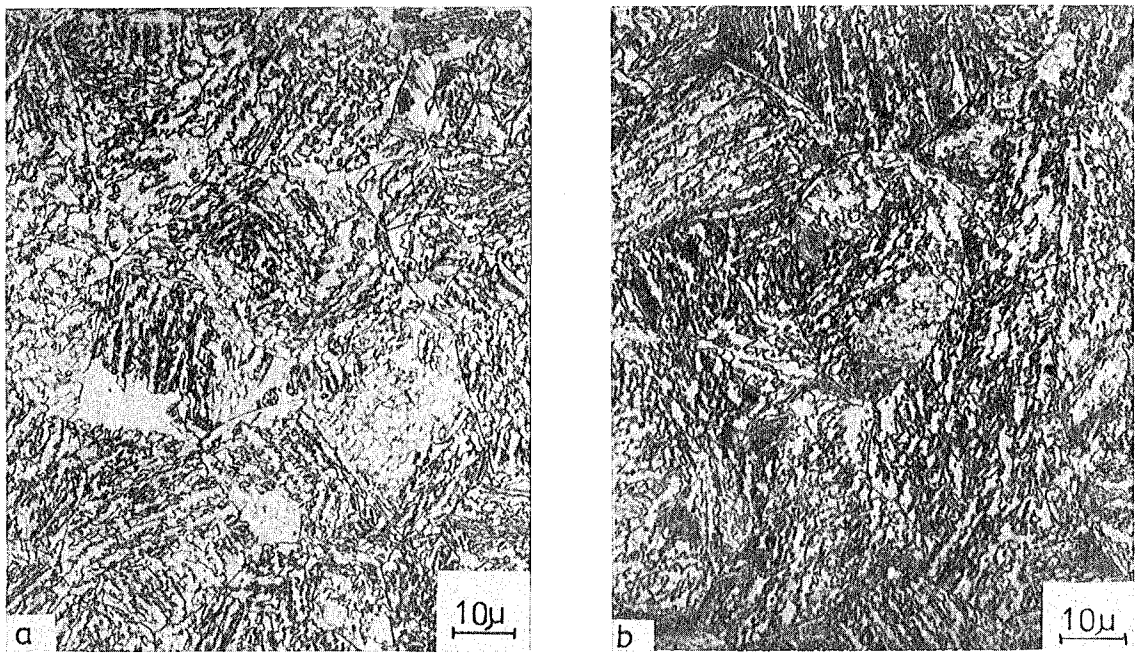

XBB 768-7617

Fig. 48.

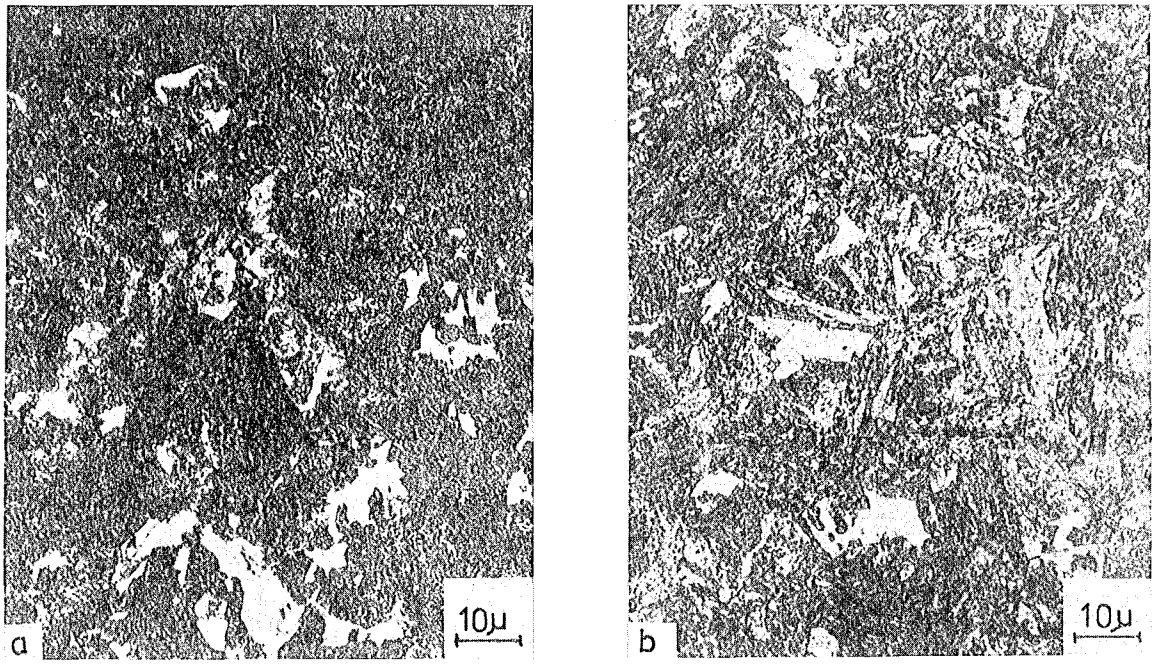

XBB 768-7618

Fig. 49.

0 0 0 0 4 7 0 6 7 8 9

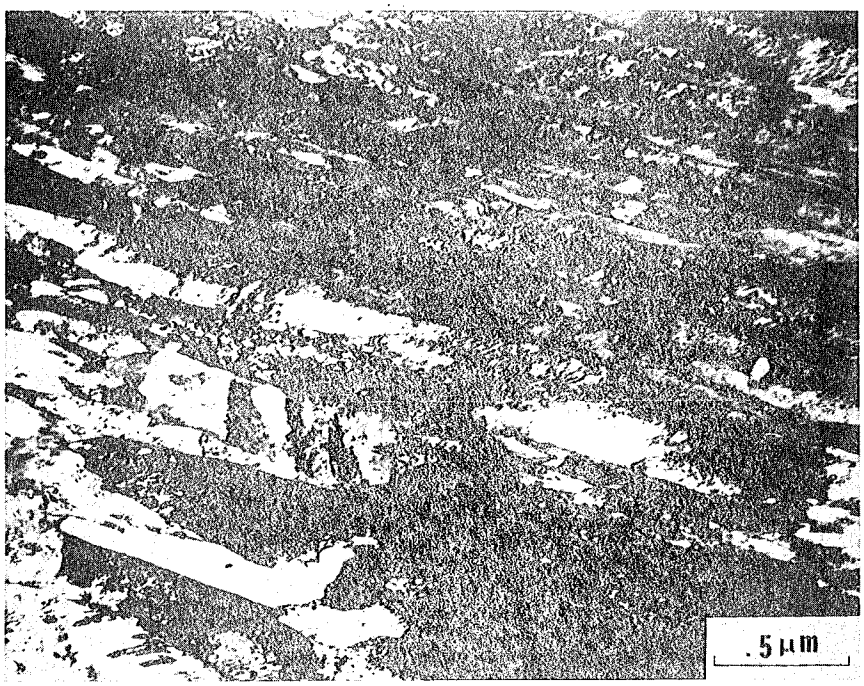

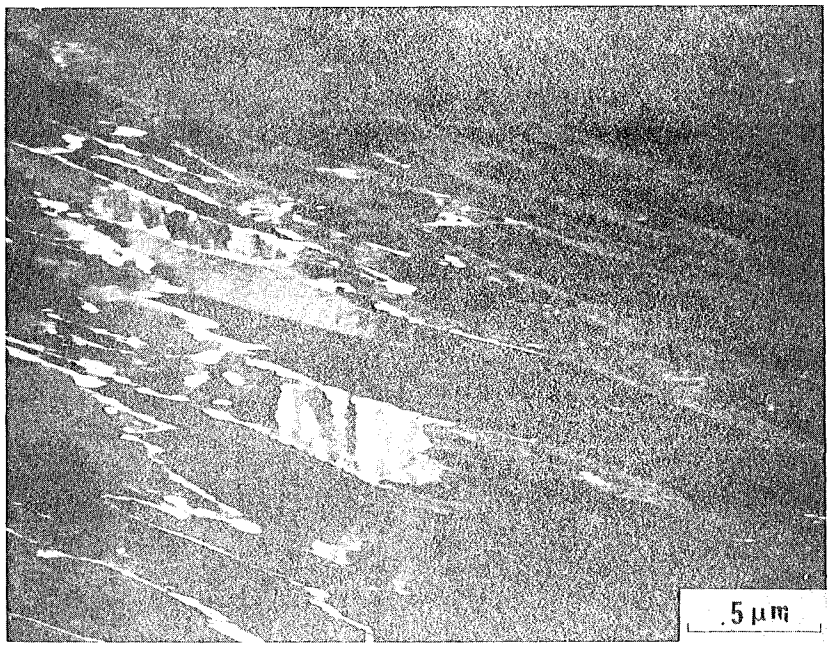

XBB 763-2464

Fig. 50.

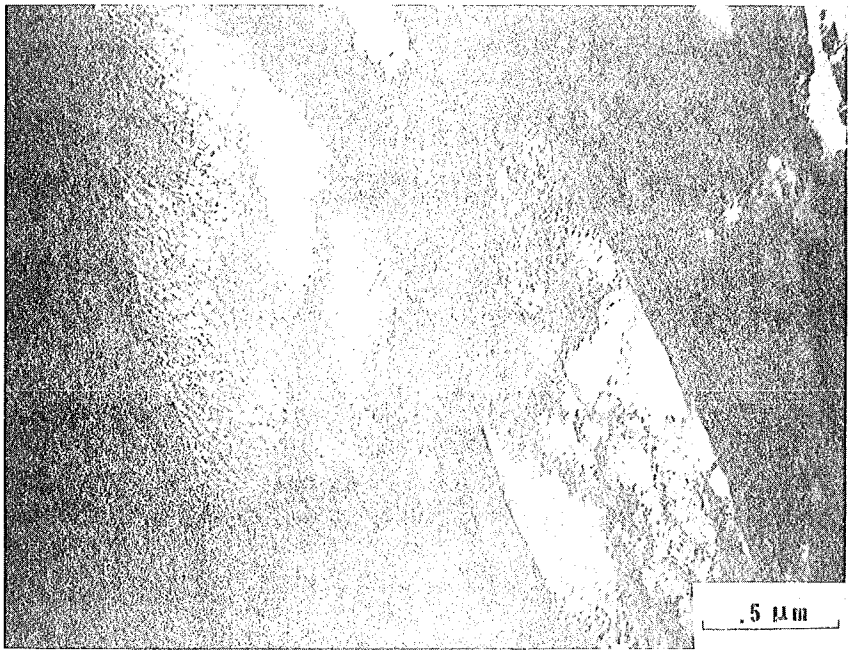

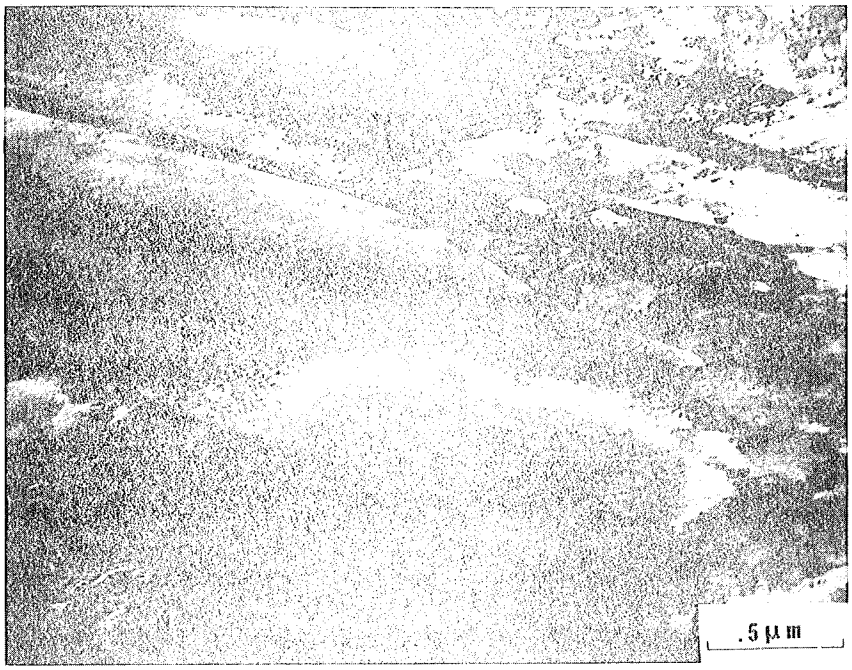

XBB 763-2465

Fig. 51.

0 0 0 0 4 7 0 0 0 9 0

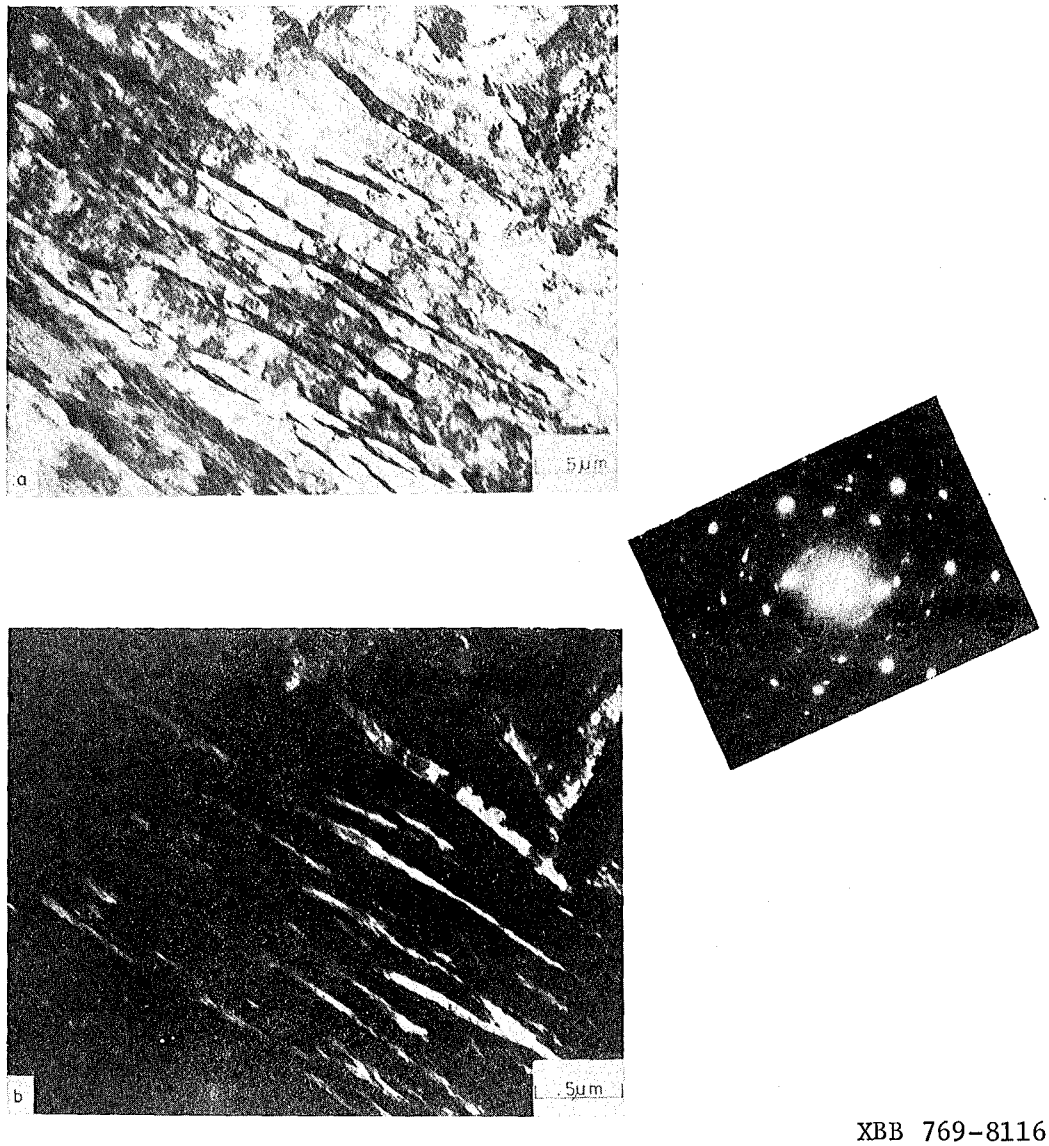

XBB 769-8116

Fig. 52.

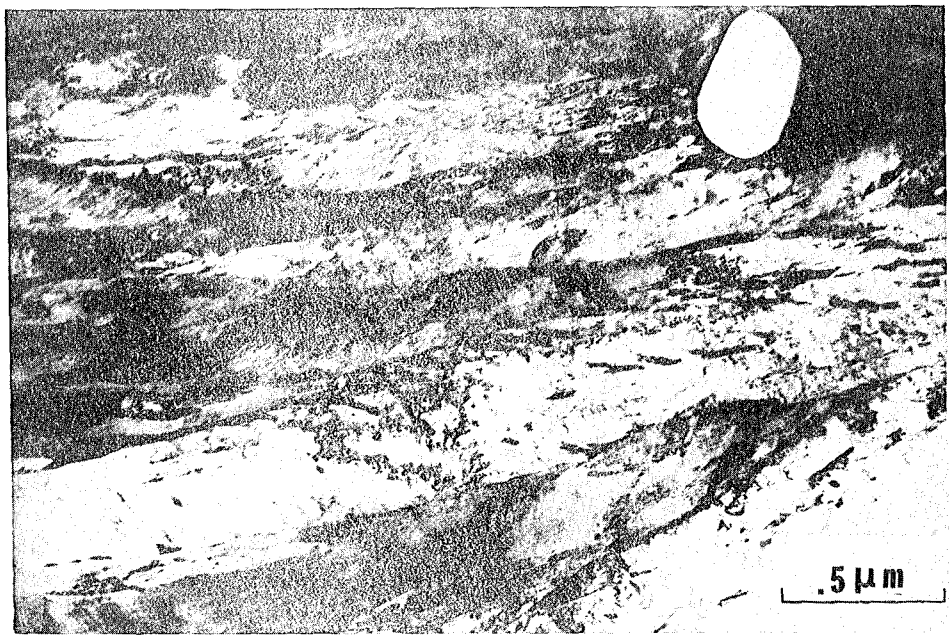

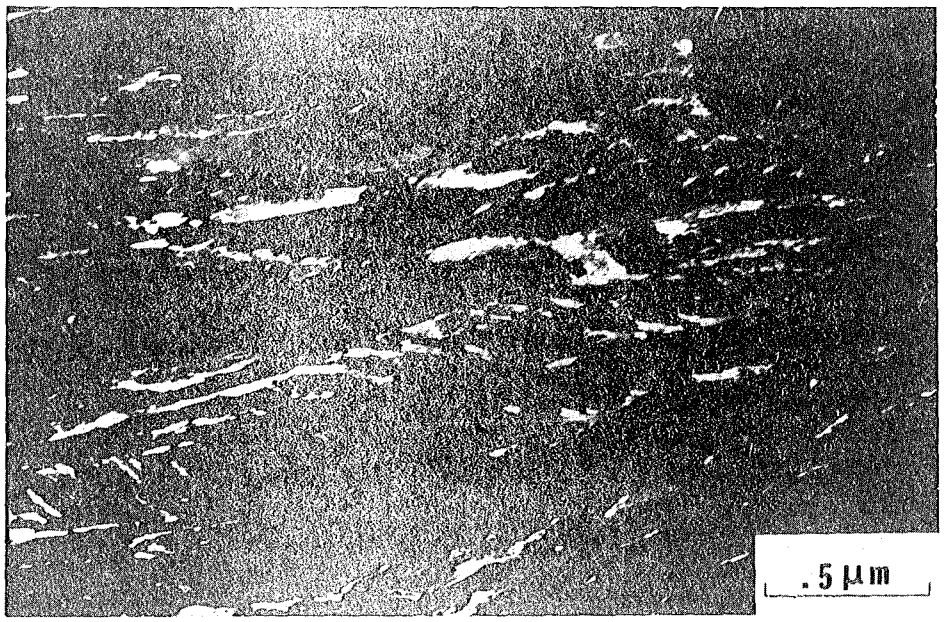

XBB 763-2463

Fig. 53.

0 0 0 0 4 7 0 0 9 0 1

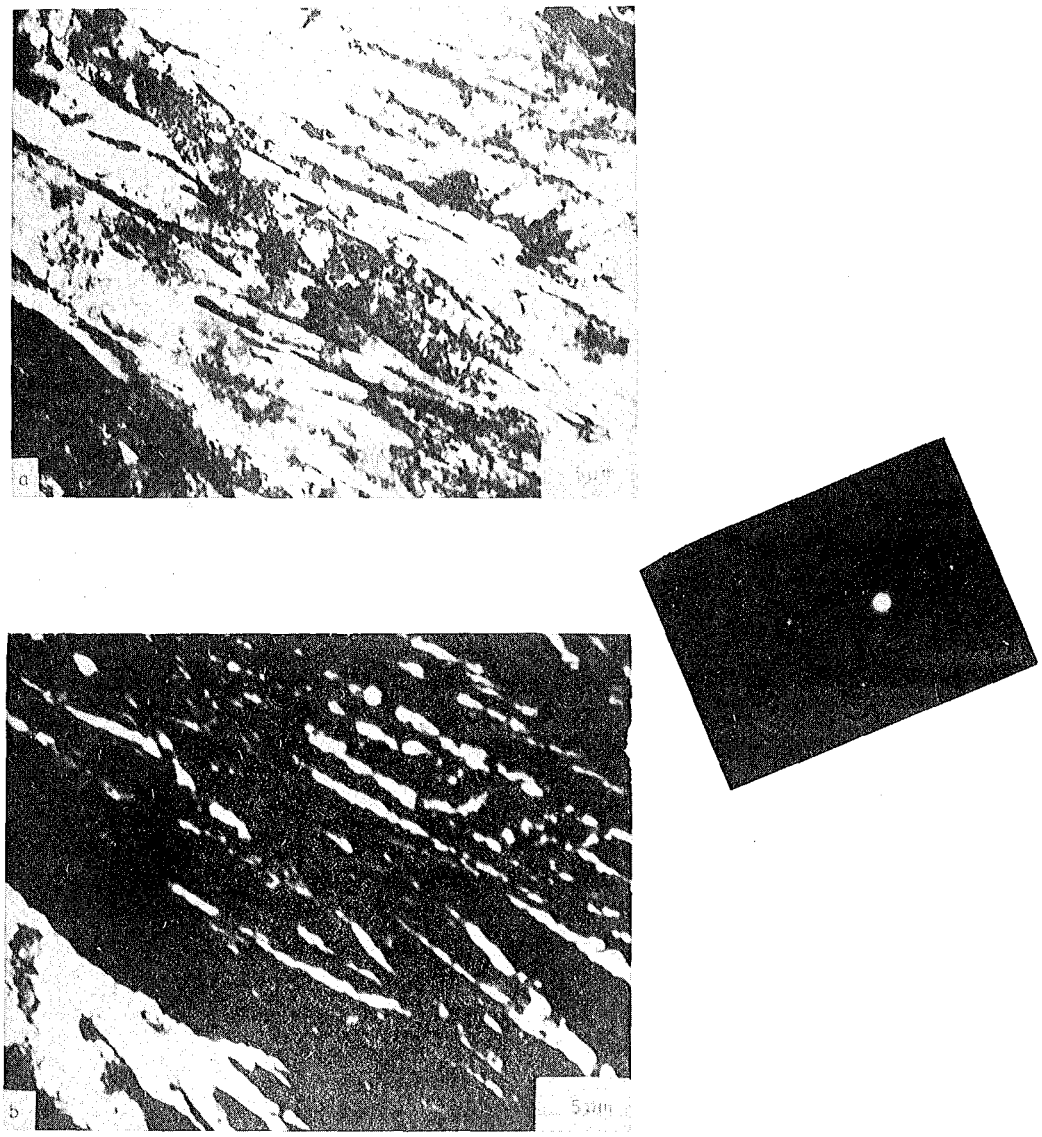

XBB 769-8113

Fig. 54.

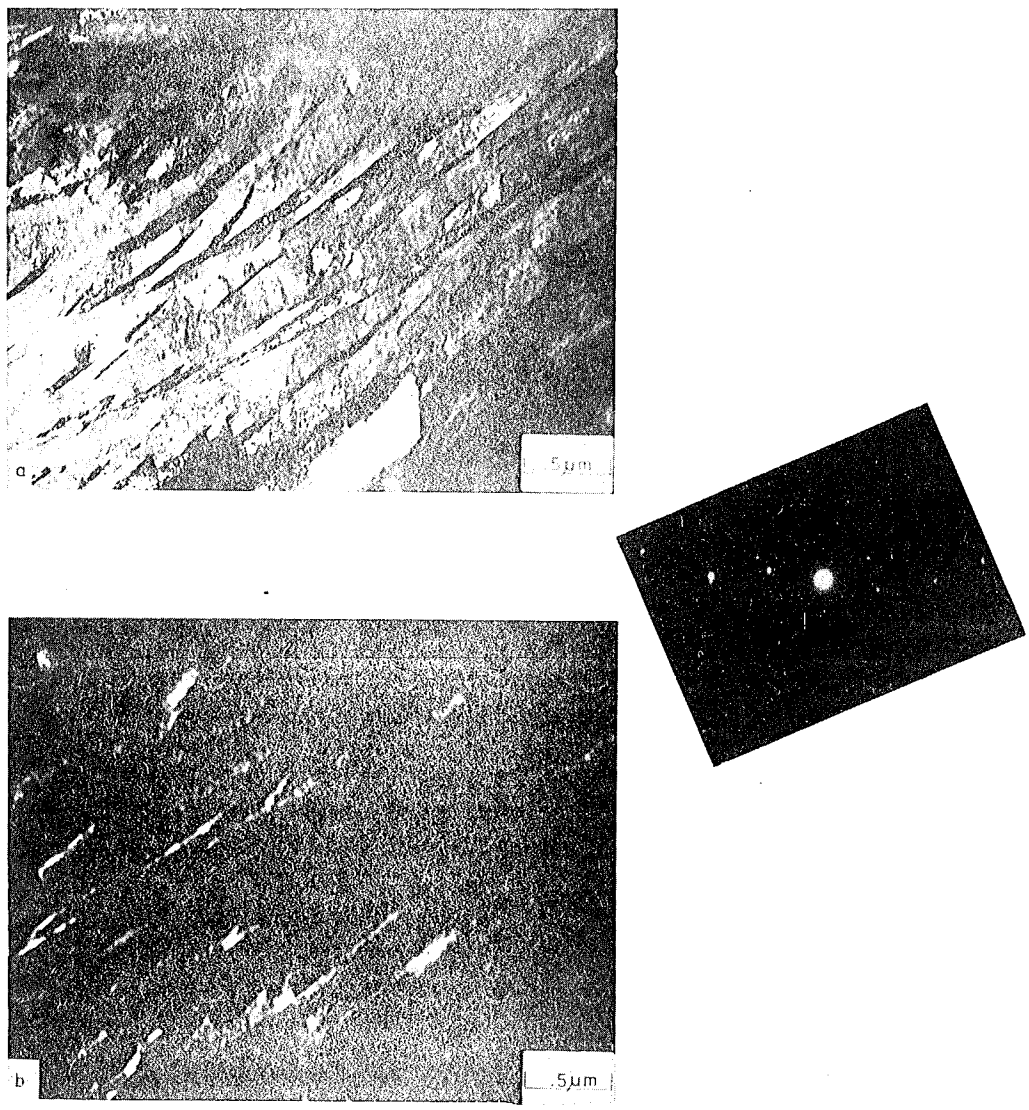

XBB 769-8117

Fig. 55.

8 8 0 0 4 7 8 0 9 9 2

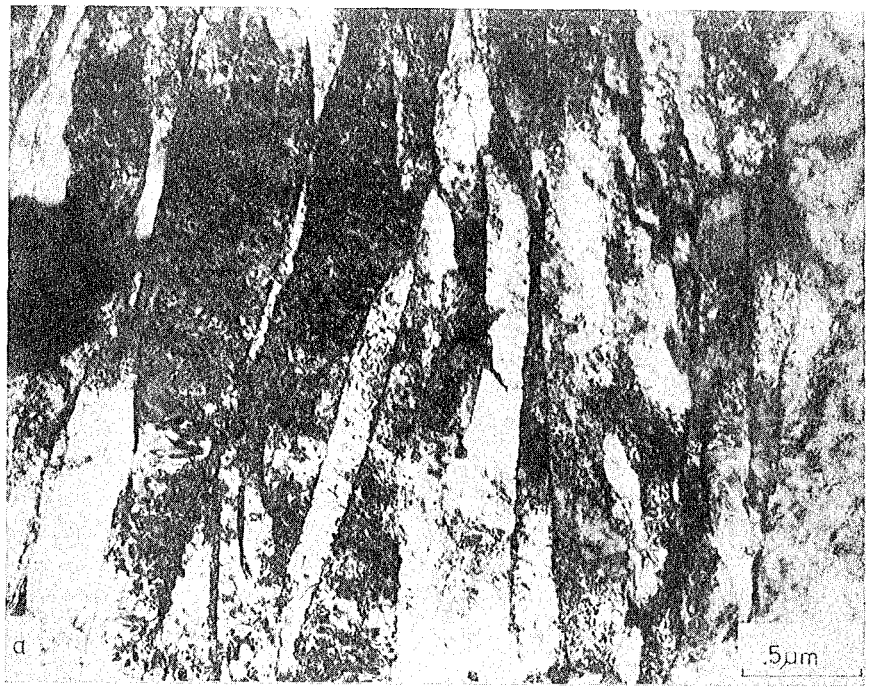

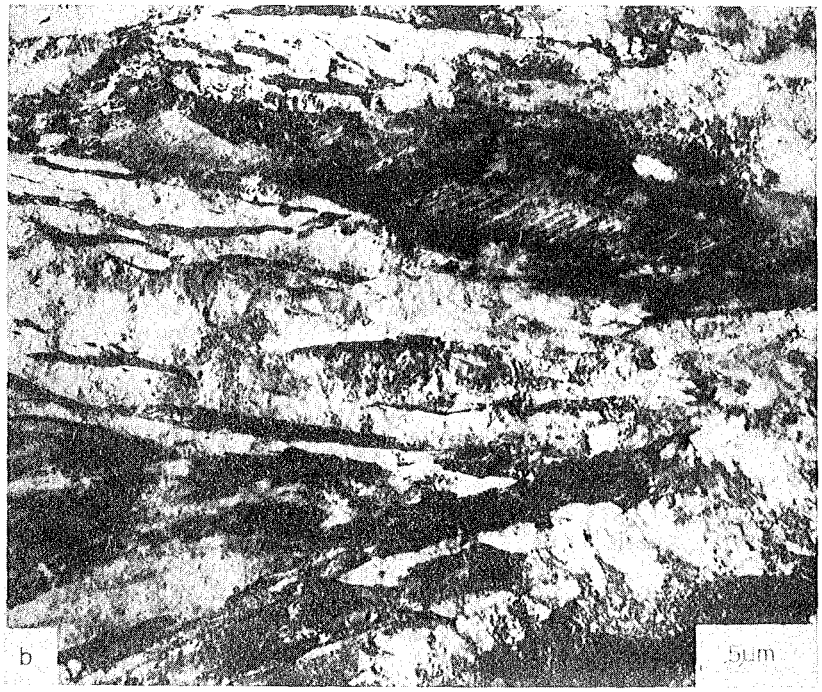

XBB 769-8120

Fig. 56.

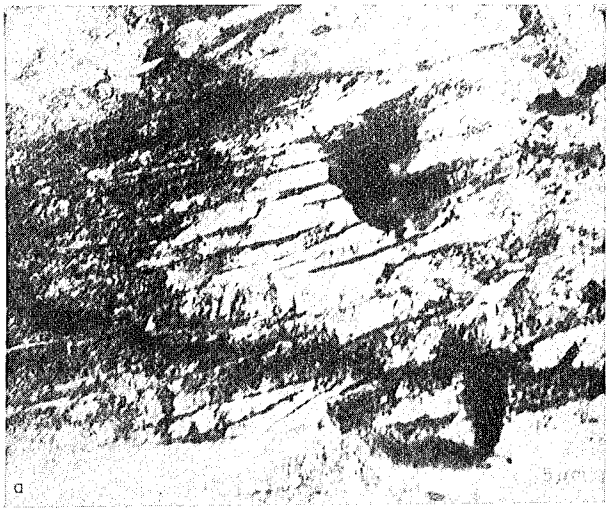

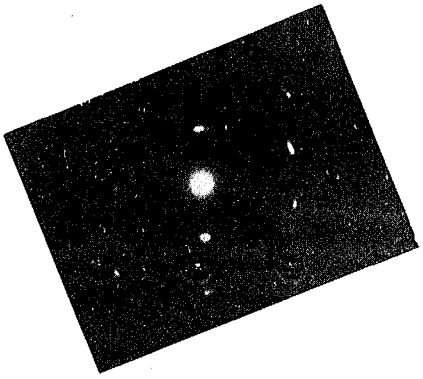

XBB 769-8114

Fig. 57.

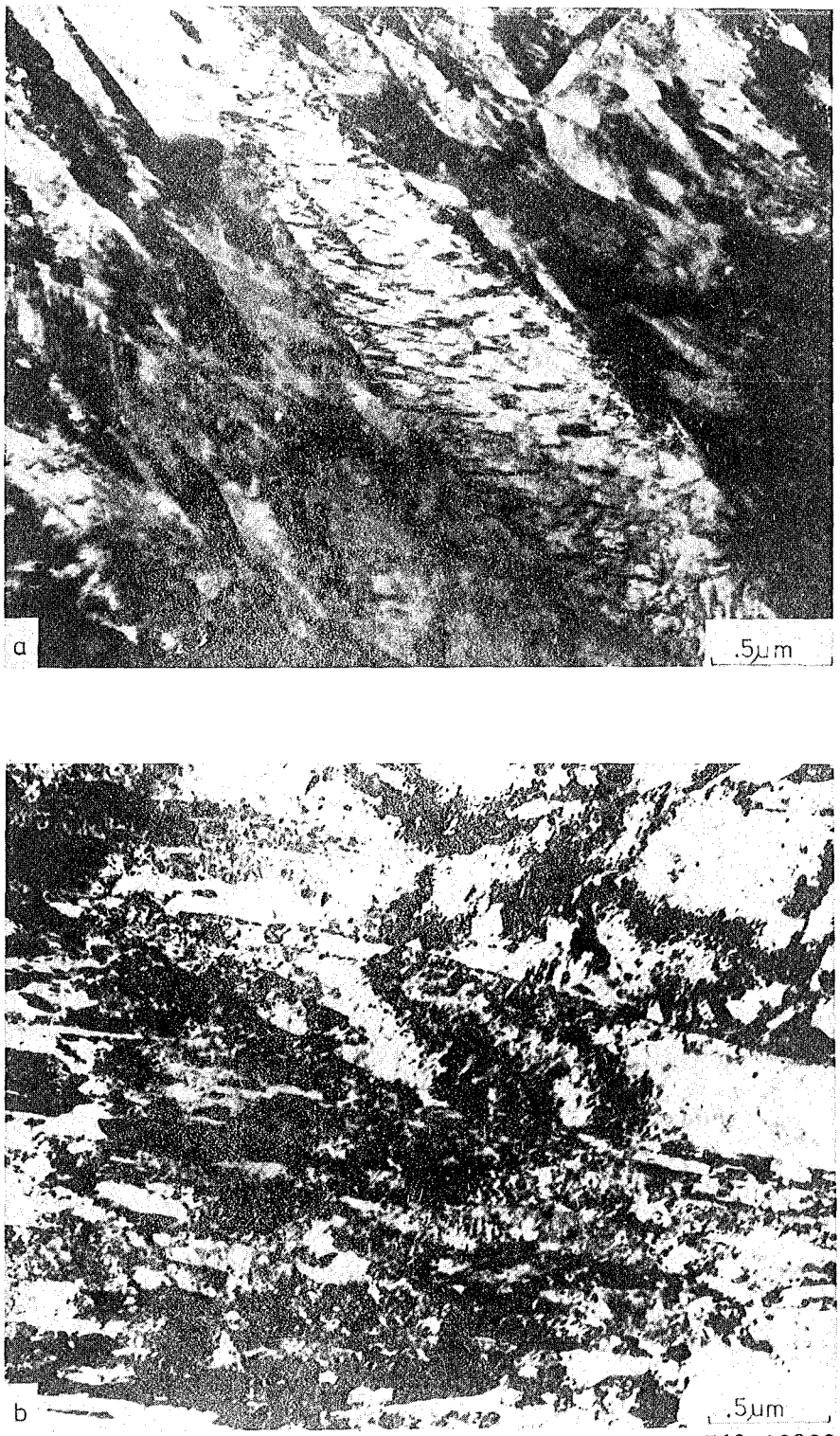

XBB 760-10002

Fig. 58.

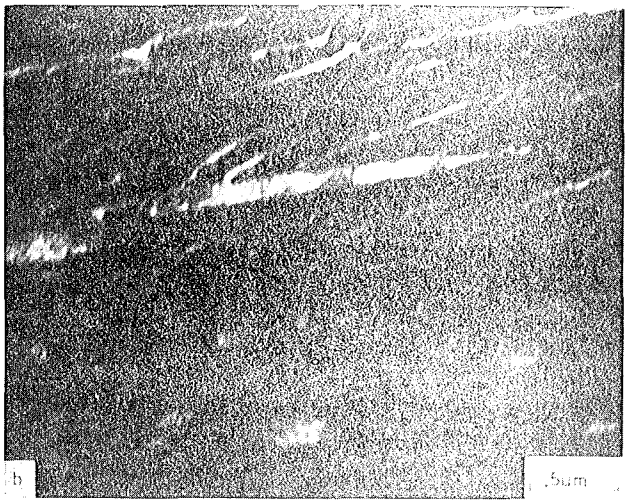

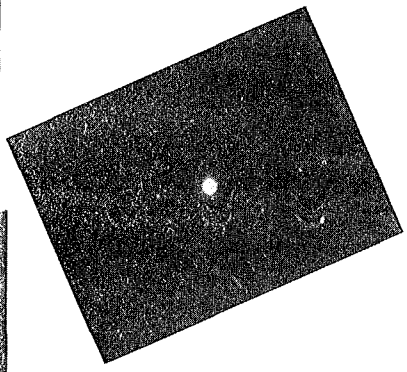

XBB 769-8115

Fig. 59.

8 8 9 9 4 7 8 0 9 9 3

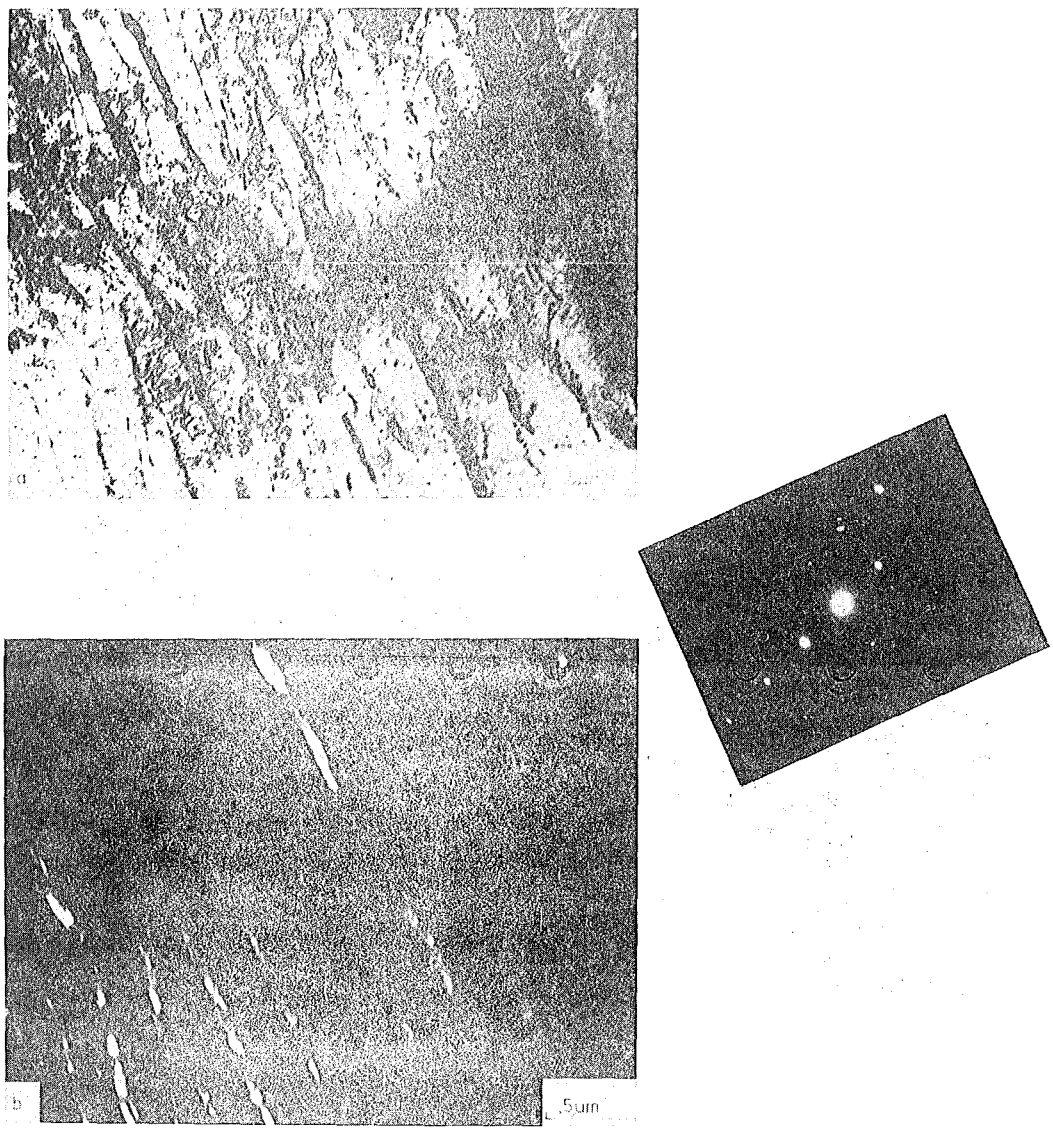

XBB 769-8119

Fig. 60.

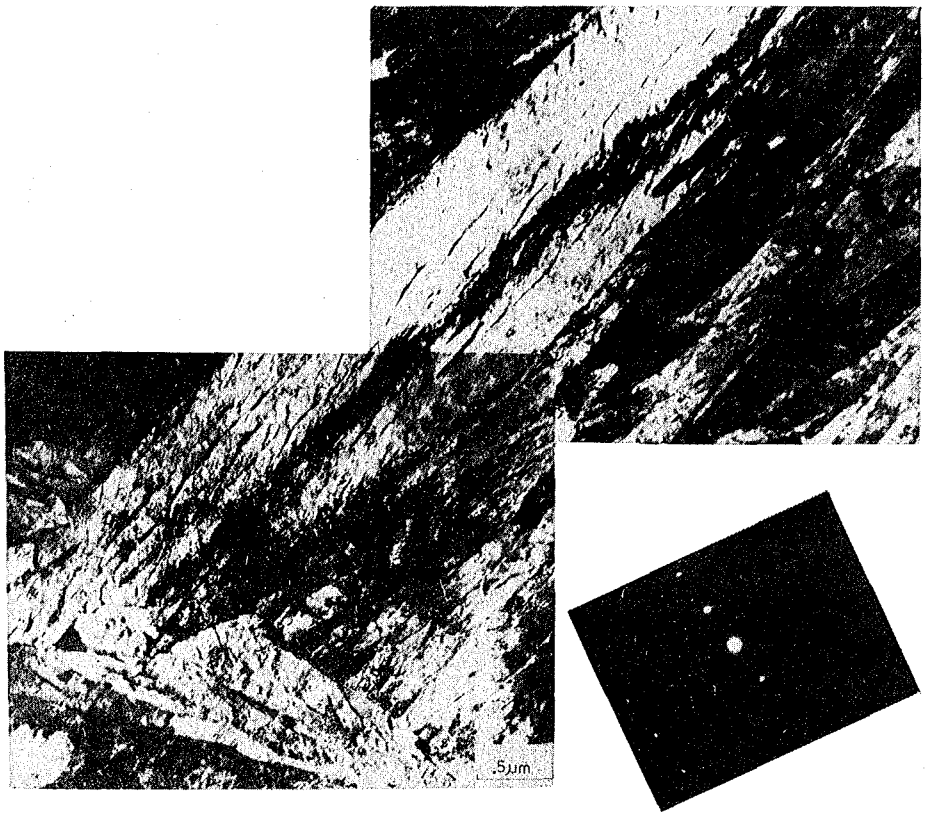

XBB 769-8112

Fig. 61.

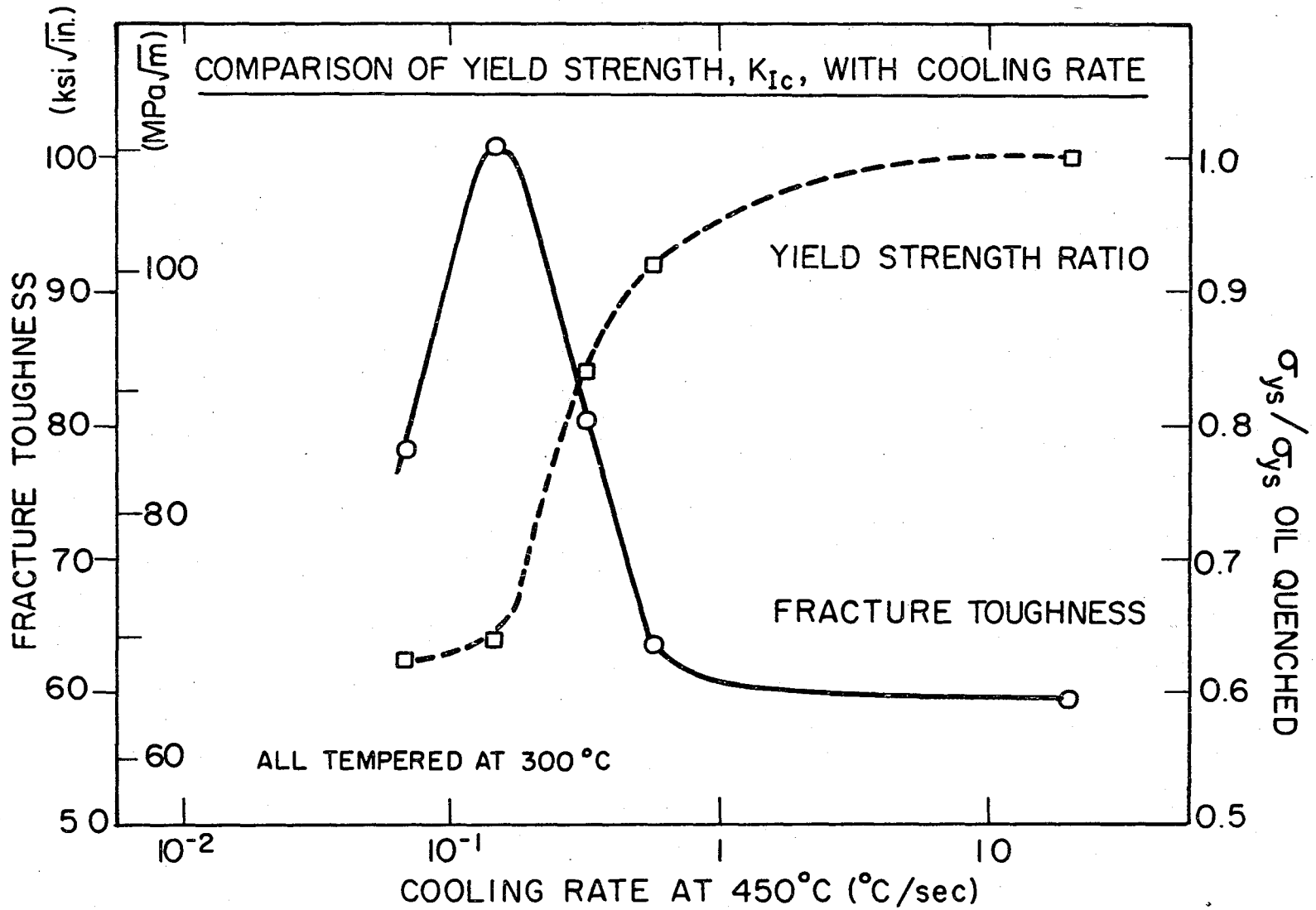

Fig. 62.

XBL 769-7517

0 0 0 0 4 7 8 8 9 0 4